

Abstract

TELEKE, SERCAN. Control Methods for Energy Storage for Dispatching Intermittent Renewable Energy Sources. (Under the direction of Dr. Mesut Baran.)

Solar, wind and other renewable energy sources are becoming an important part of energy supply to the power grid. Integrating a battery energy storage system (BESS) with a solar photovoltaic (PV) system or a wind farm can make these intermittent renewable energy sources more dispatchable. In this thesis, three different control methods for BESS are proposed for this purpose.

For dispatching, the set point for the controllers is determined first using the historical data. Then using this reference, the power and energy ratings required for the BESS is calculated, and the battery operation in terms of charge/discharge duration is characterized.

For optimal use of a BESS to minimize the deviations from dispatch set points, three control methods for BESS have been developed. The simulations have shown that the dispatch performance obtained with SOC feedback method is unsatisfactory compared to the other two methods namely optimal control and rule based control. The rule based control, and the optimal control performs very similar since the rule based control corresponds to the closed loop implementation of the optimal control. Moreover, the rule based method has several advantages over the optimal control such as less computation time, closed loop implementation, and no need for development of a mathematical model for BESS.

In terms of BESS operation, it is seen that the BESS charge/discharge frequency is relatively high in this application; and hence, new type of batteries with high

charge/discharge cycling rates are needed. Moreover, the control methods considered make a compromise in that they didn't utilize the BESS full capacity in order to extend the lifetime of the BESS, and hence, a large size BESS – about 15%-25% of the solar PV/wind farm capacity – is needed to have an effective hourly dispatch.

Control Methods for Energy Storage for Dispatching Intermittent
Renewable Energy Sources

by
Sercan Teleke

A dissertation submitted to the Graduate Faculty of
North Carolina State University
in partial fulfillment of the
requirements for the Degree of
Doctor of Philosophy

Electrical Engineering

Raleigh, North Carolina
2009

APPROVED BY:

Dr. Alex Huang

Dr. Johan Enslin

Dr. Mohan Putcha

Dr. Subhashish Bhattacharya
Co-Chair of Advisory Committee

Dr. Mesut Baran
Chair of Advisory Committee

Biography

Sercan Teleke was born in Ankara, Turkey, in 1983. He received the B.S. degree in electrical and electronics engineering from Middle East Technical University, Ankara, in 2005 and the M.S. degree in electric power engineering from Chalmers University of Technology, Gothenburg, Sweden, in 2006. He is currently pursuing Ph.D. degree in electrical engineering at North Carolina State University, Raleigh. His research interests are in the areas of integration of renewable energy sources using energy storage, power electronics applications to power systems.

Acknowledgements

I would like to express my deepest gratitude to my advisory committee chair Dr. Mesut Baran for his valuable guidance throughout my research. His support and suggestions made it much easier to accomplish my dissertation. Moreover, I would like to thank my other committee members, Dr. Subhashish Bhattacharya, Dr. Alex Huang, Dr. Mohan Putcha and Dr. Johan Enslin for their support during my thesis.

I also would like to thank the staff of the Quanta Technology, especially the transmission team, for their help and providing financial support throughout my thesis.

Sercan

Raleigh

09/27/2009

TABLE OF CONTENTS

LIST OF TABLES	v
LIST OF FIGURES	vi
1. Introduction.....	1
1.1 Scope.....	4
1.2 Thesis Structure	4
2. Literature Review.....	5
2.1 Energy Storage Technologies	5
2.1.1 Battery Energy Storage (BES).....	5
2.1.2 Other Storage Technologies.....	10
2.2 Application of Energy Storage to Intermittent Renewable Energy Sources.....	14
2.2.1 Wind.....	14
2.2.2 Solar	15
3. BESS for Wind and Solar Energy.....	17
3.1 Constraints with BESS and Converter	17
3.2 Sizing of BESS and Reference Power Profile Selection for Dispatchability	24
4. Proposed Methods.....	40
4.1 SOC Feedback [4].....	41
4.1.1 Simulation Setup.....	43
4.1.2 Simulation Results	44
4.2 Optimal Control	59
4.2.1 Simulation Setup.....	67
4.2.2 Simulation Results	68
4.3 Rule Based Control.....	90
4.3.1 Simulation Setup.....	92
4.3.2 Simulation Results	93
4.4 Control of STATCOM.....	108
4.5 Comparison of Methods.....	109
4.6 Experimental Validation of the Rule Based Method	111
5. BESS for Contingency Support	117
6. Conclusions and Future Work	123
References.....	125
Appendices.....	131
Appendix A: Battery Model.....	132
Appendix B: Derivation of the mathematical model	134
Appendix C: Experimental Setup details.....	135

LIST OF TABLES

Table 3.1: DOD vs. Number of Cycles.....	21
Table 3.2: Required BESS size for different P_{set} s	38
Table A.1: Used Parts	135

LIST OF FIGURES

Figure 1-1: Typical intermittent renewable energy source power output (a) Solar PV system (b) Wind Farm	2
Figure 1-2: Daily power output from a utility scale PV system [6].....	3
Figure 3-1: BESS integration with a renewable energy source	17
Figure 3-2: Thevenin battery model	19
Figure 3-3: Third order battery model [48].....	20
Figure 3-4: Battery capacity with different DOD	23
Figure 3-5: P_{set} with and without 10% error for wind	26
Figure 3-6: Power and energy ratings for ideal BESS (a) $P_{bess,ref} = P_{set} - P_{wind}$ (in megawatts) (b) Energy required for dispatch $E_{bess,ideal}$ (in megawatthours)	27
Figure 3-7: P_{set} with and without 10% error for solar.....	28
Figure 3-8: Power and energy ratings for ideal BESS (a) $P_{bess,ref} = P_{set} - P_{solar}$ (in megawatts) (b) Energy required for dispatch $E_{bess,ideal}$ (in megawatthours)	29
Figure 3-9: P_{set} incorporating RDRL and RURL with and without 10% error for wind..	30
Figure 3-10: Power and energy ratings for ideal BESS (a) $P_{bess,ref} = P_{set} - P_{wind}$ (in megawatts) (b) Energy required for dispatch $E_{bess,ideal}$ (in megawatthours)	31
Figure 3-11: P_{set} incorporating RDRL and RURL with and without 10% error for solar	32
Figure 3-12: Power and energy ratings for ideal BESS (a) $P_{bess,ref} = P_{set} - P_{solar}$ (in megawatts) (b) Energy required for dispatch $E_{bess,ideal}$ (in megawatthours)	33
Figure 3-13: P_{set} incorporating RDRL, RURL and $P_{set,UL}$ with and without 10% error for wind.....	34
Figure 3-14: Power and energy ratings for ideal BESS (a) $P_{bess,ref} = P_{set} - P_{wind}$ (in megawatts) (b) Energy required for dispatch $E_{bess,ideal}$ (in megawatthours)	35
Figure 3-15: P_{set} incorporating RDRL, RURL and $P_{total,UL}$ with and without 10% error for solar.....	36
Figure 3-16: Power and energy ratings for ideal BESS (a) $P_{bess,ref} = P_{set} - P_{solar}$ (in megawatts) (b) Energy required for dispatch $E_{bess,ideal}$ (in megawatthours)	37
Figure 4-1: Overall control block diagram	40
Figure 4-2: SOC feedback method	41
Figure 4-3: Dispatching of wind farm power with BESS; P_{set} : desired set point, P_{wind} : wind power, P_{total} : net injected power (in megawatts).....	45
Figure 4-4: 10 MWh BESS performance. (a) State of charge of one battery. (b) Current profile of one battery (kA). (c) DC link voltage (p.u.). (d) Power injected by the BESS (MW).....	46
Figure 4-5: Power deviations in net power supplied P_{total} around the desired set point P_{set} with 10 MWh BESS. (a) Power deviations $dP = P_{set} - P_{total}$ (in megawatts). (b) Histogram of power deviations (%).....	49

Figure 4-6: Power deviations in the power supplied P_{wind} around the desired set point P_{set} without BESS. (a) Power deviations = $P_{set} - P_{wind}$ (in megawatts). (b) Histogram of power deviations (%).....	50
Figure 4-7: Dispatching of solar PV power with BESS; P_{set} : desired set point, P_{solar} : solar power, P_{total} : net injected power (in megawatts).....	51
Figure 4-8: 300 kWh BESS performance. (a) State of charge of one battery. (b) Current profile of one battery (kA). (c) DC link voltage (p.u.). (d) Power injected by the BESS (kW).....	53
Figure 4-9: Power deviations in net power supplied P_{total} around the desired set point P_{set} with 300 kWh BESS. (a) Power deviations $dP = P_{set} - P_{total}$ (in megawatts). (b) Histogram of power deviations (%).....	57
Figure 4-10: Power deviations in the power supplied P_{solar} around the desired set point P_{set} without BESS. (a) Power deviations = $P_{set} - P_{solar}$ (in megawatts). (b) Histogram of power deviations (%).....	58
Figure 4-11: Simplified battery model with used circuit parameters	61
Figure 4-12: Current applied to both battery models (kA)	62
Figure 4-13: Battery voltage error (%)	62
Figure 4-14: Dispatching of wind farm power with BESS; P_{set} : desired set point, P_{wind} : wind power, P_{total} : net injected power (in megawatts) - 30 min prediction window	69
Figure 4-15: 10 MWh BESS performance with 30 min prediction window. (a) State of charge of one battery. (b) Current profile of one battery (kA). (c) DC link voltage (p.u.). (d) Power injected by the BESS (MW).....	70
Figure 4-16: Power deviations in net power supplied P_{total} around the desired set point P_{set} with 10 MWh BESS. (a) Power deviations $dP = P_{set} - P_{total}$ (in megawatts). (b) Histogram of power deviations (%).....	74
Figure 4-17: Dispatching of wind farm power with BESS; P_{set} : desired set point, P_{wind} : wind power, P_{total} : net injected power (in megawatts) - 100 sec prediction window	75
Figure 4-18: 10 MWh BESS performance with 100 sec prediction window. (a) State of charge of one battery. (b) Current profile of one battery (kA). (c) DC link voltage (p.u.). (d) Power injected by the BESS (MW).....	77
Figure 4-19: Power deviations in net power supplied P_{total} around the desired set point P_{set} with 10 MWh BESS. (a) Power deviations $dP = P_{set} - P_{total}$ (in megawatts). (b) Histogram of power deviations (%).....	81
Figure 4-20: Dispatching of solar PV power with BESS; P_{set} : desired set point, P_{solar} : solar power, P_{total} : net injected power (in megawatts) - 30 min prediction window	83
Figure 4-21: 300 kWh BESS performance with 30 min prediction window. (a) State of charge of one battery. (b) Current profile of one battery (kA). (c) DC link voltage (p.u.). (d) Power injected by the BESS (kW).....	84
Figure 4-22: Power deviations in net power supplied P_{total} around the desired set point P_{set} with 300 kWh BESS. (a) Power deviations $dP = P_{set} - P_{total}$ (in megawatts). (b) Histogram of power deviations (%).....	88
Figure 4-23: Dispatching of wind farm power with BESS; P_{set} : desired set point, P_{wind} : wind power, P_{total} : net injected power (in megawatts).....	94

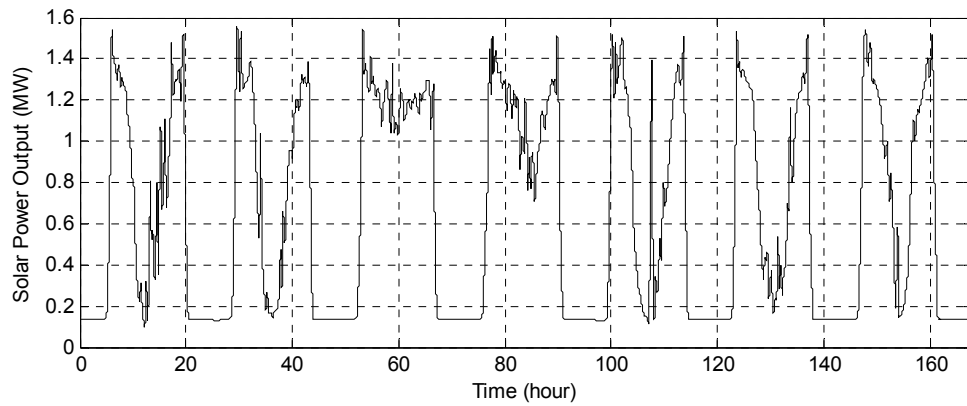
Figure 4-24: 10 MWh BESS performance. (a) State of charge of one battery. (b) Current profile of one battery (kA). (c) DC link voltage (p.u.). (d) Power injected by the BESS (MW).....	95
Figure 4-25: Power deviations in net power supplied P_{total} around the desired set point P_{set} with 10 MWh BESS. (a) Power deviations $dP = P_{set} - P_{total}$ (in megawatts). (b) Histogram of power deviations (%).....	99
Figure 4-26: Dispatching of solar PV power with BESS; P_{set} : desired set point, P_{solar} : solar power, P_{total} : net injected power (in megawatts).....	100
Figure 4-27: 300 kWh BESS performance. (a) State of charge of one battery. (b) Current profile of one battery (kA). (c) DC link voltage (p.u.). (d) Power injected by the BESS (kW).....	102
Figure 4-28: Power deviations in net power supplied P_{total} around the desired set point P_{set} with 300 kWh BESS. (a) Power deviations $dP = P_{set} - P_{total}$ (in megawatts). (b) Histogram of power deviations (%).....	106
Figure 4-29: Control block diagram of STATCOM.....	108
Figure 4-30: Comparison of the three proposed methods.....	110
Figure 4-31: Experimental Setup.....	111
Figure 4-32: Single battery performance with rule based control. (a) Power reference, $P_{bess,ref}$, power injected by the battery, P_{bess} and scaled BESS power from simulation (W). (b) Current reference, i_{bess}^* and current profile of the battery i_{bess} (A). (c) State of charge of the battery. (d) Battery voltage (V).....	113
Figure 5-1: Wind farm power output (MW).....	117
Figure 5-2: BESS application for contingency support. (a) P_{set} : desired set point, P_{wind} : wind power, P_{total} : net injected power (in megawatts). (b) State of charge of one battery. (c) Current profile of one battery (kA).....	119

1. Introduction

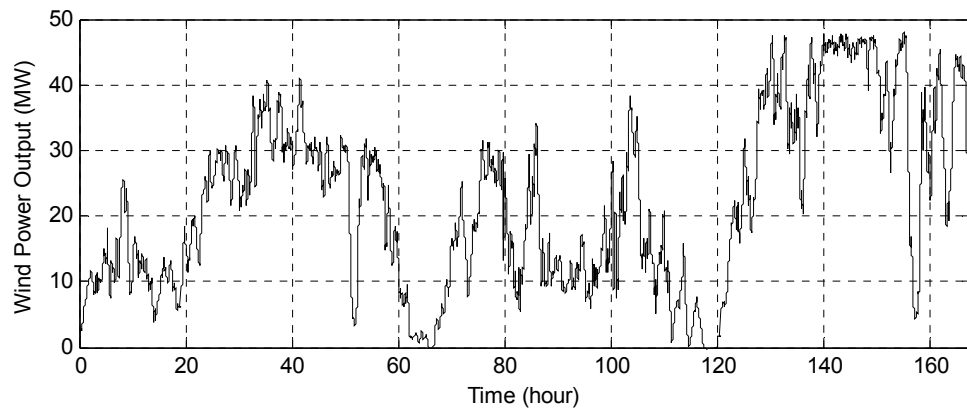
Wind, solar and other renewable energy sources are an important part of today's electricity generation and the part of energy they supply to the power grid will definitely be increasing over the next decades.

Grid-connected solar photovoltaic (PV) continued to be the fastest growing power generation technology, with a 70- percent increase in existing capacity to 13 GW in 2008 and existing wind power capacity grew by 29 percent in 2008 to reach 121 GW, more than double the 48 GW that existed in 2004 [1], [2]. However, similar to other renewable energy sources; solar and wind energy tends to be unsteady because they are influenced by natural and meteorological conditions [3]. As the output power of these sources fluctuates, it can result in network frequency and voltage deviations. Moreover, high penetration of intermittent renewable resources can introduce technical challenges including grid interconnection, power quality, reliability, protection, generation dispatch and control [4]. Therefore, the industry will need to confront the challenges associated with higher levels of penetration [5].

Figure 1-1 (a) shows the power output profile of a small scale solar PV system (3 kW capacity scaled by 1000 to represent a large scale PV system) and Figure 1-1 (b) shows a large wind farm (50 MW capacity). The wind data used was from a wind farm in northwest USA and has a resolution of 5 minutes. Due to the lack of publicly available utility scale solar data, the data obtained from a small scale solar PV system with 15 min resolution is used in this study. The typical utility scale PV system power output for one day is shown in Figure 1-2. By comparing the weekly profile shown in Figure 1-1 (a) with the daily profile seen in Figure 1-2, it is seen that the small scale solar PV system is not a typical representation of a utility scale solar PV system.



(a)



(b)

Figure 1-1: Typical intermittent renewable energy source power output (a) Solar PV system (b) Wind Farm

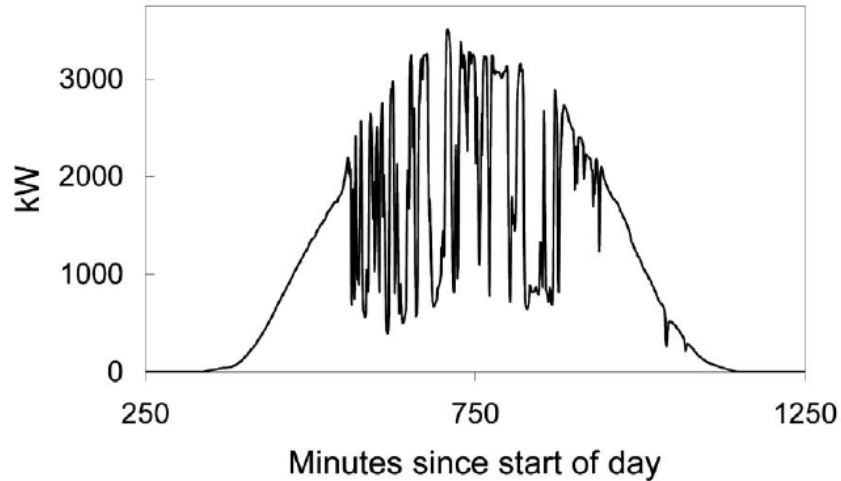


Figure 1-2: Daily power output from a utility scale PV system [6].

Figure 1-1 shows that the power output can have steep rises, sudden drops during the day and integrating such highly intermittent energy resources might adversely impact a smaller or a weaker electric power system [7], [8]. Therefore, there is a need for dispatching renewable resources so that they can be controlled like any other conventional generator, such as a thermal or a hydro power plant.

In this thesis, the focus will be the three main challenges of renewable energy sources:

- 1) Intermittency: The ability of a utility to change the power output of a generating unit as the load changes is the basis of economic dispatch [9]. For a renewable energy source to be dispatchable like the other conventional generation units, its output should be regulated at a desired dispatchability level.
- 2) Ramp Rates: Another issue with the large amount of wind/solar generation is the fast power ramps of the wind farm/solar PV system output, both positive and negative [10]. These ramps should be limited in order to integrate the large amount of generation to the grid, minimize the high cost ancillary service requirements and reduce the impact on system reliability [11].

3) Transmission curtailment: Large scale wind/solar power may cause congestion on the transmission lines that carry power (for example, when a large wind farm is integrated to a weak part of a system [12]) and hence the power output of the wind farm/solar PV system may have to be curtailed to prevent congestion [13].

1.1 Scope

The aim of the thesis is to design and control a BESS for dispatchable wind farm/solar PV power. For that purpose the following steps are taken:

- Determine the reference power profile for the intermittent renewable energy source of interest;
- Determine the power and energy ratings required for the BESS and characterize the battery operation, i.e. charge/discharge duration, lifetime;
- Develop different control algorithms to charge/discharge the BESS in order to have a dispatchable wind farm/solar PV power output and validate the final method with an experiment;

1.2 Thesis Structure

The thesis consists of following chapters:

Chapter 2 - Literature Review: General information about different energy storage types and their applications to solar and wind energy;

Chapter 3 - BESS for Wind and Solar Energy: Challenges with BESS, BESS sizing and reference power selection for dispatching;

Chapter 4 - Proposed Methods: Explanation of the three proposed methods for the control of BESS, comparison of the methods and experimental validation;

Chapter 5 - BESS for contingency support: Control of BESS with rule based method for contingency support;

Chapter 6 - Conclusions and Future Work: Conclusions and ideas for future work.

2. Literature Review

In this chapter, different energy storage technologies are introduced briefly and their applications to intermittent renewable energy sources are summarized using the existing literature.

2.1 Energy Storage Technologies

Different battery technologies and other storage types are briefly described below:

2.1.1 Battery Energy Storage (BES)

Batteries are one of the most cost-effective energy storage options available, which store energy electrochemically [14]. A battery system is made up of a set of low voltage or power battery modules connected in series and/or parallel to achieve a desired electrical characteristic. Batteries are charged when they undergo an internal chemical reaction under a potential applied to the terminals. They deliver the absorbed energy, or discharge, when they reverse the chemical reaction. Some of the key factors of batteries for storage applications include: high energy density, round trip efficiency, cycling capability, life span, and initial cost [15].

Batteries store dc charge, so power conversion is necessary to interface a battery with an ac power system. Advances in battery technologies offer increased energy storage densities, greater cycling capabilities, higher reliability, and lower cost [16]. Battery energy storage systems have emerged as one of the most promising near-term storage technologies for power applications, offering a wide range of power system applications such as area regulation, spinning reserve, and power factor correction [17]. Common battery types are described below:

Lead Acid Battery

Lead acid batteries were invented in 1859 by Gaston Plante and first demonstrated to the French Academy of Sciences in 1860. They are the most mature and oldest of all battery technologies and due to the wide use of lead acid batteries in a wide variety of applications, they have the lowest cost of all battery technologies [18].

Lead acid batteries still remain the technology of choice for automotive starting, lighting and ignition (SLI) applications because they are robust, tolerant to abuse, tried and tested and because of their low cost [19]. Their application for energy management, however, has been very limited due to their limited cycling capability. The amount of energy that a lead-acid battery can deliver is not fixed and depends on its rate of discharge.

Lead-acid batteries, nevertheless, have been used in a few commercial and large-scale energy management applications. The largest one was a 40 MWh system in Chino, California, built in 1988. It demonstrated the value of stored energy in the grid but the short cycle life of lead acid batteries made the overall economics of the system unacceptable.

There is still research going on to develop advanced lead acid batteries with improved life cycles. Adding as much as 40% of activated carbon to the negative electrode composition increases battery's life up to 2000 cycles which represent a three to four times improvement over the conventional lead acid designs [18].

Lithium Ion Battery

Pioneer work with the lithium batteries began in 1912 under G.N. Lewis but it was not until the early 1970s that the first non-rechargeable lithium batteries became commercially available. Attempts to develop rechargeable lithium batteries followed in the 1980s, but failed due to safety problems [20].

The cathode in lithium ion batteries is a lithiated metal oxide (LiCoO_2 , LiMO_2 , etc.) and the anode is made of graphitic carbon with a layer structure. The electrolyte is made up of lithium salts (such as LiPF_6) dissolved in organic carbonates [21].

When the battery is being charged, the lithium atoms in the cathode become ions and migrate through the electrolyte toward the carbon anode where they combine with external electrons and are deposited between carbon layers as lithium atoms. The reverse of this process occurs during discharge.

The main advantages of Li-ion batteries, compared to other advanced batteries, are their high energy density, high efficiency, and long cycle life. The main difficulty with these batteries is the high cost due to special packaging and internal overcharge protection circuits.

Nickel Cadmium Battery

Waldmar Jungner invented the nickel-cadmium battery in 1899. At that time, due to the expense of the materials used in the battery, its use was limited to special applications. In 1932, the active materials were deposited inside a porous nickel-plated electrode and in 1947 research began on a sealed nickel-cadmium battery [22].

Among rechargeable batteries, nickel-cadmium still remains a popular choice for two-way radios, emergency medical equipment and power tools. There is a shift towards batteries with higher energy densities and less toxic metals but alternative chemistries can not always match the durability and low cost of nickel-cadmium. The advantages of Nickel-cadmium (Ni-Cd) batteries are their long lives in stationary applications, and typically being quite resistant to abuse [15].

Sodium Sulfur Battery

The sodium sulfur (NaS) battery technology was originally developed in the 1960s for use in early electric cars but was abandoned later for this application [18].

NaS battery consists of sulfur at positive electrode, sodium at negative electrode as active materials, and beta alumina of sodium ion conductive ceramic which separates both electrodes. This hermetically sealed battery is operated under the condition that the active materials at both electrodes are liquid, and its electrolyte is solid.

During discharge, positive sodium ions flow through the electrolyte and electrons flow in the external circuit of the battery to produce about 2V. This process is reversible since charging causes sodium polysulfides to release the positive sodium ions back through the electrolyte to recombine the sodium element.

This type of battery has a high energy density, a high efficiency of charge/discharge (89–92%) [23], long cycle life, and is fabricated from inexpensive materials. However, because of the operating temperatures of 300°C, and the highly corrosive nature of the sodium polysulfides, such cells are primarily suitable for large-scale non-mobile applications such as grid energy storage.

NaS battery technology has been demonstrated over 190 sites in Japan totaling more than 270 MW of capacity with stored energy suitable for 6 hours of daily peak shaving. The largest NaS installation is a 34 MW, 245 MWh system for wind farm stabilization in Northern Japan [21]. Utilities in US have deployed 9 MW of NaS batteries for peak shaving, backup power, smoothing wind power and other applications [18].

Flow Battery

Flow batteries allow storage of the active materials external to the battery and these reactants are circulated through the cell stack as required. The first such battery was Zinc Chlorine battery in which the chlorine was stored in a separate cylinder. It was first used in 1884 by Charles Renard to power his airship La France which contained its own on board chlorine generator [24].

Flow batteries differ from conventional rechargeable batteries in one significant way which is the ability to scale the power and energy ratings of a flow battery independent of each other [18]. This is made possible by the separation of the electrolyte and the battery stack (or fuel cell stack). More cell stacks allows for an increase in power rating; a greater volume of electrolytes results in more runtime.

Some leading flow battery technologies are Zinc Bromine (ZnBr) and Vanadium Redox batteries (VRB).

The ZnBr battery was developed by Exxon in the early 1970's. Integrated ZnBr energy storage systems are now available on transportable trailers (storage systems including power electronics) with unit capacities of up to 1MW/3MWh for utility-scale applications [21].

VRB was pioneered by the University of New South Wales (UNSW) in Australia in early 1980's. The Australian Pinnacle VRB bought the basic patents in 1998 and licensed them to Sumitomo Electric Industries (SEI) and VRB Power Systems. VRB storages up to 500kW, 10 hrs (5MWh) have been installed in Japan by SEI. VRBs have also been applied for power quality applications (3MW, 1.5 sec., SEI) [21].

2.1.2 Other Storage Technologies

Compressed Air Energy Storage (CAES)

Compressed Air Energy Storage refers to the compression of air to be used later as energy source. CAES is a peaking gas turbine power plant that consumes less than 40% of the gas used in a conventional gas turbine to produce the same amount of electric output power. This is because, unlike conventional gas turbines that consume about 2/3 of their input fuel to compress air at the time of generation, CAES pre-compresses air using the low cost electricity from the power grid at off-peak times and utilizes that energy later along with some gas fuel for use during peak periods [21].

To make the CAES concept work depends on locating the plants near appropriate underground geological formations, such as underground mines, caverns created inside salt rocks or depleted gas wells.

The first commercial CAES plant was a 290 MW unit built in Germany in 1978. The second one was a 110 MW unit built in US. These units can come on line in 15 minutes when called upon for power. Today, Electric Power Research Institute (EPRI) has a research program to develop advanced CAES designs with a power range varying between 150 MW and 400 MW. In addition to this, an aboveground CAES alternative is also studied by EPRI [18].

Electrochemical Capacitors (Supercapacitors)

Electrochemical capacitors commonly called supercapacitors store electrical energy in two series capacitors of the electric double layer (EDL), which is formed between each of the electrodes and the electrolyte ions. The distance over which the charge separation occurs is just a few angstroms. The extremely large surface area makes the capacitance and energy density of these devices thousands of times larger than conventional electrolytic capacitors [18].

The electrodes of these supercapacitors are often made with porous carbon material. The electrolyte is either aqueous or organic. The aqueous capacitors have a lower energy density due to a lower cell voltage but are less expensive and work in a wider temperature range. The asymmetrical capacitors that use metal for one of the electrodes have a significantly larger energy density than the symmetric ones do and also have a lower leakage current [21].

Electrochemical capacitors have lower energy density compared to lead-acid batteries, but they can be cycled tens of thousands of times and they have faster charge and discharge capability compared to batteries.

While the small electrochemical capacitors are well developed, the larger units with energy densities over 20 kWh/m³ are still under development. Rather than operate as a main battery, supercapacitors are more commonly used as memory backup to bridge short power interruptions. Another application is improving the current handling of a battery. The electrochemical capacitor is placed in parallel to the battery terminal and provides current boost on high load demands. The electrochemical capacitors will also find a ready market for portable fuel cells to enhance peak-load performance. Because of their ability to rapidly charge, large supercapacitors are used for regenerative braking on vehicles [25].

Flywheel Energy Storage (FES)

Modern flywheel energy storage systems consist of a huge rotating cylinder (comprised of a rim attached to a shaft) that is substantially supported on a stator by magnetically levitated bearings that eliminate bearing wear and increase system life. To maintain efficiency, the flywheel system is operated in a vacuum environment to reduce drag. The

flywheel is connected to a motor/generator mounted onto the stator that interacts with the utility grid through power electronics [21].

The stored energy on a flywheel depends on the moment of inertia of the rotor and the square of the rotational velocity of the flywheel. The moment of inertia depends on the radius, mass, and height (length) of the rotor. Energy is transferred to the flywheel when the machine operates as a motor i.e. the flywheel accelerates, charging the energy storage device. The flywheel is discharged when the electric machine regenerates through the drive i.e. the flywheel decelerates [14].

The energy storage capability of flywheels can be improved either by increasing the moment of inertia of the flywheel or by rotating it at higher velocities, or both. Some designs utilize hollow cylinders for the rotor allowing the mass to be concentrated at the outer radius of the flywheel, improving storage capability with a smaller weight increase [26].

Some of the key features of flywheels are long life (20 years or 10s of thousands of deep cycles), low maintenance and environmentally inert material. Flywheels can bridge the gap between short term ride-through and long term storage with excellent cyclic and load following characteristics [21].

While high-power flywheels are developed and deployed for aerospace and UPS applications, there is an effort going on to optimize low cost commercial flywheel designs for long duration operation (up to several hours). At present, high speed flywheel systems rated 1000kW (15 min duration) or larger are being deployed in US for frequency regulation [18].

Pumped Hydro

A typical pumped hydro plant consists of two interconnected reservoirs i.e. lakes, tunnels that connect one reservoir to another, hydro machinery, valves, a generator-motor, transformers, a transmission switchyard and connection to transmission system. The product of the total volume of water and the differential height between the reservoirs is proportional to the amount of stored energy [18].

Pumped hydro was first used in Italy and Switzerland in the 1890's. Beginning in the early 1900's, several small hydroelectric pumped storage plants were constructed in Europe, primarily in Germany. The first unit in US was constructed in 1929 in Connecticut. Today, adjustable speed machines are being used to improve efficiency and pumped hydro is available at almost any scale with discharge times ranging from several hours to a few days. Their efficiency is in the 70% to 85% range [21].

The global capacity of pumped hydro storage plants installed up to day totals more than 95 GW with around 20 GW operating in US. The main function of these plants was to provide off peak base loading for large coal and nuclear power plants to optimize the overall performance and provide peaking energy each day. Nowadays, their duties have been expanded to include providing ancillary services such as frequency regulation [18].

Superconducting Magnetic Energy Storage (SMES)

Superconducting magnetic energy storage systems store energy in the field of a large magnetic coil with direct current flowing. It can be converted back to alternative current as needed. Although superconductivity was discovered in 1911, it was not until the 1970s that SMES was first proposed as an energy storage technology for power systems [27].

A magnetic field is created by circulating a DC current in a closed coil of superconducting wire. The path of the coil circulating current can be opened with a solid

state switch which is modulated to be either on or off. Due to the high inductance of the coil, when the switch is off i.e. open, the magnetic coil behaves as a current source and will force current into the capacitor which will charge to some voltage level. Proper modulation of the solid-state switch can hold the voltage across the capacitor within the proper operating range of the inverter. An inverter then converts the DC voltage into AC voltage [28].

SMES systems have attracted the attention of both utilities and the military due to their fast response and high efficiency (charge/discharge efficiency over 95%). Possible applications of this technology include load leveling, dynamic stability, transient stability, voltage stability, frequency regulation, transmission capability enhancement, and power quality improvement [14]. Low temperature SMES cooled by liquid helium is commercially available and high temperature SMES cooled by liquid nitrogen is still in the development stage and may become a viable commercial energy storage source in the future.

2.2 Application of Energy Storage to Intermittent Renewable Energy Sources

Application of energy storage to address the intermittency of renewable energy sources has been addressed in many papers and a summary of these papers focusing on the application of wind and solar power is given below.

2.2.1 Wind

Some of the BESS applications for wind farms involve a simple scheme to charge and discharge the BESS, such as storing excess power if the wind power output exceeds a threshold [13], [29], [30].

In [31], a washout filter based scheme is adopted to smooth out short term power fluctuations of a wind farm with Vanadium Redox-Flow Batteries (VRB) as energy storage. Similarly, in [32], washout filter is used for an off-shore wind farm application with Supercapacitors as the energy storage.

Another application of Supercapacitors for wind farms can be found in [5]. In this paper, smoothing of fast wind induced power variations is studied and various size of storage is tested to show the improvement in the low voltage ride through (LVRT) capability of the wind farm.

Design of a BESS consisting of lead acid batteries for attenuating the effects of unsteady power from wind farms is made in [3] and it is shown that the economic benefit obtained from the BESS by dispatching wind can be represented as a maximization of an objective function and the solution of the problem can be used to determine the BESS size for perfect dispatch.

Moreover, in [33], prediction of the wind farm power output have been proposed to be used in BESS control in order to limit the maximum ramp rate of the wind farm power output. It is concluded from the paper that the wind forecast can reduce the required BESS size for ramp rate limiting drastically.

Large scale energy storage system (ESS) such as pumped hydro or compressed air for regulating the wind farm power output variation is studied in [34] and it is shown that besides dispatching voltage stability can also be improved with the energy storage.

2.2.2 Solar

The application of energy storage to solar systems is an emerging concept and not many papers in literature have addressed this issue yet.

Application of batteries to solar PV systems is proposed in [8]. In this paper, sodium sulfur (NaS) battery is used for dispatching a PV system using forecasted solar radiation and it is concluded that the accuracy of the solar radiation forecast is very important for dispatch performance.

Combining concentrating solar power (CSP) with thermal energy storage (TES) is suggested in [35]. In this article, the purpose of using storage was to match the load profile with the solar production and it is claimed that with the storage, the utilities can enhance dispatchability with the CSP plants.

3. BESS for Wind and Solar Energy

Amongst the storage technologies mentioned in the previous chapter, battery energy storage is the most appropriate and common storage technology with low losses for utility scale application [14]. Since the battery energy storage system (BESS) possesses higher energy capacity than several other energy storage media, it is suitable for the long-term load-tracking operation [36]. Moreover in [14], BESS is also shown to be cost-effective for use in power systems. Therefore, BESS can be selected a suitable choice for energy storage type that will be complemented with wind/solar energy.

Figure 3-1 illustrates the use of BESS to compensate for the intermittent power output of the PV system/wind farm. The BESS is connected to the system at the point of common coupling and is charged/discharged through a power converter to smooth the net power injected to the system.

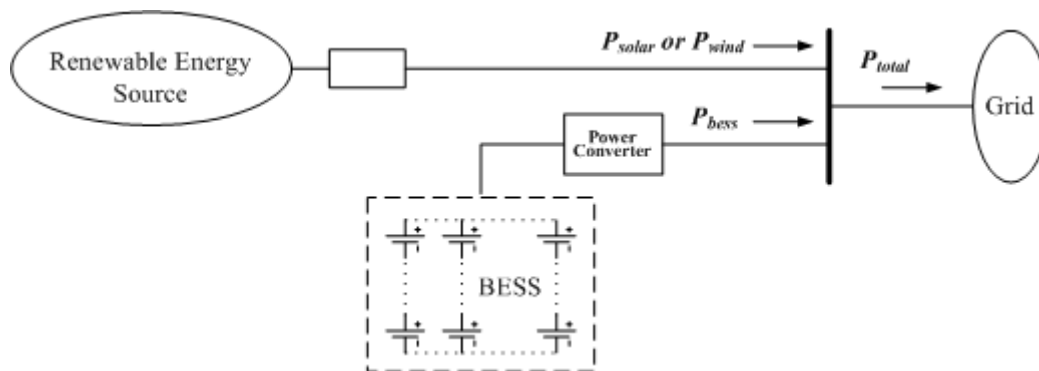


Figure 3-1: BESS integration with a renewable energy source

A STATCOM can be used as a power converter in this scheme in order to achieve the reactive power control [7] besides the active power control by BESS.

3.1 Constraints with BESS and Converter

Since BESS with STATCOM is proposed to tackle with renewable sources' variability, we need to look at the limitations of the components in this proposed structure.

State of Charge (SOC): The State of Charge of a battery is its available capacity expressed as a percentage of its rated capacity. Knowing the amount of energy left in a battery, compared with the energy it had when it was new, gives the user an indication of how much longer a battery will continue to discharge before it needs recharging. Using the analogy of a fuel tank in a car, SOC estimation is often called the “Fuel Gauge” function [25].

As it is not desired to deplete or overcharge the battery, the SOC of the battery should be kept within proper limits (i.e. between 30-100%) and need to be determined accurately for the controller operation [8], [31].

Several methods exist in literature which can be used in SOC estimation [38]-[43]. Some of these methods are discharge test, Ah counting, artificial neural network and Kalman filter. A summary and a brief explanation of these methods can be found in [44].

It should be noted that the SOC reference is normally the rated capacity of a cell which is a new cell. It is not the fully charged capacity of the cell when it was last charged (i.e. the current charge-discharge cycle). This is because the cell capacity gradually reduces as the cell ages and it is also affected by temperature and discharge rate. For example, towards the end of the cell’s life its actual capacity will be approaching only 80% of its rated capacity and in this case, even if the cell were fully charged, its SOC would only be 80%. This difference is important if the user is depending on the SOC estimation as he would in a real gas gauge application in a car. Therefore, these ageing and environmental factors must be taken into account if an accurate estimate is required.

In order to get a good estimation of SOC during the simulations, a suitable battery model is needed. Several papers exist in literature with different approach to battery modeling.

The simplest and commonly used model of a battery consists of a constant internal resistance in series with an ideal voltage source [45], [46]. Another commonly used battery model, namely, Thevenin battery model [47], [48] consists of an ideal no-load battery voltage, series internal resistance in series with parallel combination of overvoltage resistance and capacitance seen in Figure 3-2.

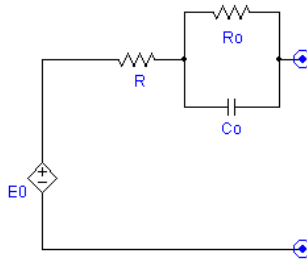


Figure 3-2: Thevenin battery model

Recently more realistic models have been proposed to take into account of the non-linear parameters [46], [47]. These models characterized the battery internal resistance, self-discharge resistance and overcharge resistance; and separated the charging and discharging process. In this thesis, one of these improved models, a third order model developed by Ceraolo [49], [50] has been considered for accurate representation of battery charge/discharge characteristics and estimating the SOC of the battery. Figure 3-3 shows the model.

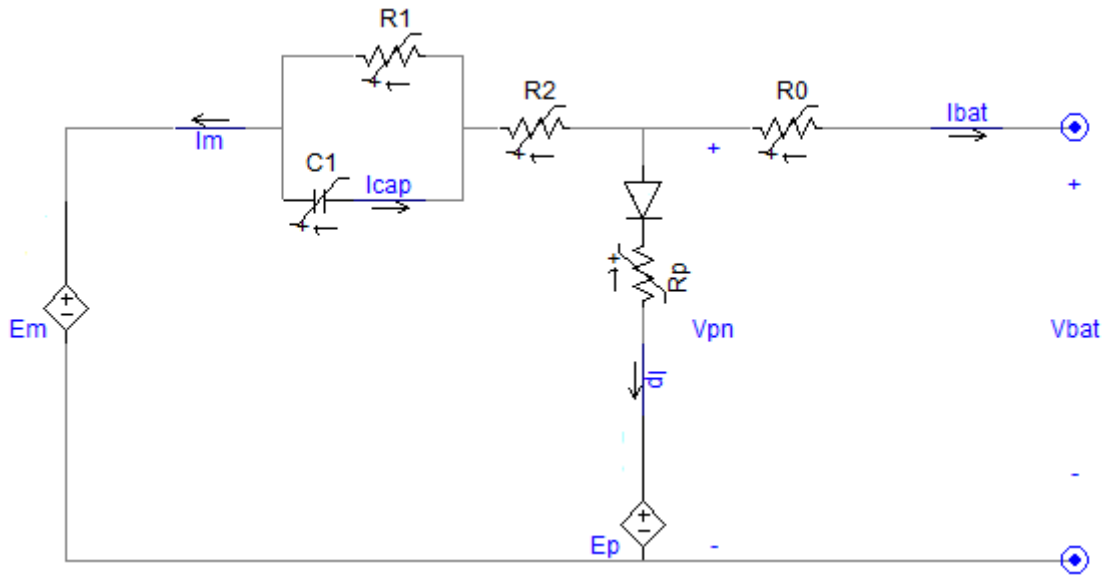


Figure 3-3: Third order battery model [48]

In this model, the main branch (containing the elements Em , $R1$, $C1$ and $R2$) approximates the battery charge/discharge dynamics, the parasitic branch (containing Rp and Ep) accounts for the self-discharge, and $R0$ approximates the overcharge resistance. As the figure indicates, most of the resistive elements are non-linear, current dependent, and are determined empirically [51]. For this study, the parameters were taken from [49] which are derived for a flooded lead acid battery with a capacity of 500 Ah. The equations to represent the elements of the battery model are given in Appendix A.

According to this model the SOC is defined as:

$$SOC = 1 - \frac{Q_e}{C(0, \theta)} \quad (3-1)$$

$$Q_e = Q_{e_init} + \int_0^{\tau} -I_m(\tau) d\tau \quad (3-2)$$

where C is the battery's capacity in Amp-seconds, Q_e is the extracted charge in Amp-seconds, Q_{e_init} is the initial extracted charge in Amp-seconds, I_m is the main branch current in Amps.

The battery capacity C is defined as:

$$C(I, \theta) = \frac{K_c C_0^* \left(1 + \frac{\theta}{-\theta_f}\right)^\varepsilon}{1 + (K_c - 1) \left(\frac{I}{I^*}\right)^\delta} \quad (3-3)$$

where K_c , δ , ε are constants, C_0^* is the no load capacity at 0°C in Amp-seconds, θ is electrolyte temperature in °C, θ_f is the electrolyte freezing temperature, I is the discharge current in Amps, I^* is the nominal battery current in Amps.

By looking at the C definition, if we assume that the temperature of the battery constant, then the capacity of the battery becomes constant in SOC definition which assumes that the battery never ages. However, as mentioned before, the ageing in the battery must be taken into account if an accurate estimate is required. Therefore the battery model needs to be modified in order to implement aging.

In order to represent the effect of aging on the battery capacity, first of all, several lead acid battery data sheets are reviewed to get typical numbers for number of cycle vs. depth of discharge (DOD) of a lead acid battery. After the review, the following numbers are assumed for the aging implementation:

Table 3.1: DOD vs. Number of Cycles

Depth of Discharge (DOD)	Number of Cycles
0%<DOD<20%	5000
20%<DOD<40%	3500
40%<DOD	1850

After selecting life cycle associated with lead acid batteries, the number of cycles is counted for a typical one week wind power dispatchability application to get approximate charge/discharge time. The results of this counting shows that in wind farm application, the average charge/discharge cycle is 25 mins. Therefore, assuming an average discharge time of 25 mins, we can calculate the life time of the battery for different DOD levels by multiplying discharge time with number of cycles.

To implement the aging to the battery model, the battery capacity should decrease over time. Since how long battery will last with different DOD levels is known, the capacity in the battery model is made to decrease with different slope depending on the DOD to get an approximate aging implementation to the model. Simulation results obtained from the battery model explained above with aging implemented is shown in Figure 3-4.

The faster decrease of battery capacitance with higher discharge current is seen in Figure 3-4. By looking at this result, we can conclude that the aging is implemented properly depending on DOD as we described above.

To sum up, the battery capacity is decreased with a slope corresponding to 5000 cycles for $0\% < \text{DOD} < 20\%$; when DOD changes between 20% and 40%, the slope changes corresponding to 3500 cycles; and when DOD is higher than 40%, the slope changes corresponding to 1850 cycles. Therefore, the battery capacity is decreased continuously by observing the DOD all the time.

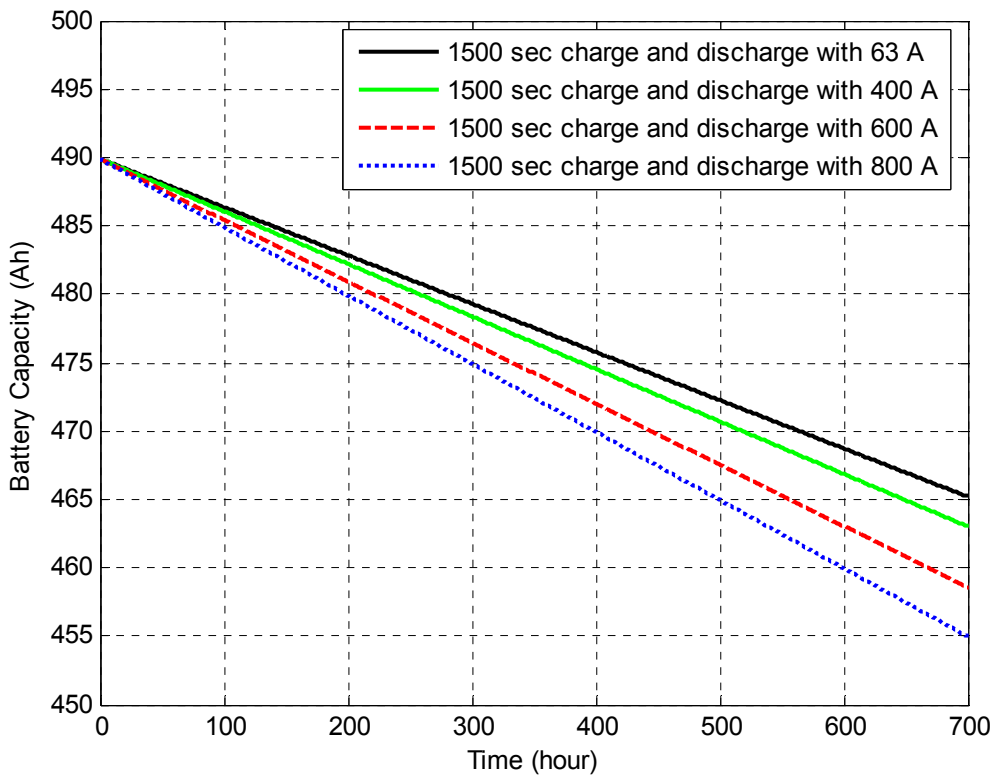


Figure 3-4: Battery capacity with different DOD

Deep Discharge: Cycle life of a battery decreases with increased depth of discharge (DOD) as shown in Table 3.1 and many cell chemistries will not tolerate deep discharge and may be permanently damaged if fully discharged. Therefore, to increase the cycle life of a battery and; moreover, to protect the battery from death, a limitation needs to be put on the maximum discharge current of the battery [52].

Converter Limit: Since the STATCOM consists of power electronics switches, the maximum power output of the BESS should be limited in order not to exceed STATCOM MVA rating.

3.2 Sizing of BESS and Reference Power Profile Selection for Dispatchability

We can use historical data to select a reference power profile for the intermittent renewable energy source of interest and to characterize the BESS for the dispatchability application, i.e., determine the power and energy ratings, the charge/discharge duration.

Looking at our proposed scheme which is shown in Figure 3-1, we note that total power injected to the grid is:

$$P_{total} = P_{wind} + P_{bess} \quad (3-4)$$

or

$$P_{total} = P_{solar} + P_{bess} \quad (3-5)$$

In these equations, P_{wind} is the wind farm power output, P_{solar} is the solar PV system power output, P_{bess} is the BESS power output, and P_{total} is the total power injected to the grid. To make P_{total} dispatchable, a power reference needs to be selected in order to define the power that BESS needs to inject:

$$P_{bess,ref} = P_{set} - P_{wind} \quad (3-6)$$

or

$$P_{bess,ref} = P_{set} - P_{solar} \quad (3-7)$$

where P_{set} is the reference power that needs to be selected in order to make P_{total} to be dispatchable, $P_{bess,ref}$ is the reference power that BESS needs to inject/absorb in order to obtain P_{set} .

To find a suitable P_{set} that will provide the dispatchable total power output, a dispatch period needs to be selected and in this study, it is chosen as one hour. Having selected the period, now the magnitude of P_{set} for each dispatch period i.e. for each hour needs to be selected.

To select the magnitude of P_{set} , assume that we can forecast the average solar and wind power output for the next hour, then selecting P_{set} to be the average of these hourly forecasts will minimize the required size of the BESS since the area under $P_{set} - P_{wind}$ or $P_{set} - P_{solar}$ which is the energy that needs to be provided by BESS will add up to zero for each hour [4]. Several papers exist in literature that addresses hourly wind/solar forecasting methods with 10% mean relative error of the rated resource capacity [10], [53]-[55].

Having determined what P_{set} needs to be for hourly dispatch while minimizing the required BESS size, we can now analyze this quantitatively to characterize the BESS required for this application.

In order to obtain the BESS ratings, the actual wind farm and solar PV system profile given in Figure 1-1 will be used and to calculate the BESS energy size, the following equation will be used:

$$E_{bess,ideal}(t) = E_{bess,ideal}(0) + \int_0^t P_{bess,ref}(t) dt \quad (3-8)$$

where $E_{bess,ideal}$ is the required energy for the BESS.

Figure 3-5 shows the P_{set} with and without 10% error in wind forecast obtained from Figure 1-1 (b); and Figure 3-6 shows the required BESS power and energy ratings i.e., $P_{bess,ref}$ and $E_{bess,ideal}$ for these two P_{sets} .

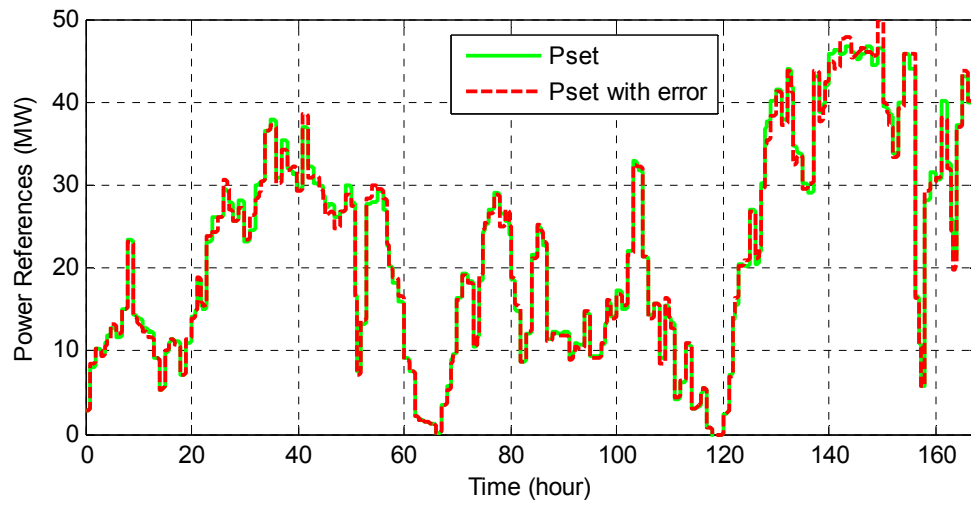
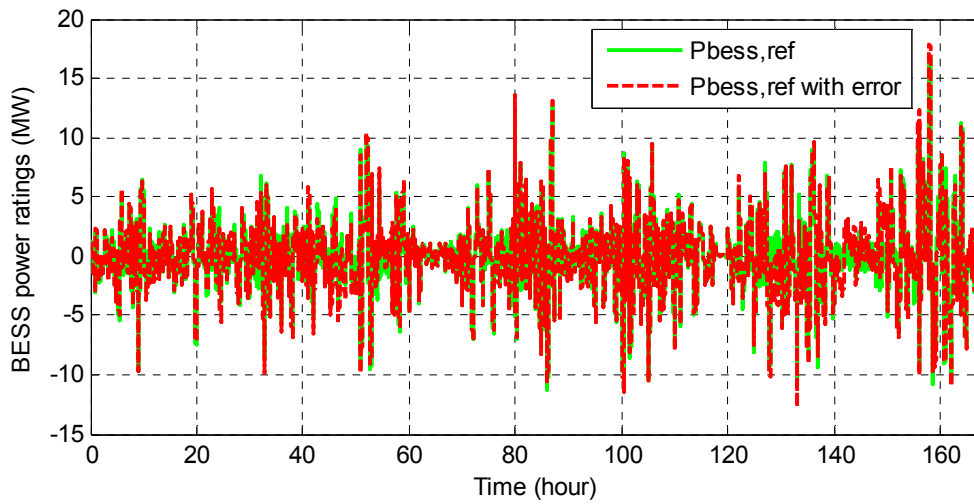
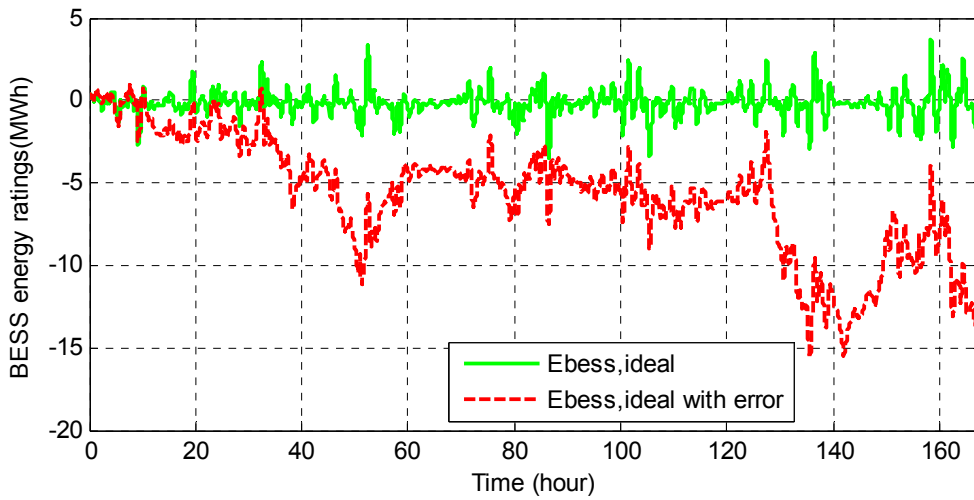


Figure 3-5: P_{set} with and without 10% error for wind



(a)



(b)

Figure 3-6: Power and energy ratings for ideal BESS (a) $P_{bess,ref} = P_{set} - P_{wind}$ (in megawatts) (b) Energy required for dispatch $E_{bess,ideal}$ (in megawatthours)

It is seen from Figure 3-6 that we need a converter size of ± 17 MW and a minimum BESS size of 8 MWh (i.e. 16% of the wind farm capacity) if we forecast wind power with no error, a converter size of ± 18 MW and a minimum BESS size of 17 MWh (i.e. 34% of the wind farm capacity) when we have 10% error in wind forecast.

Figure 3-7 shows the P_{set} with and without 10% error in solar forecast obtained from Figure 1-1 (a); and Figure 3-8 shows the required BESS power and energy ratings i.e., $P_{bess,ref}$ and $E_{bess,ideal}$ for these two P_{set} s.

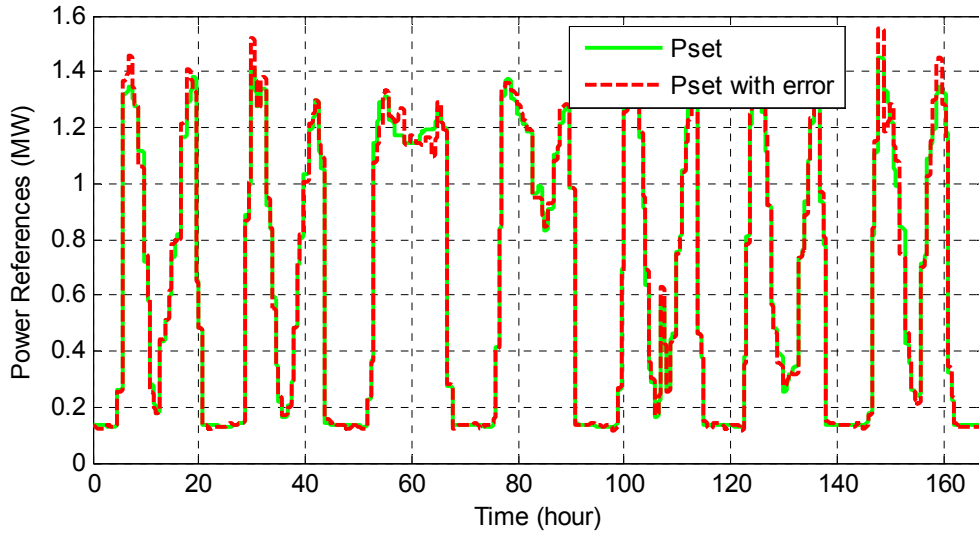
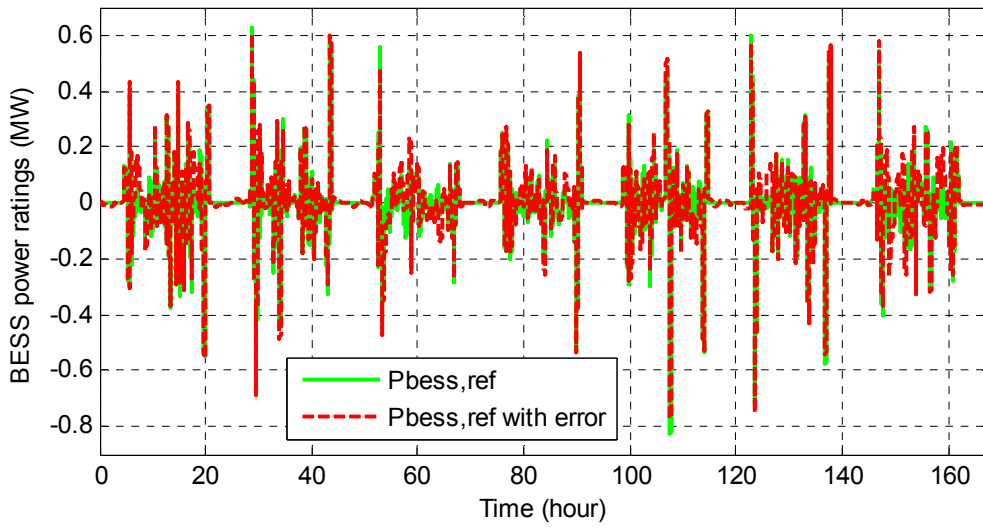
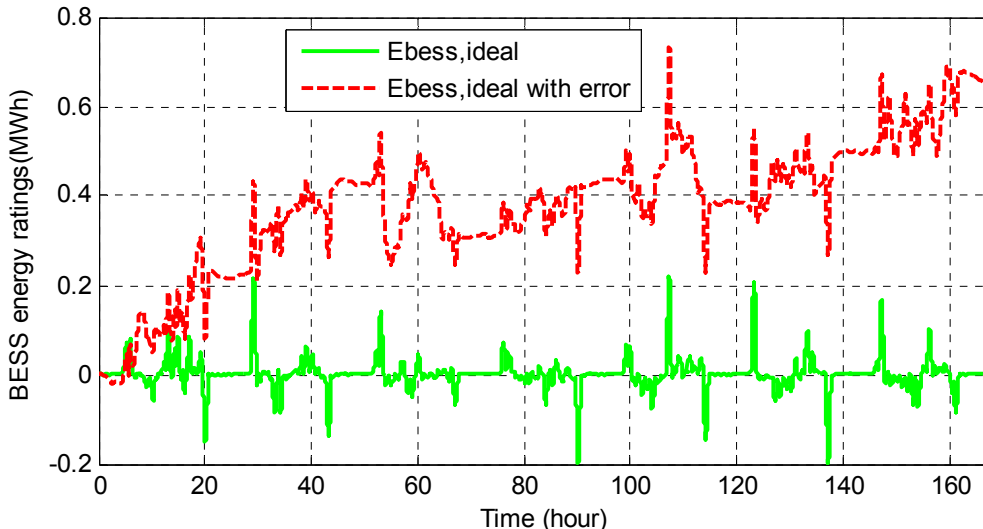


Figure 3-7: P_{set} with and without 10% error for solar



(a)



(b)

Figure 3-8: Power and energy ratings for ideal BESS (a) $P_{bess,ref} = P_{set} - P_{solar}$ (in megawatts) (b) Energy required for dispatch $E_{bess,ideal}$ (in megawatthours)

It is seen from Figure 3-8 that we need a converter size of ± 0.9 MW and a minimum BESS size of 0.5 MWh (i.e. 30% of the PV system capacity) if we forecast solar power with no error, a converter size of ± 0.8 MW and a minimum BESS size of 0.8 MWh (i.e. 53% of the wind farm capacity) when we have 10% error in solar forecast.

As we obtained the required sizes for an hourly dispatch, now we can focus on the second challenge which is ramp rate limiting. For ramp rate limiting, we want:

$$RDRL \leq P_{set}(t) - P_{set}(t-1) \leq RURL \quad (3-9)$$

where $RDRL$ and $RURL$ are ramp down rate limit and ramp up rate limit, respectively. In order to limit ramp up and ramp down rates, we can modify the P_{set} and add a ramp limiter to its output. Figure 3-9 shows the new P_{set} with and without 10% error in wind power forecast obtained from Figure 1-1 (b) with a $RDRL$ and a $RURL$ of $-1\text{MW}/\text{min}$ and $+1\text{MW}/\text{min}$, respectively. Figure 3-10 shows the required BESS power and energy ratings i.e., $P_{bess,ref}$ and $E_{bess,ideal}$ for these two new P_{set} s.

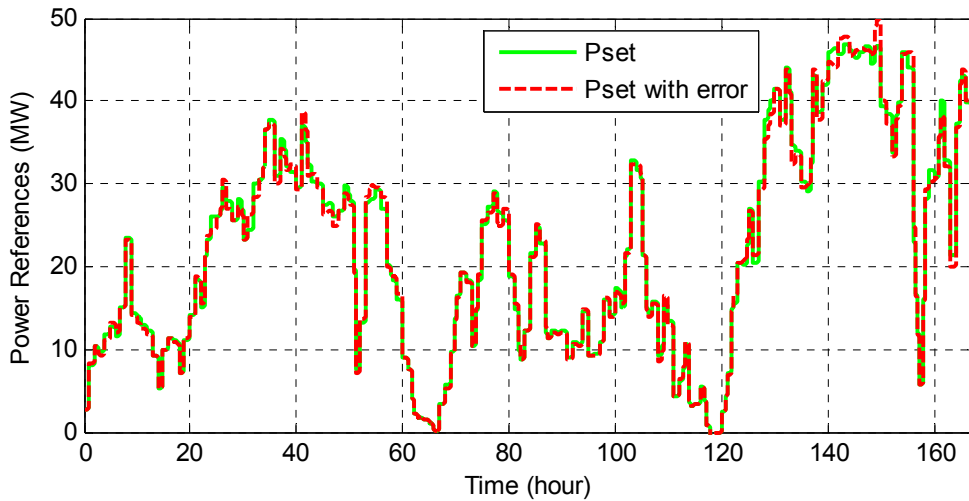
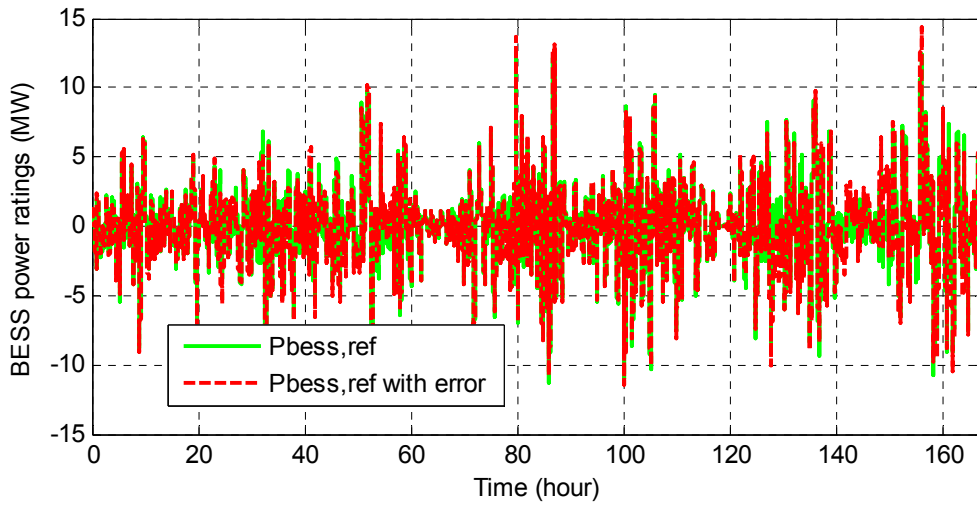
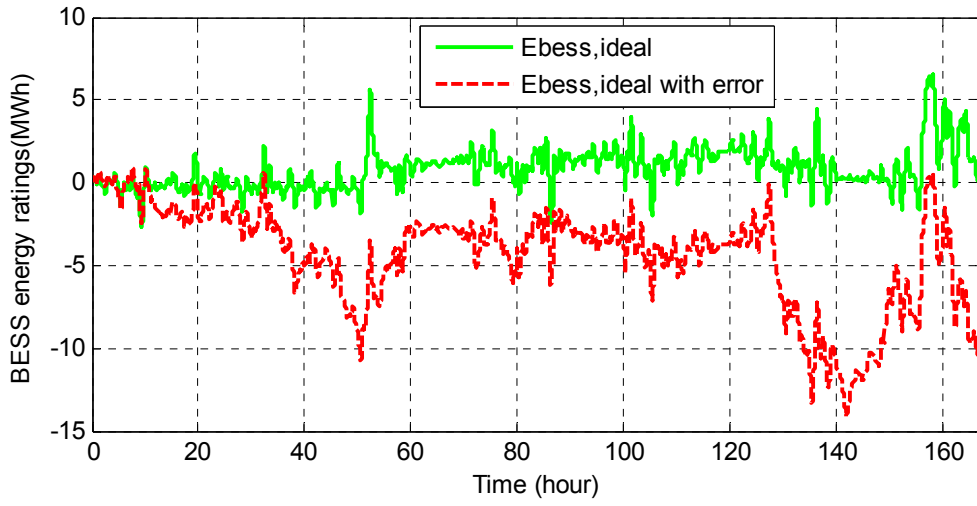


Figure 3-9: P_{set} incorporating $RDRL$ and $RURL$ with and without 10% error for wind



(a)



(b)

Figure 3-10: Power and energy ratings for ideal BESS (a) $P_{bess,ref} = P_{set} - P_{wind}$ (in megawatts) (b) Energy required for dispatch $E_{bess,ideal}$ (in megawatthours)

It is seen from Figure 3-10 that we need a converter size of ± 13 MW and a minimum BESS size of 10 MWh if we forecast wind power with no error, a converter size of ± 15 MW and a minimum BESS size of 15 MWh when we have 10% error in wind forecast for a wind farm with 50 MW capacity.

Figure 3-11 shows the new P_{set} with and without 10% error in solar power forecast obtained from Figure 1-1 (a) with a RDRL and a RURL of $-0.03\text{MW}/\text{min}$ and $+0.03\text{MW}/\text{min}$, respectively. Figure 3-12 shows the required BESS power and energy ratings i.e., $P_{bess,ref}$ and $E_{bess,ideal}$ for these two P_{set} s.

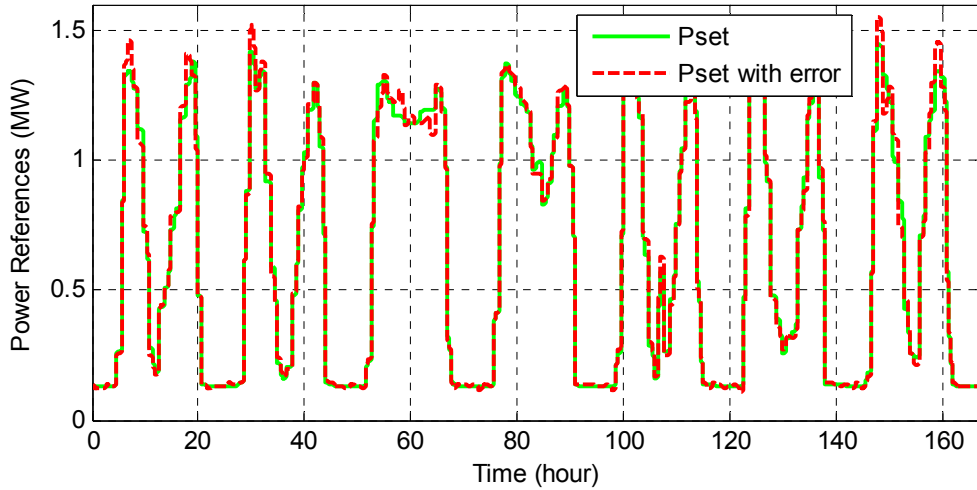
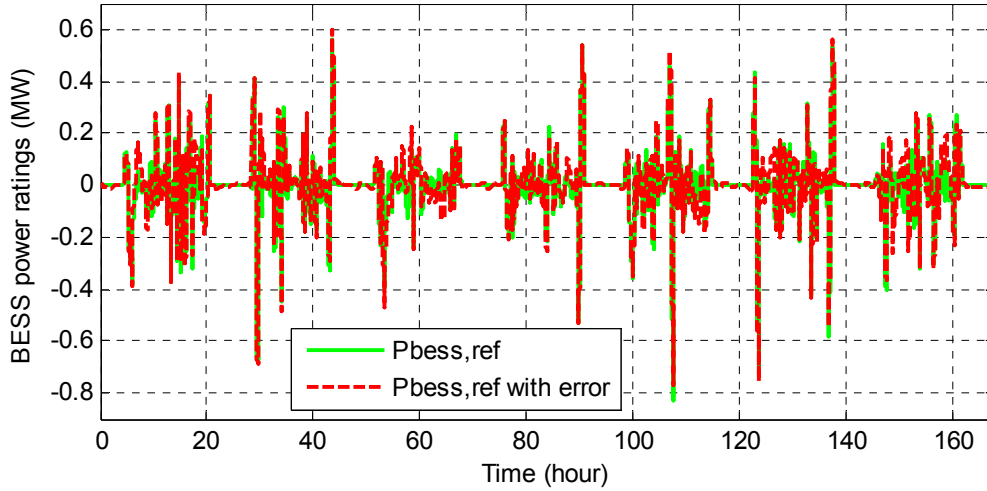
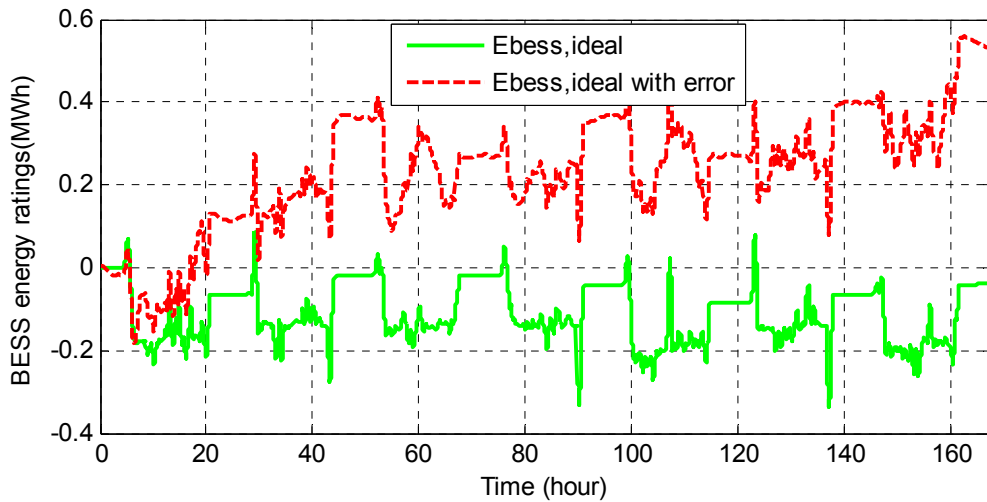


Figure 3-11: P_{set} incorporating RDRL and RURL with and without 10% error for solar



(a)



(b)

Figure 3-12: Power and energy ratings for ideal BESS (a) $P_{bess,ref} = P_{set} - P_{solar}$ (in megawatts) (b) Energy required for dispatch $E_{bess,ideal}$ (in megawatthours)

It is seen from Figure 3-12 that we need a converter size of ± 0.9 MW and a minimum BESS size of 0.5 MWh if we forecast solar power with no error, a converter size of ± 0.8 MW and a minimum BESS size of 0.8 MWh when we have 10% error in solar forecast for a solar PV system with 1.5 MW peak output.

To prevent congestion on the transmission lines that carry the wind farm/solar PV system power when the power generation is high, we need to utilize the BESS in order to limit total power flow such that:

$$P_{set} \leq P_{set,UL} \quad (3-10)$$

where $P_{set,UL}$ is the upper limit selected to prevent congestion. In order to incorporate this constraint, an upper limit can be placed after P_{set} which ensures that there is no overloading on the lines. Figure 3-13 shows the new P_{set} with and without 10% error in wind forecast obtained from Figure 1-1 (b) while incorporating a RDRL and a RURL of $-1\text{MW}/\text{min}$ and $+1\text{MW}/\text{min}$, respectively and a $P_{set,UL}$ of 90% of wind farm capacity (45MW); and Figure 3-14 shows the required BESS power and energy ratings i.e., $P_{bess,ref}$ and $E_{bess,ideal}$ for these two P_{set} s.

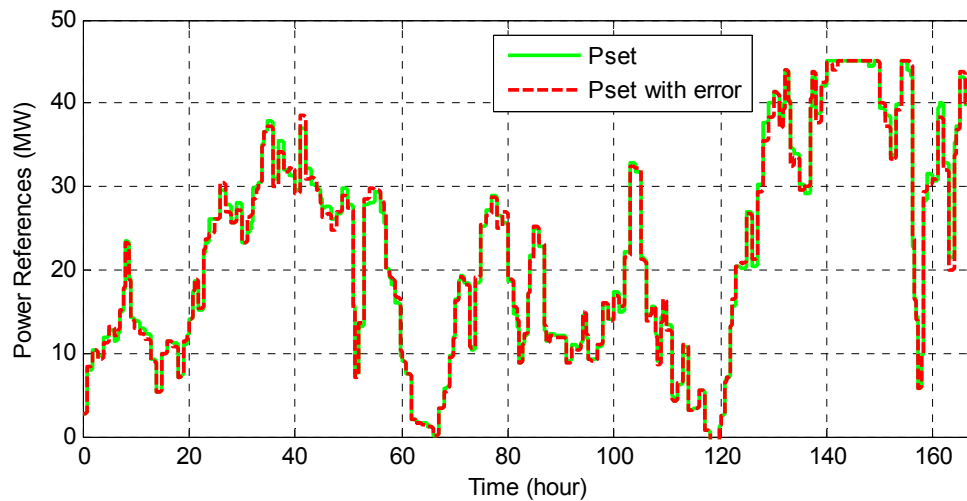
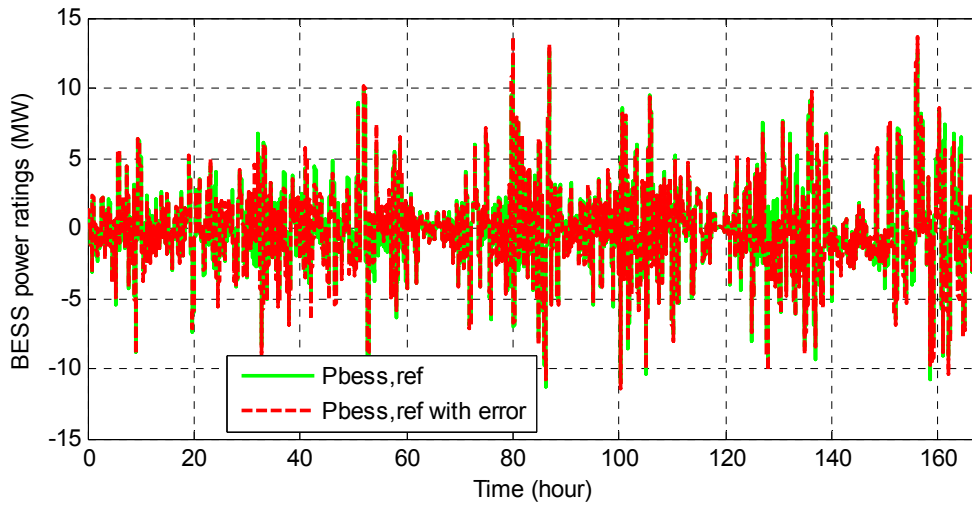
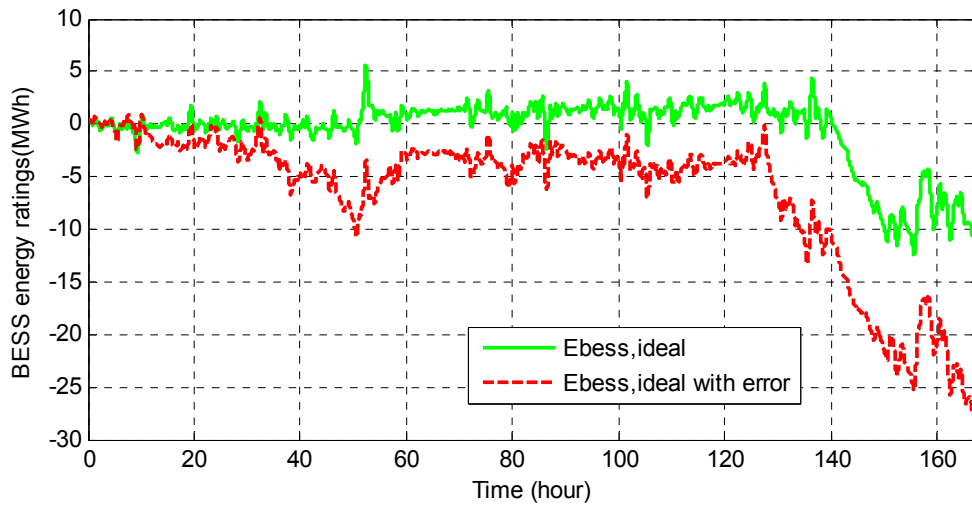


Figure 3-13: P_{set} incorporating RDRL, RURL and $P_{set,UL}$ with and without 10% error for wind



(a)



(b)

Figure 3-14: Power and energy ratings for ideal BESS (a) $P_{bess,ref} = P_{set} - P_{wind}$ (in megawatts) (b) Energy required for dispatch $E_{bess,ideal}$ (in megawatt-hours)

It is seen from Figure 3-14 that we need a converter size of ± 13 MW and a minimum BESS size of 18 MWh if we forecast wind power with no error, a converter size of ± 14 MW and a minimum BESS size of 29 MWh when we have 10% error in wind forecast with the P_{sets} incorporating rate limiters and upper limit.

Figure 3-15 shows the new P_{set} with and without 10% error in solar power forecast obtained from Figure 1-1 (a) while incorporating a RDRL and a RURL of $-0.03\text{MW}/\text{min}$ and $+0.03\text{MW}/\text{min}$, respectively and a $P_{total,UL}$ of 90% of solar PV system peak power (1.35MW); and Figure 3-16 shows the required BESS power and energy ratings i.e., $P_{bess,ref}$ and $E_{bess,ideal}$ for these two P_{set} s.

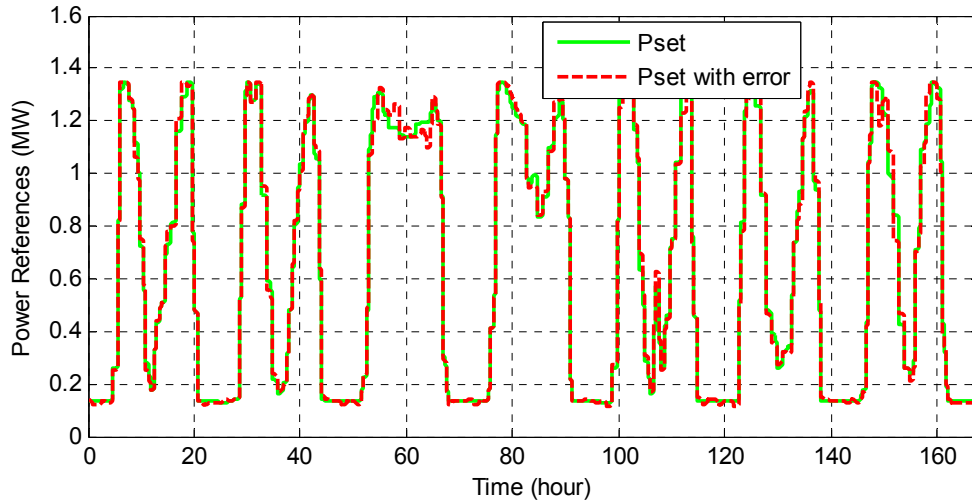
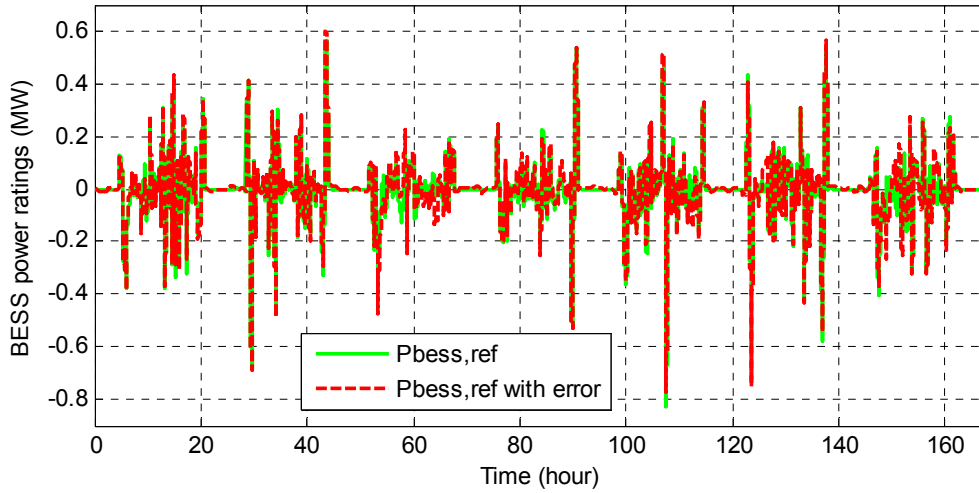
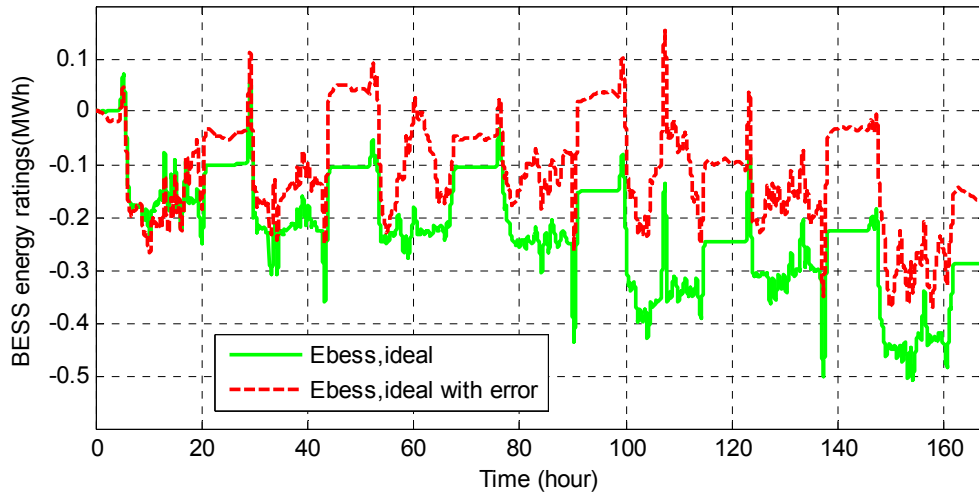


Figure 3-15: P_{set} incorporating RDRL, RURL and $P_{total,UL}$ with and without 10% error for solar



(a)



(b)

Figure 3-16: Power and energy ratings for ideal BESS (a) $P_{bess,ref} = P_{set} - P_{solar}$ (in megawatts) (b) Energy required for dispatch $E_{bess,ideal}$ (in megawatthours)

It is seen from Figure 3-16 that we need a converter size of ± 0.9 MW and a minimum BESS size of 0.6 MWh if we forecast solar power with no error, a converter size of ± 0.8 MW and a minimum BESS size of 0.6 MWh when we have 10% error in solar forecast with the P_{sets} incorporating rate limiters and upper limit.

The summary of the results are shown in Table 3.2:

Table 3.2: Required BESS size for different P_{set} s

Application		Hourly Dispatch	Hourly Dispatch + RL	Hourly Dispatch + RL + $P_{total,UL}$
Wind Farm (50 MW Capacity)	Required energy rating with no error in P_{set} (MWh)	8	10	18
	Required energy rating with 10% error in P_{set} (MWh)	17	15	29
	Required power rating with no error in P_{set} (MW)	17	13	13
	Required power rating with 10% error in P_{set} (MW)	18	15	14
Solar PV System (1.5 MW peak output)	Required energy rating with no error in P_{set} (MWh)	0.5	0.5	0.6
	Required energy rating with 10% error in P_{set} (MWh)	0.8	0.8	0.6
	Required power rating with no error in P_{set} (MW)	0.9	0.9	0.9
	Required power rating with 10% error in P_{set} (MW)	0.8	0.8	0.8

By observing Table 3.2, it is seen that the ratio of the required BESS energy and power rating to the renewable energy peak output power is higher for solar case compared to the wind case. Hence, this requires bigger size of BESS system in order to dispatch solar energy. Moreover, if it is desired to limit the power output the wind farm during high generation this will also drastically increase the required BESS energy and power rating.

From these results, it can also be concluded that the BESS charge/discharge period typically varies between 5 min to 25 min for these applications and the charge/discharge for BESS occurs both daytime and nighttime for wind case; however, for solar case, the charge/discharge for BESS mostly occurs during the daytime only since there is not generation in the night.

4. Proposed Methods

From the results of the previous chapter, it is seen that the required BESS energy and power rating for dispatching is higher than 30% of the capacity of the wind farm/solar PV system. Since the cost of the BESS is proportional to the size of the BESS, using these required high BESS sizes for perfect dispatch becomes economically unfeasible and hence necessitates the use of a smaller BESS size. Moreover, even if we try to use the required BESS size, we also need to consider the challenges with the BESS mentioned before such as limiting SOC, preventing deep discharge and preventing to exceed converter power limits.

Because of the aforementioned economical and practical challenges with the BESS, there is a need for designing a controller for BESS so that BESS can be utilized in an optimum way for dispatching while its SOC, charge/discharge current stay within its limits during operation.

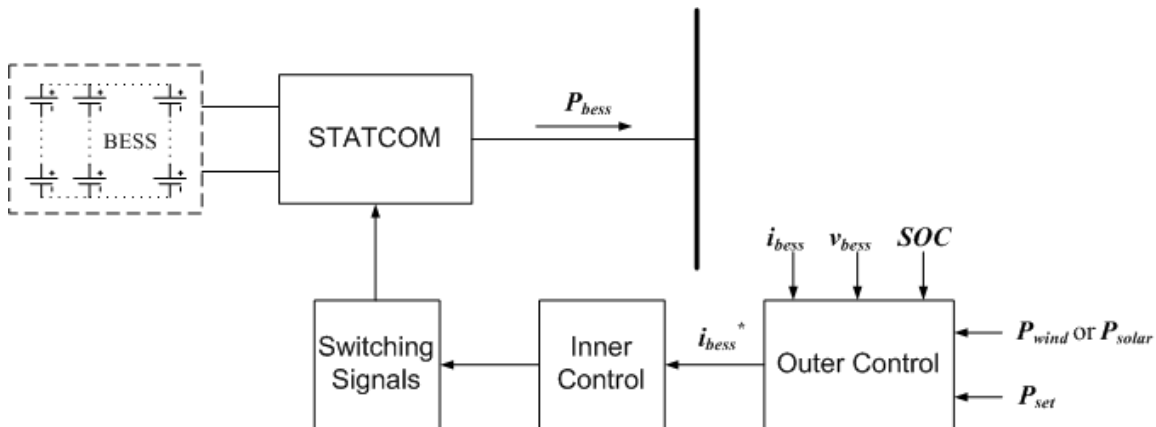


Figure 4-1: Overall control block diagram

The overall control block diagram for the BESS and converter is shown in Figure 4-1. It is seen that the power converter is replaced by STATCOM so that reactive power compensation can also be provided. Moreover, we can see that the controller has two

loops, the outer used for generating reference charge/discharge current i_{bess}^* , and the inner used for generating switching signals for the switches in STATCOM which will control the power flow.

In order the controller to perform properly, it requires several signals such as current (i_{bess}), voltage (v_{bess}) and SOC of the BESS. The voltage and current can be obtained by using voltage and current sensors; the SOC can be obtained by using power management integrated circuits. Moreover, the reference input to the controller is P_{set} which is the hourly dispatch set point as explained in the previous chapter. P_{wind} or P_{solar} can be seen as a disturbance input since we don't have any control on either and they will be used to calculate the reference power that needs to be absorbed/injected by BESS. Using this controller scheme, three novel control algorithms for the outer loop are developed.

4.1 SOC Feedback [4]

The first control scheme developed for the outer loop is based on the controller design of [31] which uses the SOC as a feedback signal in order to keep the SOC of the battery within proper limits. This basic control scheme which uses a washout filter for smoothing intermittent renewable energy source power output, however, needs to be modified in order to work for hourly dispatching and also address the constraints of BESS as pointed out in the previous chapter. Figure 4-2 shows the proposed control scheme.

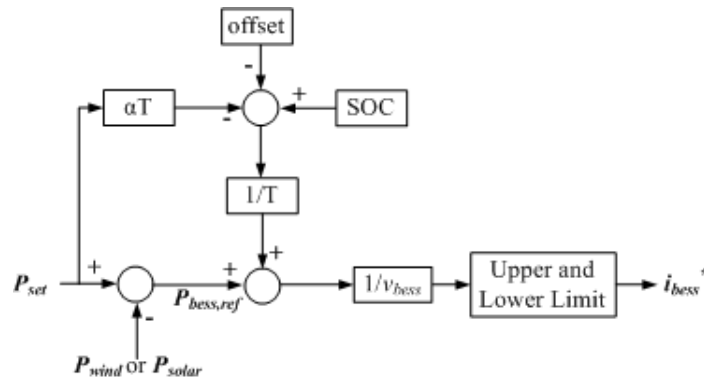


Figure 4-2: SOC feedback method

As Figure 4-2 shows, the inputs to the outer loop controller are P_{set} which can be selected as hourly dispatch or hourly dispatch plus rate limiter or hourly dispatch plus rate limiter plus upper limit as described in the previous chapter and P_{wind} or P_{solar} depending on the application. Using these inputs, $P_{bess,ref}$ i.e. the power that BESS should compensate is obtained by subtracting the disturbance input P_{wind} or P_{solar} from the desired set point P_{set} .

After this, the SOC feedback signal is added to $P_{bess,ref}$ in order to ensure that SOC stays within proper limits. In order to get the SOC feedback signal, the 3rd order battery model shown in Figure 3-3 is used. In this feedback loop, $offset = M.C$ (where C is the BESS capacity in MWh and M is SOC margin rate), and $\alpha = (C - 2.C.M)/(T.P_{WF})$ (where P_{WF} is the rated output of the wind farm or solar PV system in MW). Hence, the design parameters for the controller are smoothing time constant, T and SOC margin rate, M .

In this controller, the smoothing time constant, T and SOC margin rate, M are determined by using the guidelines given in [31]. The guidelines suggest a time constant of $T \leq C/P_{WF}$ for smoothing case but since our case is for dispatchability, this formula may not be optimal; hence, T needs to be tuned depending on the size of the BESS. The SOC margin rate, M , is selected as 0.3 in order to keep SOC of the BESS within 30%-70% as recommended in [31].

Finally, a gain block of $1/v_{bess}$ is used to get the current reference signal from the power reference, i.e. $P_{bess,ref} = v_{bess} \times i_{bess}^*$, and an upper and lower limit block is employed immediately after that to ensure that the output of the outer loop controller, i_{bess}^* , i.e. the reference charge/discharge current that BESS should provide stays within proper current limits of the BESS.

4.1.1 Simulation Setup

Power system computer-aided design (PSCAD)/ electromagnetic transients including dc (EMTDC) is used in order to verify the effectiveness of the proposed control method and two different cases, one with PV system and storage; the other with wind farm and storage are simulated. During the simulations in PSCAD, the actual solar and wind power data is used for P_{solar} and P_{wind} (Figure 1-1 (a) and (b) respectively) and the setup shown in Figure 3-1 is realized.

It is assumed that the converter (i.e. STATCOM) can follow the current reference coming from the SOC feedback control perfectly and hence it is represented as a gain block of 0.97 (i.e. 3 % loss) since its time constant (i.e. ms) is an order of magnitude lower than the average battery charge/discharge time (i.e. min) for this application.

The next step was to select the size of the BESS and to design it accordingly. For this purpose, preliminary study with different BESS sizes were carried out and 300 kWh (300 kW 1 hour discharge) BESS is selected for the case with solar and 10 MWh (10 MW 1 hour discharge) BESS is chosen for the wind case.

To realize the 300 kWh BESS with the lead acid batteries described in chapter 3, it is assumed that the converter DC side has a voltage of 600V and to reach that voltage level we need to connect 282 of the lead acid batteries of 2.135 Volt in series. These number of batteries will also provide us roughly the required energy rating of 300 kWh.

For the realization of 10 MWh BESS, the DC side voltage is selected to be 2 kV for the converter and to reach that voltage level, we need to connect 937 of the lead acid batteries in series to get the desired voltage, and connect 10 of these series strings in parallel to obtain the desired energy rating which results in a total number of 9370 batteries.

During the simulations, it is assumed that each of these batteries contributes the same amount of current and the current limits in the upper and lower limit block are selected as $\pm 500\text{A}$ for the batteries.

The set point P_{set} is selected as hourly dispatch reference which is obtained by taking the actual next hour average of P_{wind} for wind case and P_{solar} for the solar case and adding 10% noise to it as mentioned before in chapter 3.

The smoothing time constant, T is selected to be 0.19 hour for the wind case and 0.25 hour for the solar case.

Using this setup, one week long simulations were made in PSCAD/EMTDC with a time step of 1 sec.

4.1.2 Simulation Results

The results with 10 MWh BESS connected to 50 MW wind farms are presented first. Figure 4-3 shows the P_{set} , P_{wind} and the net power injected $P_{total} = P_{wind} + P_{bess}$ for one day zoom-in of the weekly long simulation. It is seen that the total injected power follows the desired set points occasionally; however, large deviations occur time to time which is not desired.

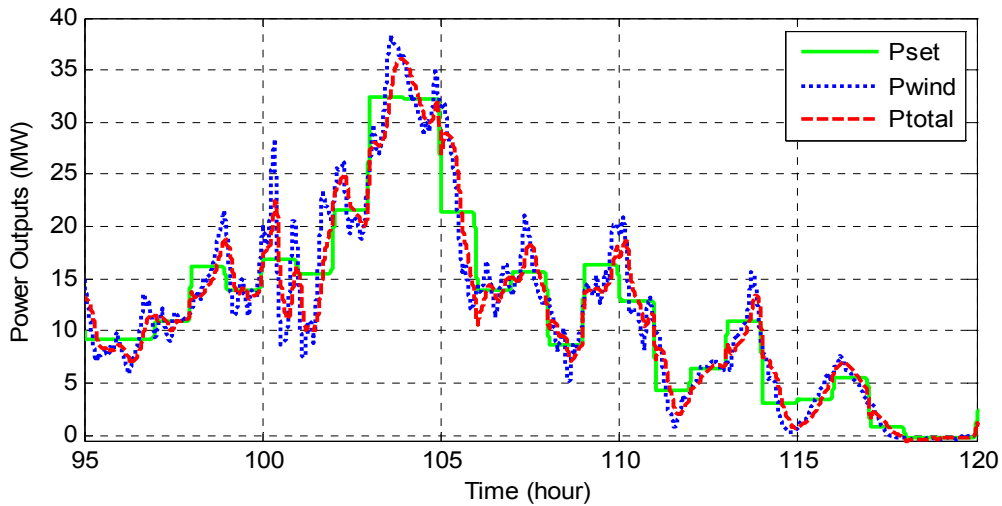
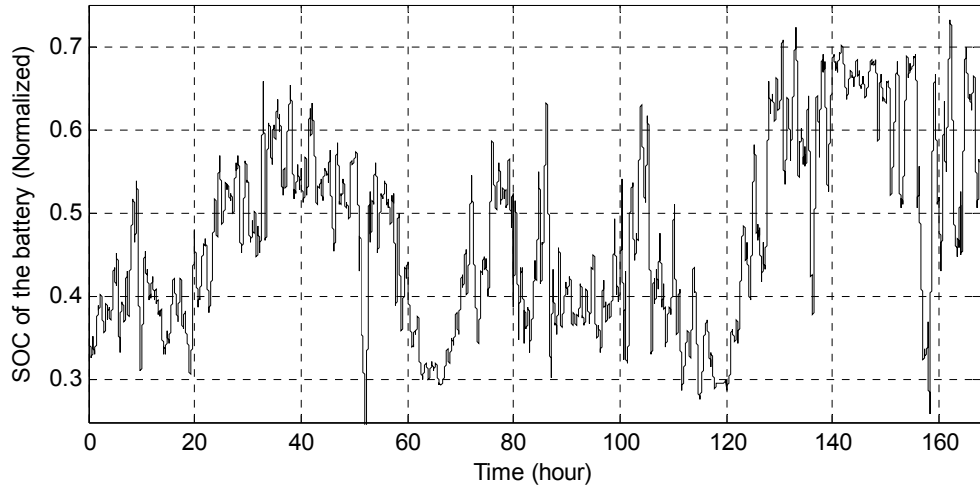


Figure 4-3: Dispatching of wind farm power with BESS; P_{set} : desired set point, P_{wind} : wind power, P_{total} : net injected power (in megawatts)

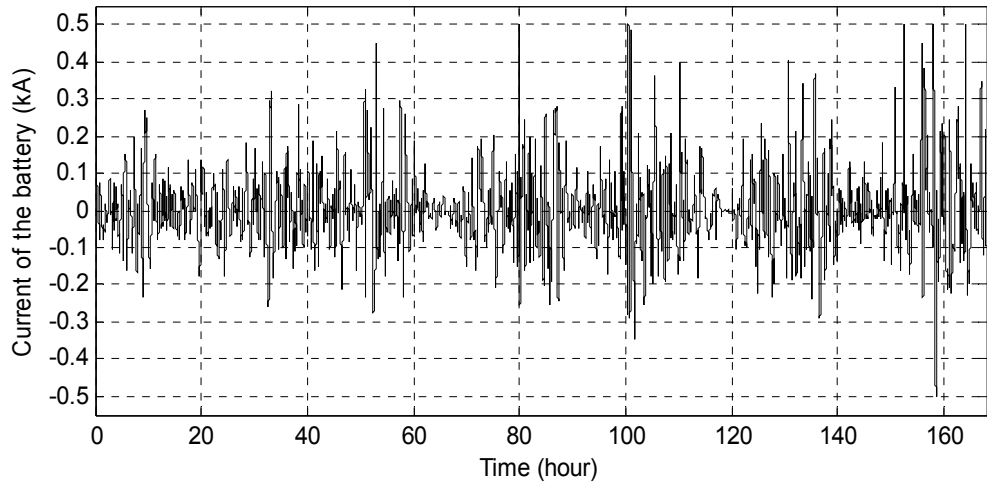
The 10 MWh BESS performance is seen in Figure 4-4. Figure 4-4 (a) shows that the SOC of the battery is kept between 30% - 70% most of the time as desired. The current profile of the battery in Figure 4-4 (b) indicates the charge/discharge current levels and cycle frequency. This figure points out that the maximum charge/discharge current is 500 A as set before, which is the 1C discharge rate of the lead acid battery considered. The figure also shows that the charge/discharge cycle is approximately every 20 min; but most of the time charging/discharging is partial and shallow. Figure 4-4 (c) shows that SOC feedback control also helps to keep the battery voltage within acceptable limits (+10/-15 % of rated voltage) during the weekly period. The power output profile of the BESS in Figure 4-4 (d) indicates that the output of the BESS is limited to ± 10 MW as desired.

Note that, by limiting the SOC to be between 30% and 70%, the deep discharge/charge cycles have been minimized in order to extend the lifetime of the battery. Hence, the new lead acid batteries with extended life cycles, or new type batteries such as flow or NaS with high discharge cycling capability [21] are feasible candidates for this application.

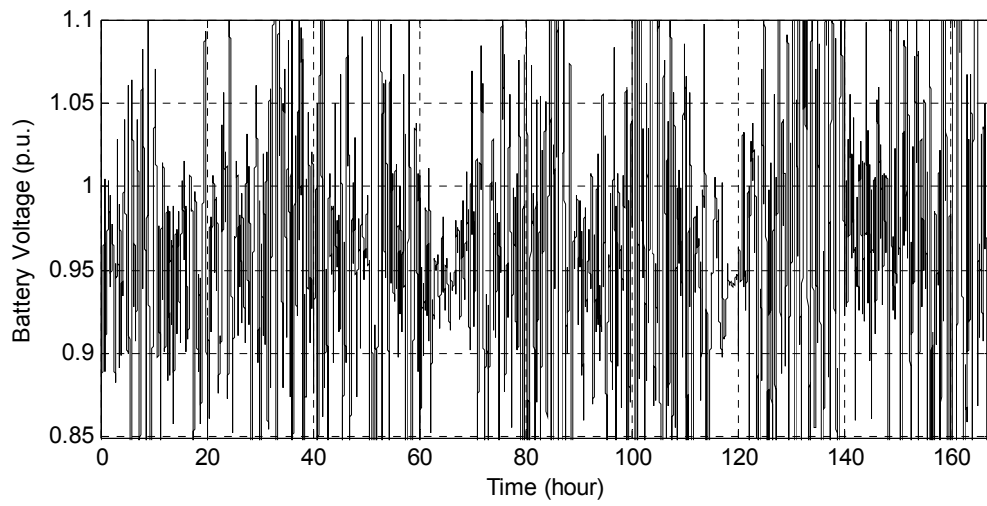
Figure 4-4: 10 MWh BESS performance. (a) State of charge of one battery. (b) Current profile of one battery (kA). (c) DC link voltage (p.u.). (d) Power injected by the BESS (MW)



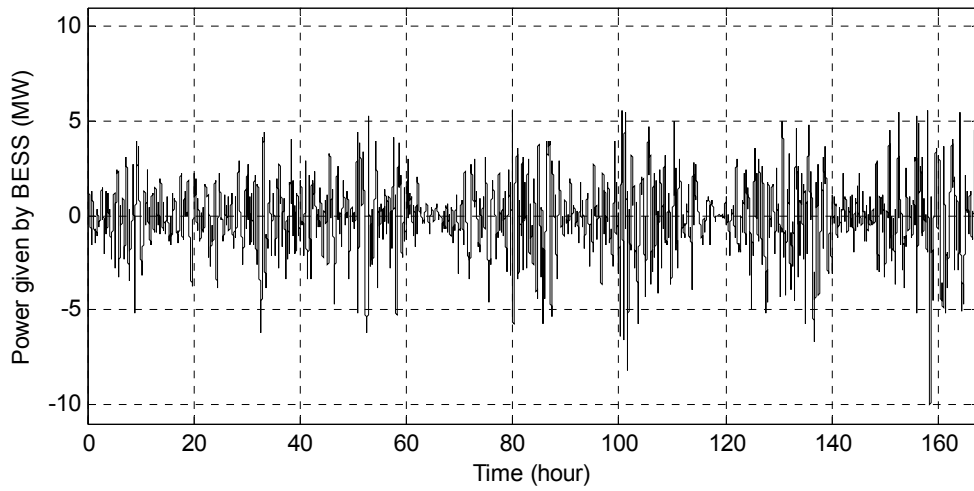
(a)



(b)

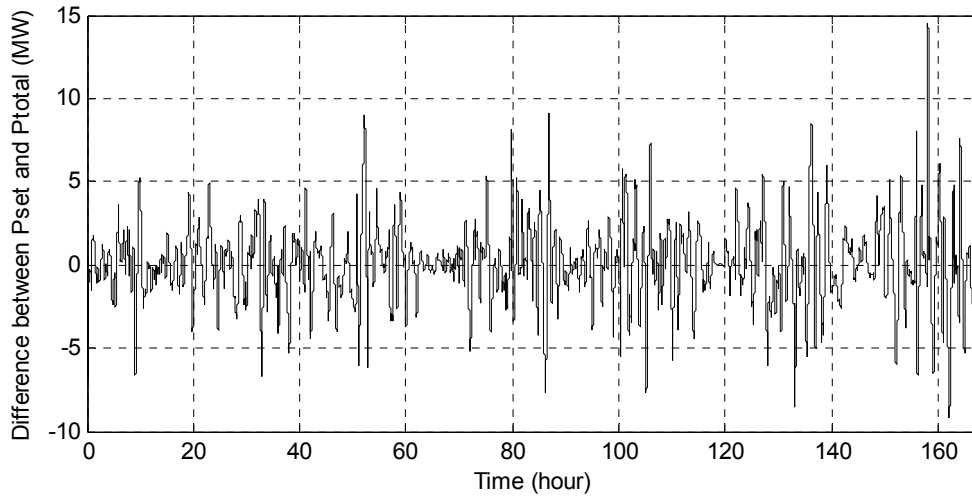


(c)

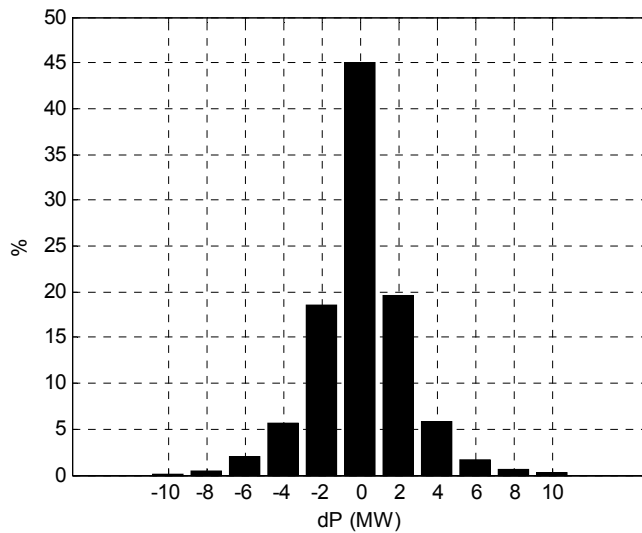


(d)

To assess the effectiveness of dispatchability provided by the BESS, the difference between the total output and the desired set points is determined. This difference $dP = P_{set} - P_{total}$ is given in Figure 4-5 (a), and Figure 4-5 (b) shows the corresponding histogram. As these figures indicate, although most of the time the deviations are within ± 3 MW, larger deviations do occur occasionally.



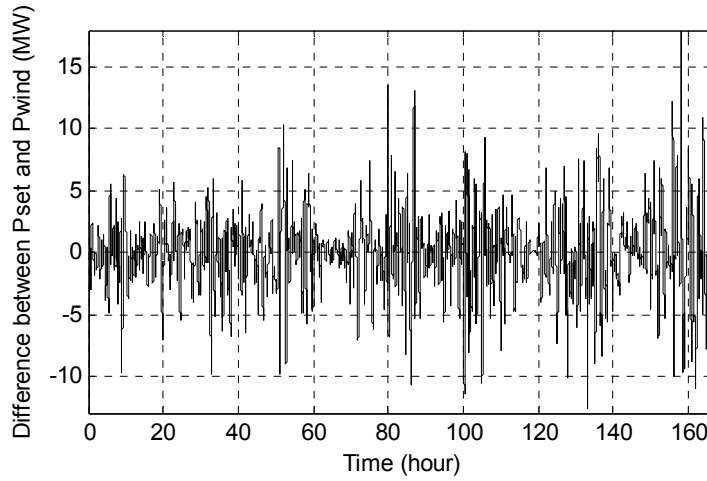
(a)



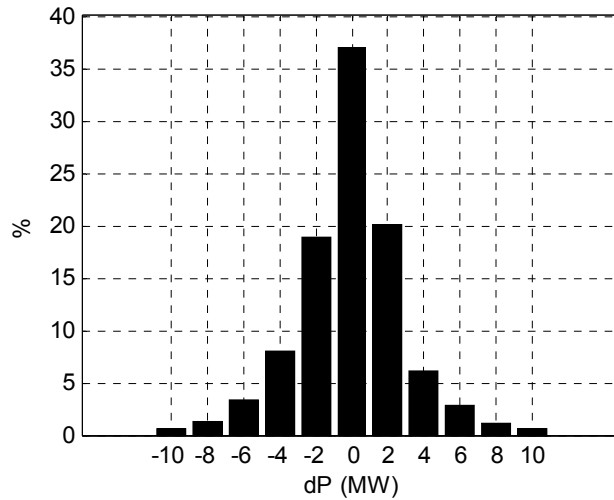
(b)

Figure 4-5: Power deviations in net power supplied P_{total} around the desired set point P_{set} with 10 MWh BESS. (a) Power deviations $dP = P_{set} - P_{total}$ (in megawatts). (b) Histogram of power deviations (%)

To analyze improvement obtained with the BESS integration furthermore, the power deviations can be compared with the case without BESS. The result without BESS is given in Figure 4-6.



(a)



(b)

Figure 4-6: Power deviations in the power supplied P_{wind} around the desired set point P_{set} without BESS. (a) Power deviations = $P_{set} - P_{wind}$ (in megawatts). (b) Histogram of power deviations (%)

Assuming that the deviations up to ± 3 MW are acceptable, it is seen that with 10 MWh BESS, we can reduce the undesired deviations from 24% (Figure 4-6 (b)) to 16.7% (Figure 4-5 (b)).

The results with 300 kWh BESS connected to a solar PV system of 1.5 MW peak output are presented next. Figure 4-7 shows the P_{set} , P_{solar} and the net power injected $P_{total} = P_{solar} + P_{bess}$ for one day zoom-in of the weekly long simulation. It is seen that the SOC feedback control method shows poor performance with the solar case and total injected power follows the desired set points rarely and large deviations do occur especially during the daytime when solar PV output peaks which is not desired.

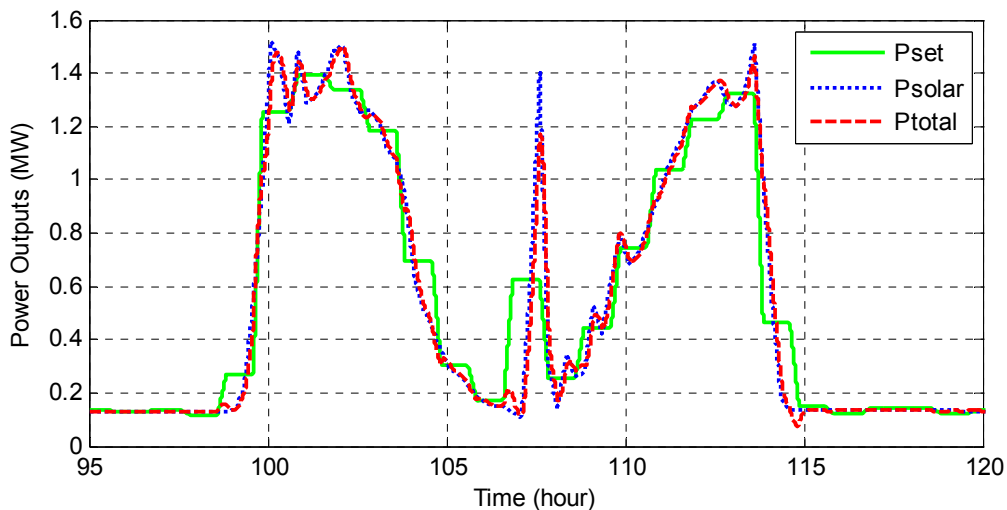


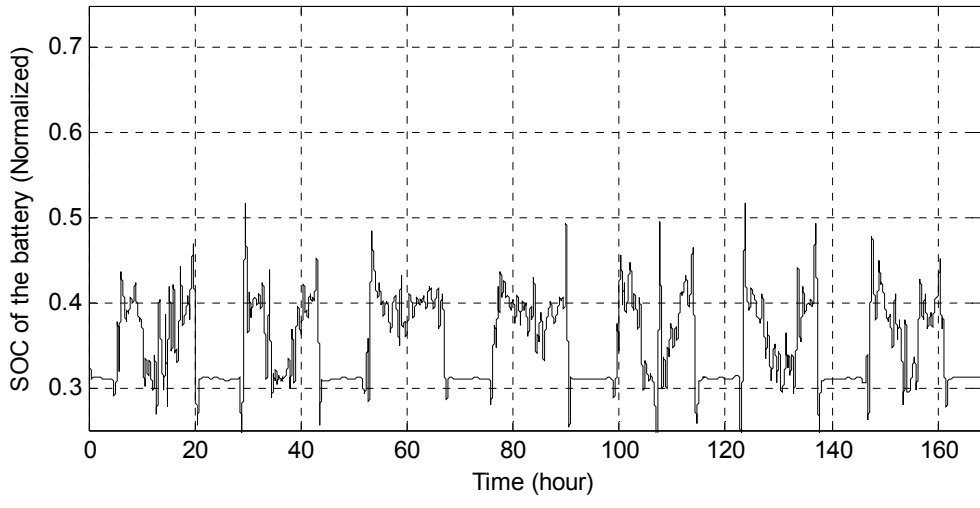
Figure 4-7: Dispatching of solar PV power with BESS; P_{set} : desired set point, P_{solar} : solar power, P_{total} : net injected power (in megawatts)

The 300 kWh BESS performance is seen in Figure 4-8. Figure 4-8 (a) shows that the SOC of the battery is kept within 30% - 50% most of the time and changes in a similar fashion to the solar PV power output. The current profile of the battery in Figure 4-8 (b) indicates the charge/discharge current levels and cycle frequency. This figure points out that the current stays within ± 500 A. The figure also shows that the charge/discharge

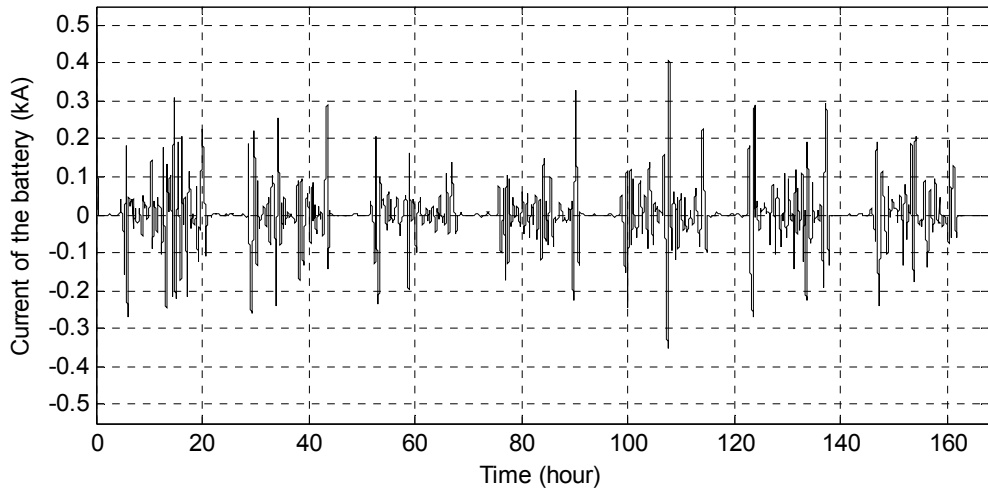
cycle is approximately every 20 min; but most of the time charging/discharging is partial, shallow and occurs during the daytime only. Figure 4-8 (c) shows that SOC feedback control also helps to keep the battery voltage within acceptable limits (+10/-15 % of rated voltage) during the weekly period. The power output profile of the BESS in Figure 4-8 (d) indicates that the output of the BESS is limited to ± 300 kW as desired.

Note that, by limiting the SOC to be between 30% and 70% similar to the wind case, the deep discharge/charge cycles have been minimized in order to extend the lifetime of the battery.

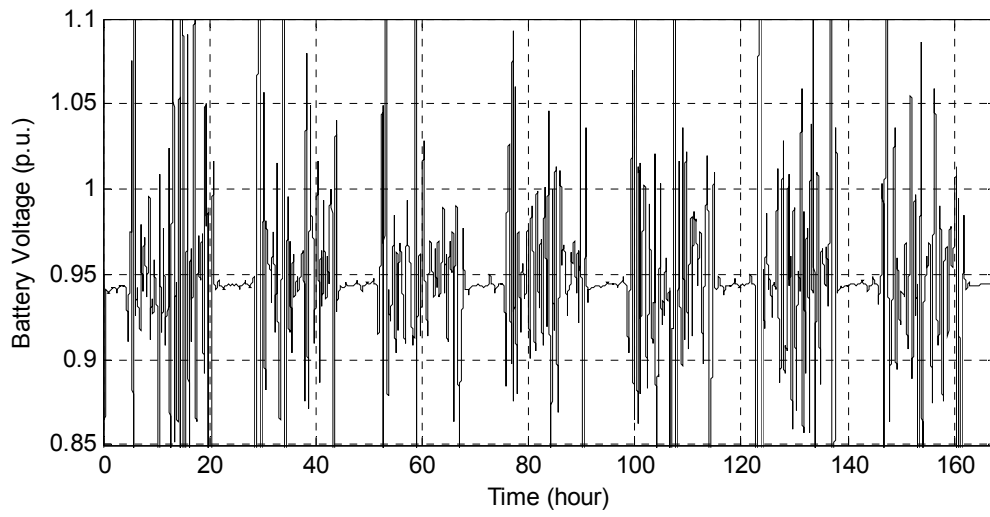
Figure 4-8: 300 kWh BESS performance. (a) State of charge of one battery. (b) Current profile of one battery (kA). (c) DC link voltage (p.u.). (d) Power injected by the BESS (kW)



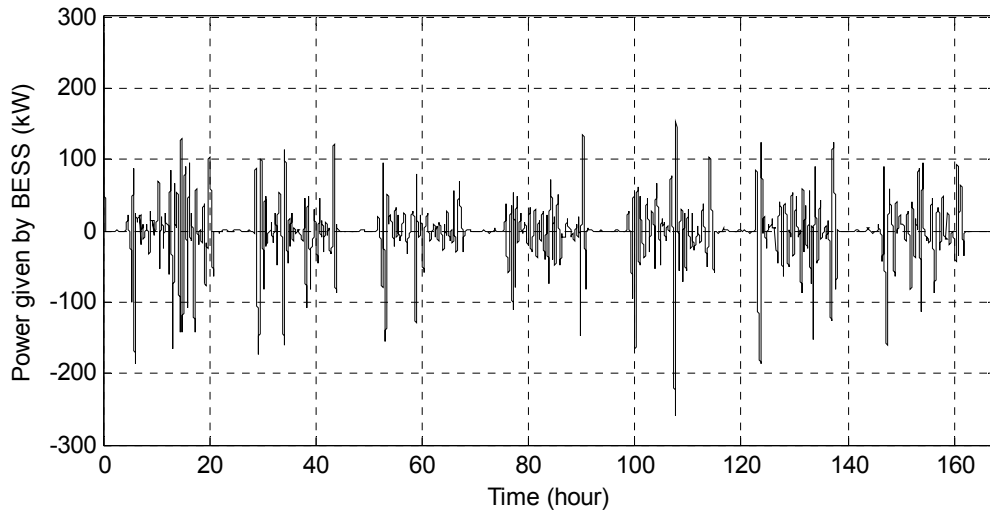
(a)



(b)

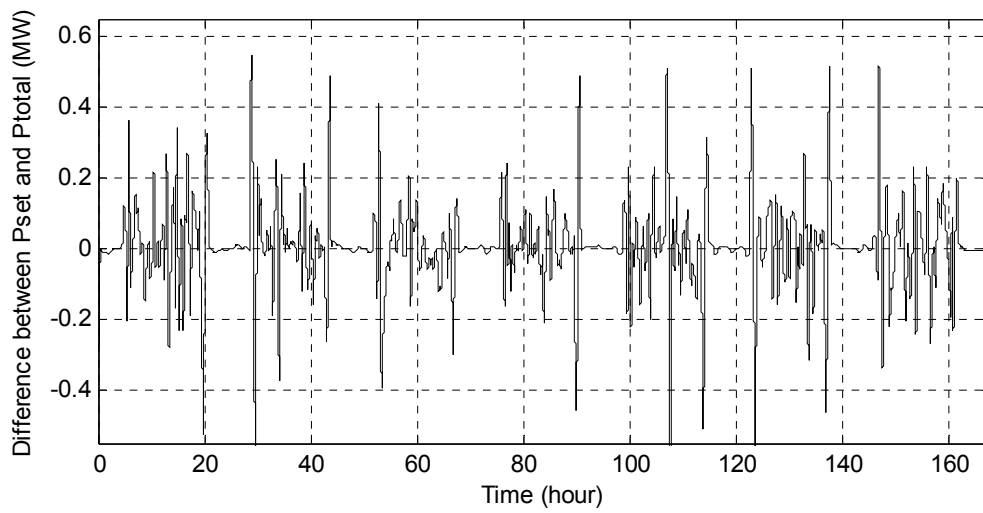


(c)

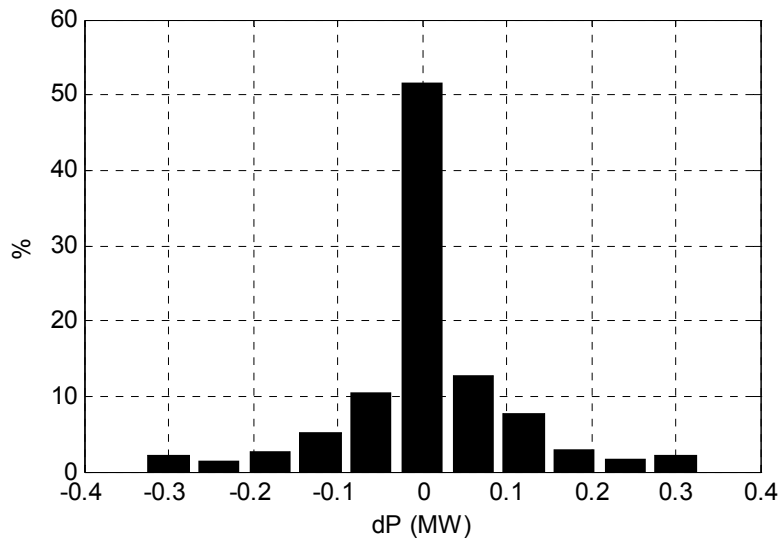


(d)

To assess the effectiveness of dispatchability provided by the BESS, the difference between the total output and the desired set points is determined for solar case, too. This difference $dP = P_{set} - P_{total}$ is given in Figure 4-9 (a), and Figure 4-9 (b) shows the corresponding histogram. As these figures indicate, larger deviations as high as 0.5 MW do occur occasionally.



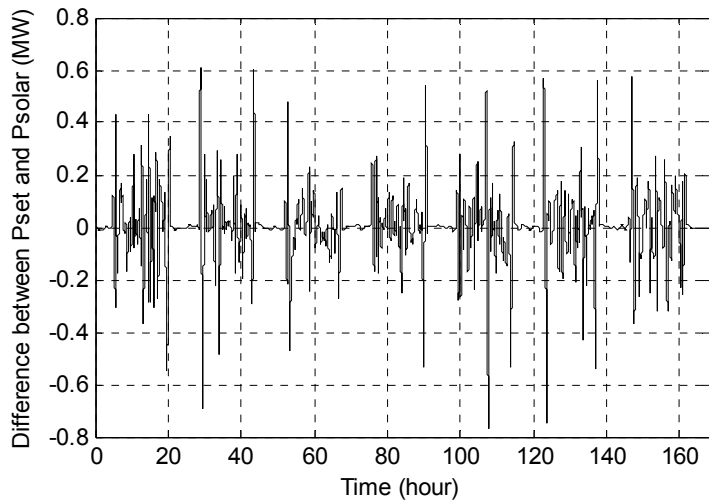
(a)



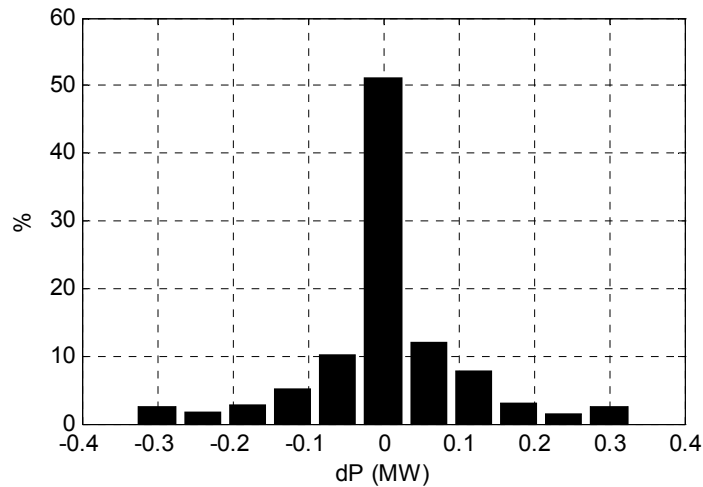
(b)

Figure 4-9: Power deviations in net power supplied P_{total} around the desired set point P_{set} with 300 kWh BESS. (a) Power deviations $dP = P_{set} - P_{total}$ (in megawatts). (b) Histogram of power deviations (%)

To analyze improvement obtained with the BESS integration furthermore, the power deviations can be compared with the case without BESS. The result without BESS is given in Figure 4-10.



(a)



(b)

Figure 4-10: Power deviations in the power supplied P_{solar} around the desired set point P_{set} without BESS. (a) Power deviations = $P_{set} - P_{solar}$ (in megawatts). (b) Histogram of power deviations (%)

Assuming that the deviations up to ± 0.09 MW are acceptable, it is seen that with 300 kWh BESS, we can reduce the undesired deviations from 27% (Figure 4-10 (b)) to only 25.4% (Figure 4-9 (b)).

From the results of the two cases with solar and wind, it is seen that the BESS charge/discharge frequency is relatively high for these applications especially for wind, and hence new type of batteries with high charge/discharge cycling rates would be needed for this application.

The control strategy considered makes a compromise in that it limits the full utilization of the BESS capacity in order to extend the lifetime of the BESS. Hence, as the results show, we need a large size BESS –about 20-30% of the wind farm/ solar PV capacity – to have an effective and smooth dispatch profile. Moreover, even if the control method is easy to implement and doesn't require much computation time, it is seen that the undesired deviations from the hourly dispatch set points was still higher than 10% and the controller showed very poor performance especially for the solar case. Because of this insufficient performance obtained with SOC feedback method and not being an optimum control method, a new method is developed which will be described next.

4.2 Optimal Control

The existence of significant percent of undesired deviations from the hourly dispatch set points with the SOC feedback method and not being sure about how good the method is, i.e. is it the optimal solution or how close it is to the optimal solution, a new method is developed.

Since the problem is to develop a controller to charge/discharge the BESS through converter such that the wind farm/solar PV power output can be dispatched on an hourly basis while considering the SOC, deep discharge limitations of the BESS, it can be formulated as an optimal control problem. The motivation for defining it as an optimal control problem is that there is an objective function which is to minimize the deviations between the wind/solar power and hourly dispatch set points using the BESS and there

are constraints on SOC and discharge current of the battery which has to be satisfied all the time.

Optimal control deals with the problem of finding a control law for a given system such that a certain optimality criterion is achieved. A control problem includes a cost functional that is a function of state and control variables. An optimal control is a set of differential equations describing the paths of the control variables that minimize the cost functional [56].

There are various types of optimal control problems, depending on the performance index, the type of time domain (continuous, discrete), the presence of different types of constraints, and what variables are free to be chosen. The formulation of an optimal control problem requires the following [57]:

- a mathematical model of the system to be controlled
- a specification of the performance index
- a specification of all boundary conditions on states, and constraints to be satisfied by states and controls

Having described what is required for optimal control problem; the next step is to develop the mathematical model of our system which will be the model of the BESS.

Mathematical Model for Optimal Control problem

In order to develop the mathematical model for our problem, the third order battery model shown in Figure 3-3 is used. As the components in this model are nonlinear and current dependent, the model is simplified first to obtain a linear model. For this purpose the following assumptions are made:

- Ignore parasitic branch (I_p is around %0.5 of I_m which is observed from a weekly simulation using the control method proposed in [4])

- All circuit parameters are constant where the values are obtained by taking the average of time varying component values of the third order battery model

The simplified model according to the above assumptions is shown in Figure 4-11.

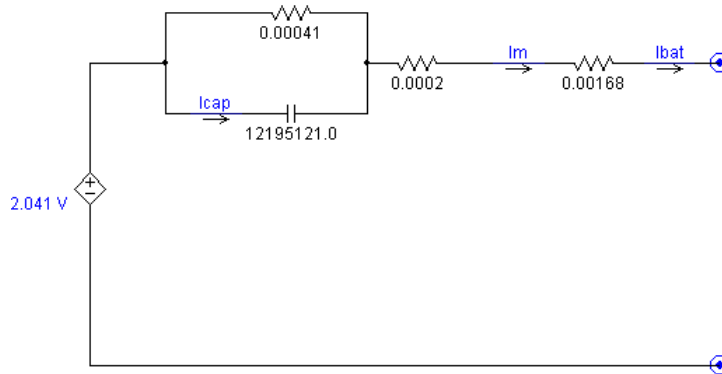


Figure 4-11: Simplified battery model with used circuit parameters

Before writing the equations for the simplified model, the validation of this model is made by comparing it with the third order battery model. For this purpose, the SOC feedback control method is simulated with the two battery models using the wind case and by taking the third order battery model as the base model, the error of the simplified model is obtained.

Figure 4-12 shows the current applied to both battery models. The battery voltage error obtained using the given current profile is shown in Figure 4-13.

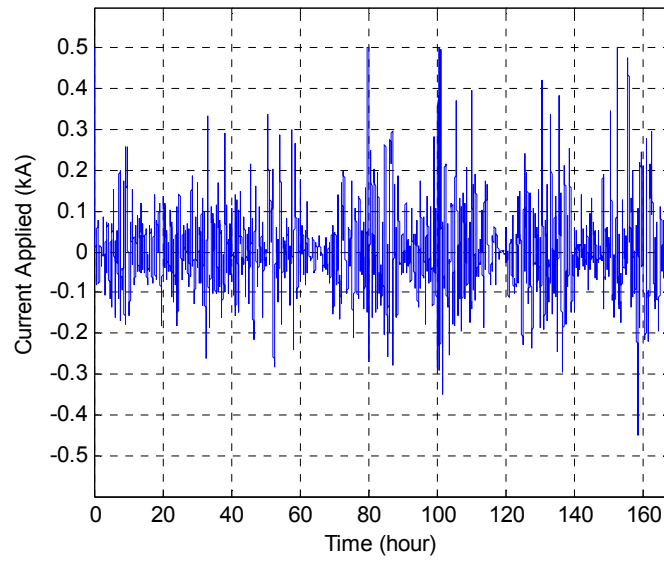


Figure 4-12: Current applied to both battery models (kA)

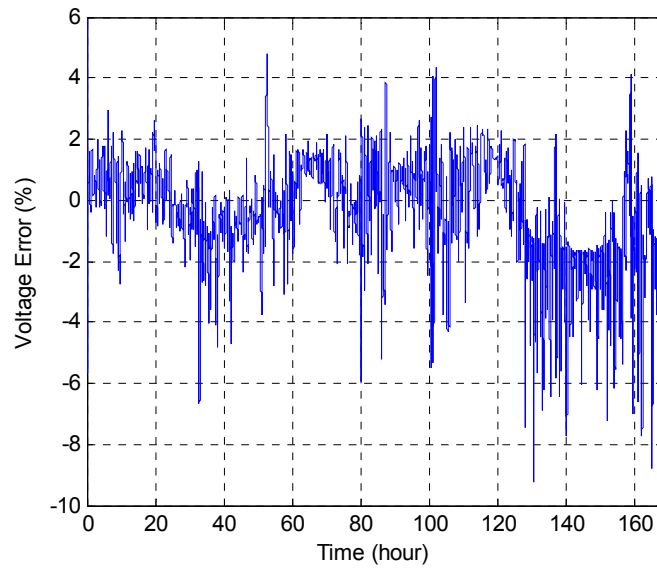


Figure 4-13: Battery voltage error (%)

By observing Figure 4-13, it is seen that the voltage error with the simplified model is between +5/-9 percent. Hence, the simplified battery model is reasonable for the development of the mathematical model for the optimal control problem.

As it is verified that the simplified BESS model is accurate enough; now, the states, control and output can be selected by looking at Figure 4-11:

$$x_1 = I_{cap} \quad (4-1)$$

$$x_2 = I_{bat} \quad (4-2)$$

$$x_3 = \int I_{bat}(t)dt \quad (4-3)$$

$$u = \frac{dI_{bat}}{dt} \quad (4-4)$$

$$y = P_{bess} = R1 \times I_{bat} \times I_{cap} + Em \times I_{bat} - (R0 + R1 + R2)I_{bat}^2 \quad (4-5)$$

Using these selections, in state space form (i.e., $\dot{x} = Ax + Bu$, $y = Cx + Du$) we get:

$$\begin{bmatrix} \dot{x}_1 \\ \dot{x}_2 \\ \dot{x}_3 \end{bmatrix} = \begin{bmatrix} \frac{-1}{\tau_1} & 0 & 0 \\ 0 & 0 & 0 \\ 0 & 1 & 0 \end{bmatrix} \begin{bmatrix} x_1 \\ x_2 \\ x_3 \end{bmatrix} + \begin{bmatrix} 1 \\ 1 \\ 0 \end{bmatrix} u \quad (4-6)$$

$$y = \begin{bmatrix} R1 \times x_2 & Em - (R0 + R1 + R2) \times x_2 & 0 \end{bmatrix} \begin{bmatrix} x_1 \\ x_2 \\ x_3 \end{bmatrix} \quad (4-7)$$

where $\tau_1 = R1 \times C1 = 5000$ and the details of the derivation of the model can be found in Appendix B.

As the standard state space form is obtained, the next step is to check the controllability of the system and from the controllability matrix it is found that the rank is 3 which guarantees that the system is controllable.

Specification of the performance index

Having verified that our system is controllable, the performance index can be specified next. For our problem, it is desired that the battery power follows the reference power that is set by the difference of hourly dispatchable P_{set} and variable P_{wind} or P_{solar} (i.e. $P_{bess,ref} = P_{set} - P_{wind}$ or $P_{bess,ref} = P_{set} - P_{solar}$). Hence, we can write our performance index as a quadratic cost functional of:

$$J(u) = \int_0^t (P_{bess,ref}(t) - P_{bess}(t))^2 dt = \int_0^t (y_{ref}(t) - y(t))^2 dt \quad (4-8)$$

which will penalize the deviations from the battery power reference y_{ref} .

Specification of all boundary conditions on states, and constraints to be satisfied by states and controls

As discussed before, the constraints consist of current of a battery and SOC of a battery. Hence we can write boundary conditions on states, and constraints to be satisfied by states as:

Initial Conditions:

$$x_1(0) = 0 \quad (4-9)$$

$$x_2(0) = 0 \quad (4-10)$$

$$x_3(0) = 0 \quad (4-11)$$

Constraints:

$$i_{max,ch} \leq x_2(t) \leq i_{max,disch} \quad (4-12)$$

$$C \times (1 - SOC_{UL}) - Q_{e_init} \leq x_3(t) \leq C \times (1 - SOC_{LL}) - Q_{e_init} \quad (4-13)$$

where $i_{max,ch}$ and $i_{max,disch}$ are the maximum charge and discharge currents respectively; the limits on x_3 is obtained by the SOC limit, i.e. $SOC_{LL} \leq SOC(t) \leq SOC_{UL}$ where SOC and Q_e are given in equations (3-1) and (3-2). For the lead acid battery model used, a suitable

selection for current limit can be ± 500 A and SOC limits can be selected as $SOC_{LL} = 0.3$, $SOC_{UL} = 1$ (i.e. the battery energy level varies between 30%–100% which is the case for similar applications) to utilize the battery more effectively compared to SOC feedback method.

Optimal Control for BESS

Having defined all the necessary requirements, the optimal control problem for BESS is defined as follows:

“Find an admissible control $u^* \in U[t_0, t_f]$ which satisfies the physical constraints in such a manner that the cost functional $J(u^*)$ has a minimum value.”

Solution of the optimal control problem and real time implementation

The optimal control problem is considered nonlinear and, thus does not have an analytic solution. As a result, it is necessary to employ numerical methods to solve this optimal control problem. Hence, our problem requires numerical methods to solve and needs to be implemented as an open loop optimal control (OLOC). For this open loop control implementation, the duration of the control window, i.e. the control signal period that needs to be applied to the BESS, needs to be selected. For this purpose four different control windows are chosen: 100s, 5 min, 15 min and 30 min. Having selected the control window, it is needed to obtain and input y_{ref} (i.e. the predicted battery power reference obtained by $P_{bess,ref} = P_{set} - P_{wind}$ or $P_{bess,ref} = P_{set} - P_{solar}$) to our cost function continuously. For this purpose it is assumed that we can predict the wind/solar PV power, i.e. P_{wind}/P_{solar} , for each window size duration with a resolution of 100s without error and we can predict the average of the wind/solar PV power, P_{set} , for the next hour with 10% error as mentioned before. Moreover, the points obtained at 100s predictions are concatenated to have continuous y_{ref} .

With these assumptions, the real time implementation of the open loop control will be as follows:

- Update your initial conditions and y_{ref} , and solve the problem
- Obtain the resulting x_2 (battery current) from the optimal control software
- Input x_2 to the converter as current reference for the control window duration, i.e. for the 30 min window solution, charge/discharge BESS through converter according to the current obtained from the optimal control software for half an hour
- Go to first step

While this implementation seems to be acceptable for short window length, it may end up in problems for window lengths of 15 min or more. Since the system will be open loop for the window duration, the actual states will be different from what is expected due to modeling errors and hence limits may be violated at the end of the control period.

In order to overcome the aforementioned challenge resulting from the OLOC, model predictive control (MPC) can be used to implement the real time control of the converter.

The model predictive control scheme makes use of the receding horizon principle such that a finite horizon optimal control problem is solved over a fixed interval of time, the prediction horizon; and the control variable is applied to the process over the control horizon which is generally shorter than prediction horizon [58]. The rest of the predicted control variable is discarded, and at the end of the control horizon the entire procedure is repeated.

Using the idea of receding horizon control, we can change the real time implementation of the OLOC to MPC as follows:

- Update your initial conditions and y_{ref} , and solve your problem for longer prediction horizon (i.e. 30 mins)
- Obtain the resulting x_2 (battery current) from the optimal control software
- Input x_2 to the converter as current reference for the control horizon, i.e. for the 5 min control horizon, charge/discharge BESS through converter according to the current obtained from the optimal control software for 5 min and ignore the rest of the solution
- Go to first step

As can be observed, this MPC implementation will reduce the open loop control period and still use the advantage of the longer prediction window.

4.2.1 Simulation Setup

PSCAD/EMTDC is again used in order to verify the effectiveness of the proposed control method and two different cases, one with PV system and storage, and the other with wind farm and storage are simulated. During the simulations in PSCAD, the actual solar and wind power data is used for P_{solar} and P_{wind} (Figure 1-1 (a) and (b) respectively) and the setup shown in Figure 3-1 is realized similar to the setup used for SOC feedback method.

It is again assumed that the STATCOM can follow the current reference coming from the optimal control perfectly and hence it is represented as a gain block of 0.97 (i.e. 3 % loss).

To solve the optimal control problem, DIDO (Ver. 7.3) [59] is used. In order to solve our optimal problem in DIDO, we just need to code our equations in the corresponding cost, dynamics, events and main function templates of DIDO and insert the numerical values for the circuit parameters and constraints.

During these simulations in PSCAD, the optimal control problem solution obtained from DIDO is used with the simplified BESS model to evaluate the performance of different prediction horizons with a 100 sec control horizon.

The same BESS sizes with the SOC feedback method were selected which were 300 kWh (300 kW 1 hour discharge) for the case with solar and 10 MWh (10 MW 1 hour discharge) for the wind case. Moreover, the same realization with SOC feedback method for the BESS is made to get the required battery number.

During the simulations, it is again assumed that each of these batteries contributes the same amount of current and the current limits are selected as $\pm 500\text{A}$ for the batteries and SOC of the batteries are limited to change between 30% and 100%.

Using this setup, one week long simulations were made in PSCAD/EMTDC with a time step of 1 sec.

4.2.2 Simulation Results

The results with 10 MWh BESS connected to 50 MW wind farms are presented first. Figure 4-14 shows the P_{set} , P_{wind} and the net power injected $P_{total} = P_{wind} + P_{bess}$ with prediction horizon of 30 min for one day zoom-in of the weekly long simulation. It is seen that the total injected power follows the desired set points perfectly most of the time.

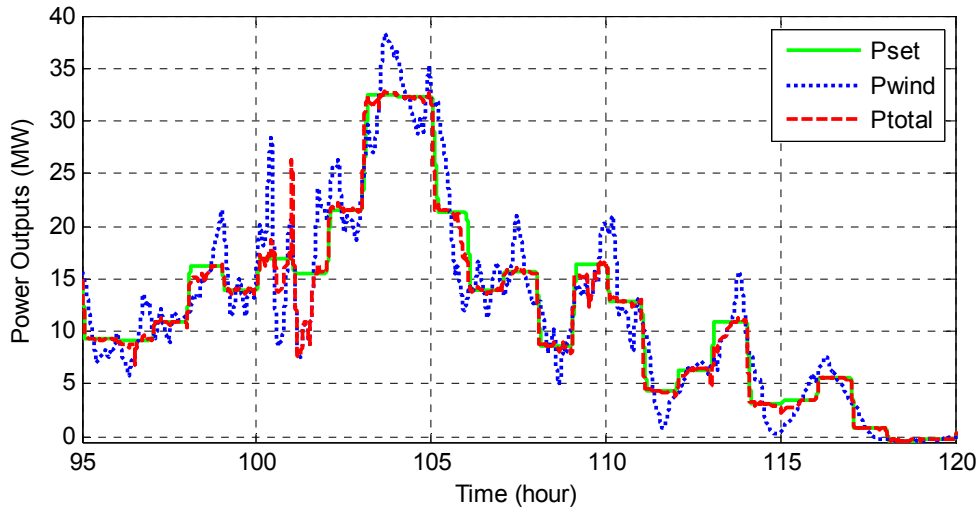
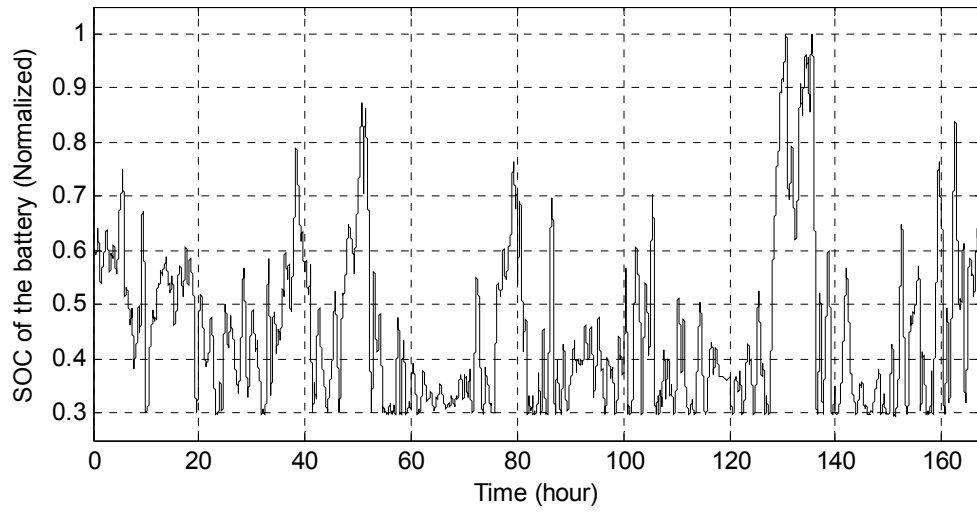


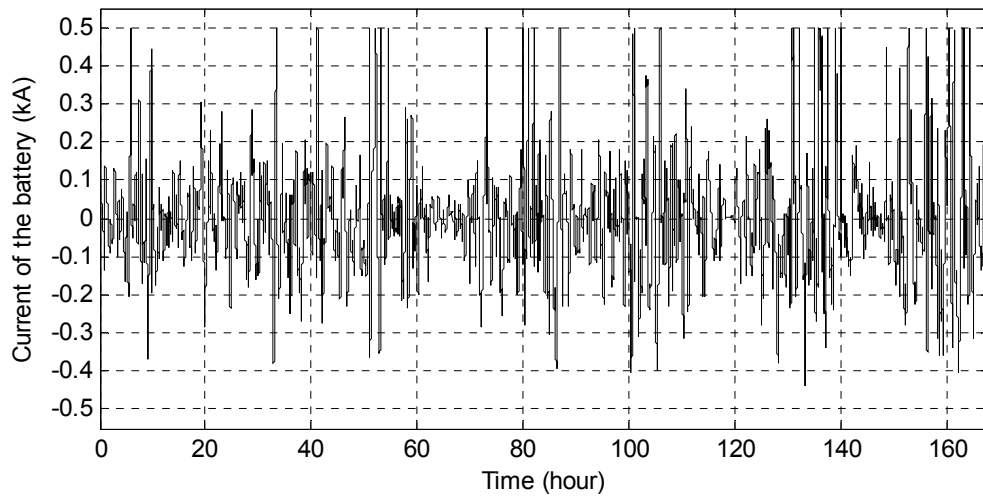
Figure 4-14: Dispatching of wind farm power with BESS; P_{set} : desired set point, P_{wind} : wind power, P_{total} : net injected power (in megawatts) - 30 min prediction window

The 10 MWh BESS performance with 30 min prediction window is seen in Figure 4-15. Figure 4-15 (a) shows that the SOC of the battery is kept between 30% - 100% as limited before. The current profile of the battery in Figure 4-15 (b) indicates the charge/discharge current levels and cycle frequency. This figure points out that the maximum charge/discharge current is 500 A as set before. The figure also shows that the charge/discharge cycle is approximately every 20 min; however, most of the time charging/discharging is partial and shallow. It can also be observed that the current reaches upper limit of 500A several times during the simulation and hence this will lead to increase in the deviations between P_{set} and P_{total} . Figure 4-15 (c) shows that limiting the SOC helps to keep the battery voltage within acceptable limits (+10/-15 % of rated voltage) during the weekly period. The power output profile of the BESS in Figure 4-15 (d) indicates that the output of the BESS is limited to ± 10 MW as desired.

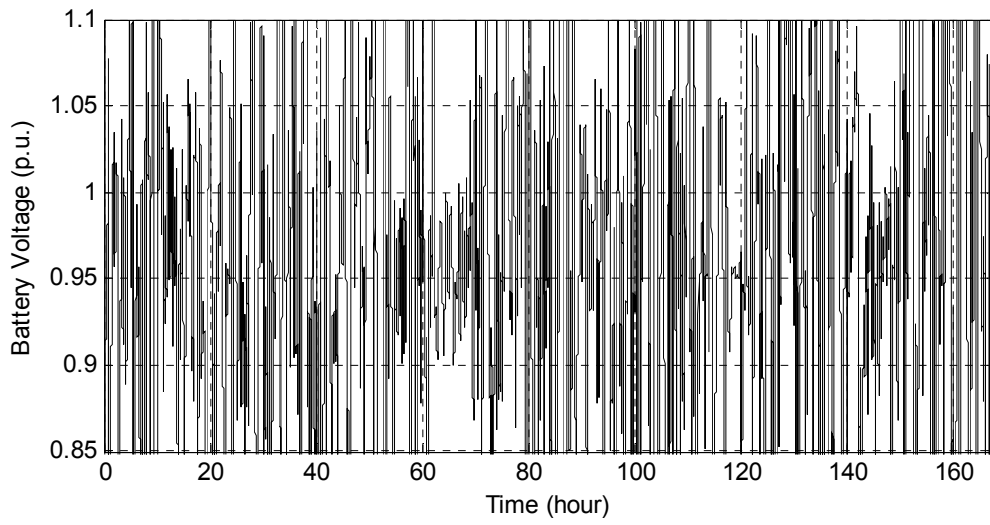
Figure 4-15: 10 MWh BESS performance with 30 min prediction window. (a) State of charge of one battery. (b) Current profile of one battery (kA). (c) DC link voltage (p.u.). (d) Power injected by the BESS (MW)



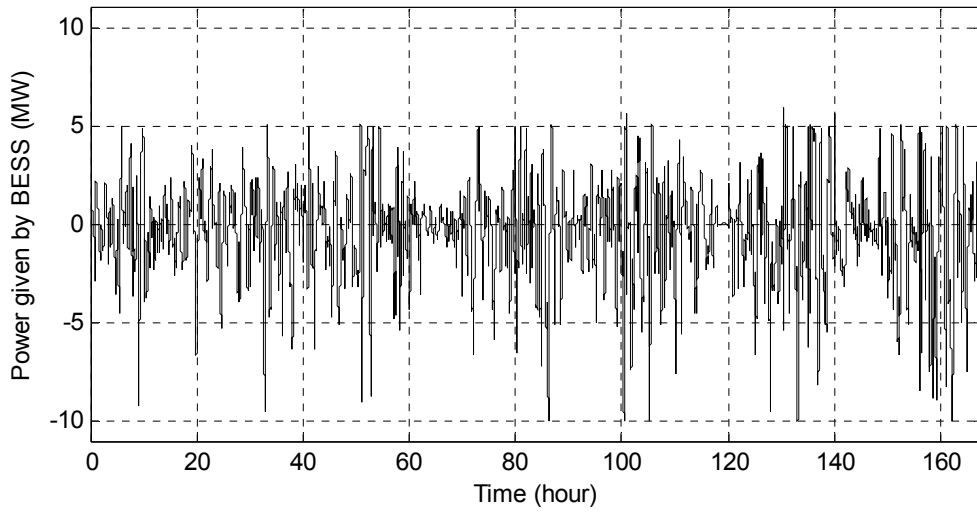
(a)



(b)

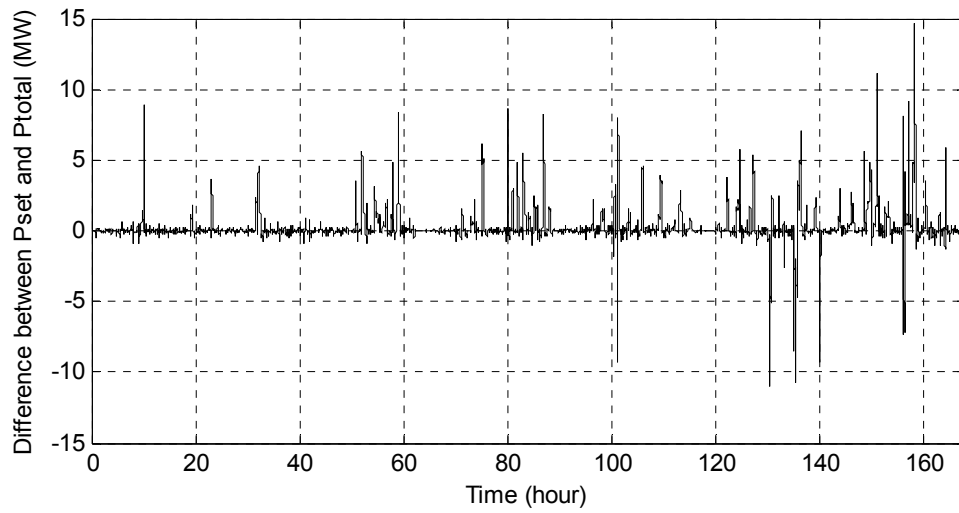


(c)

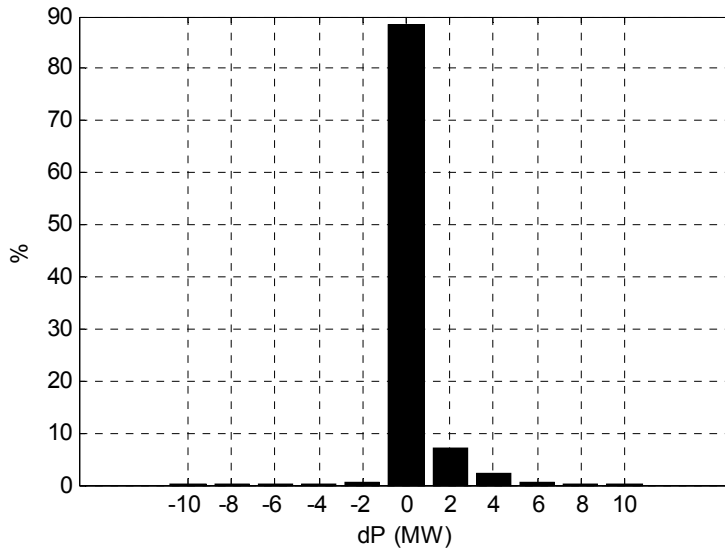


(d)

To assess the effectiveness of dispatchability provided by the BESS, the difference between the total output and the desired set points is determined. This difference $dP = P_{set} - P_{total}$ is given in Figure 4-16 (a), and Figure 4-16 (b) shows the corresponding histogram. As these figures indicate, most of the time the deviations are within ± 3 MW, and with optimal control, larger deviations occur rarely.



(a)



(b)

Figure 4-16: Power deviations in net power supplied P_{total} around the desired set point P_{set} with 10 MWh BESS. (a) Power deviations $dP = P_{set} - P_{total}$ (in megawatts). (b) Histogram of power deviations (%)

To analyze improvement obtained with the BESS integration furthermore, the power deviations can be compared with the case without BESS as done in the SOC feedback method. The result without BESS was shown in Figure 4-6. If we assume again that the deviations up to ± 3 MW are acceptable, it is seen that with 10 MWh BESS, we can

reduce the undesired deviations from 24% (Figure 4-6 (b)) to 3.7% (Figure 4-16 (b)) with the optimal control method having 30 min prediction window.

To see the effect of different prediction window, the simulations are repeated for 100 sec prediction window for the wind case. Figure 4-17 shows the P_{set} , P_{wind} and the net power injected $P_{total} = P_{wind} + P_{bess}$ with prediction horizon of 100 sec for one day zoom-in of the weekly long simulation. It is seen that similar to the 30 min prediction window case the total injected power follows the desired set points perfectly most of the time.

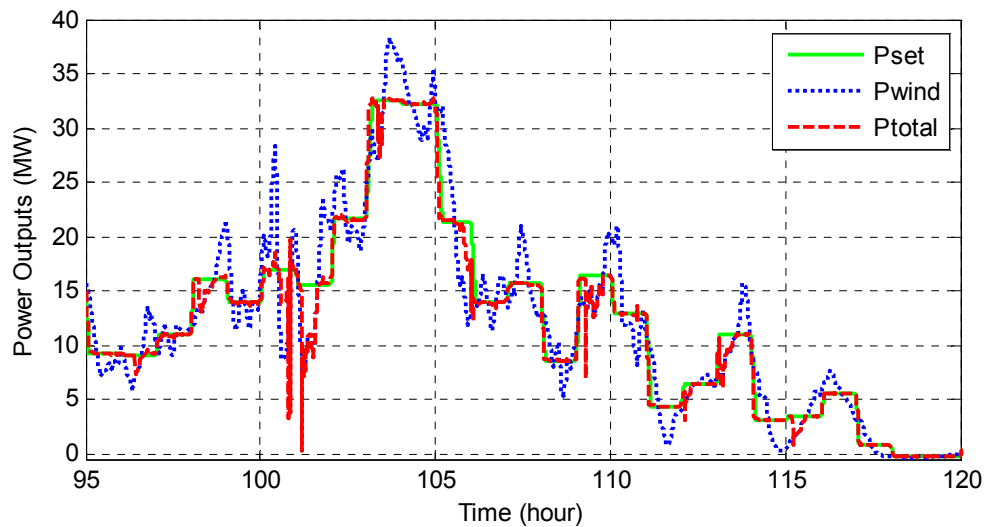
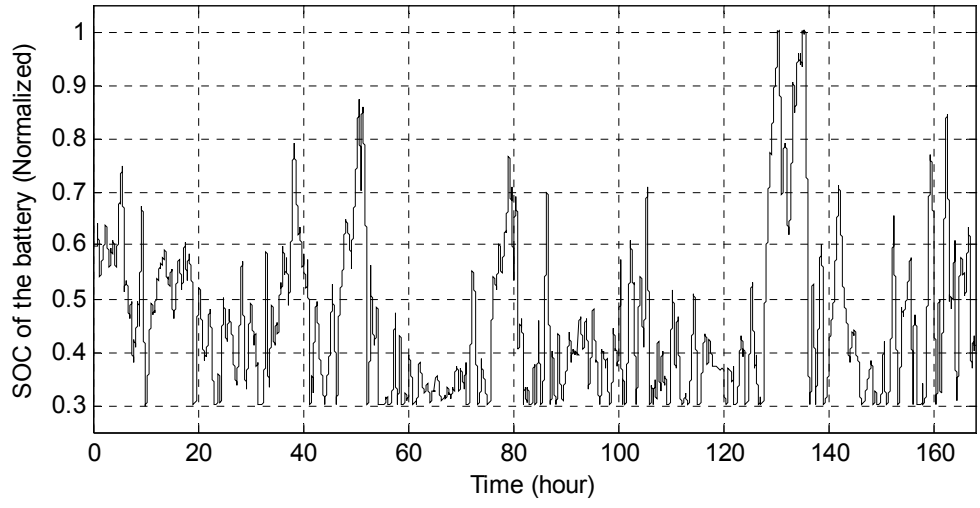


Figure 4-17: Dispatching of wind farm power with BESS; P_{set} : desired set point, P_{wind} : wind power, P_{total} : net injected power (in megawatts) - 100 sec prediction window

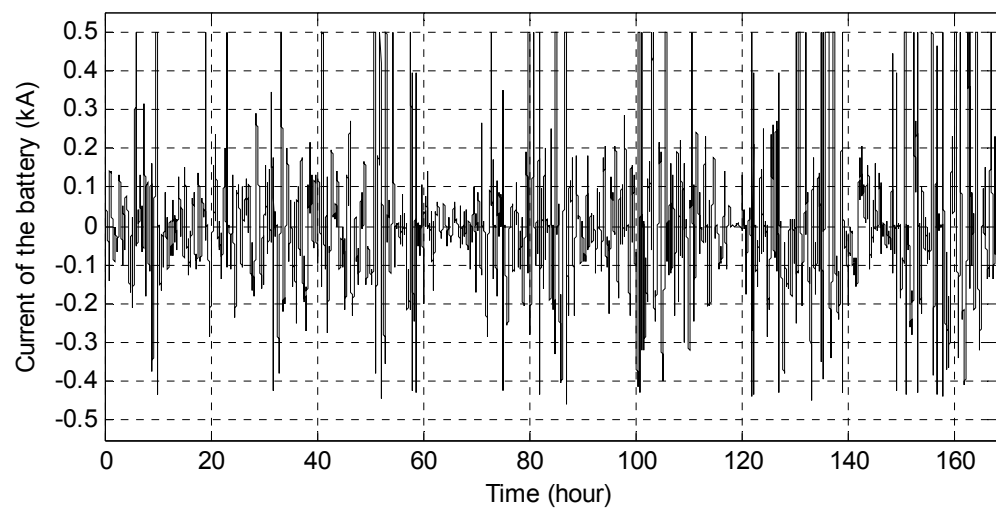
The 10 MWh BESS performance with 100 sec prediction window is seen in Figure 4-18. Figure 4-18 (a) shows that the SOC of the battery is kept between 30% - 100% as set before. The current profile of the battery which is seen in Figure 4-18 (b) has similar behavior compared to the 30 min prediction window case and it is seen that the maximum charge/discharge current is 500 A. The charge/discharge cycle is approximately every 20 min again and most of the time charging/discharging is partial and shallow. Figure 4-18 (c) shows that limiting the SOC helps to keep the battery voltage within acceptable limits

(+10/-15 % of rated voltage) during the weekly period. The power output profile of the BESS in Figure 4-18 (d) indicates that the output of the BESS is limited to ± 10 MW with 100 sec prediction window, too.

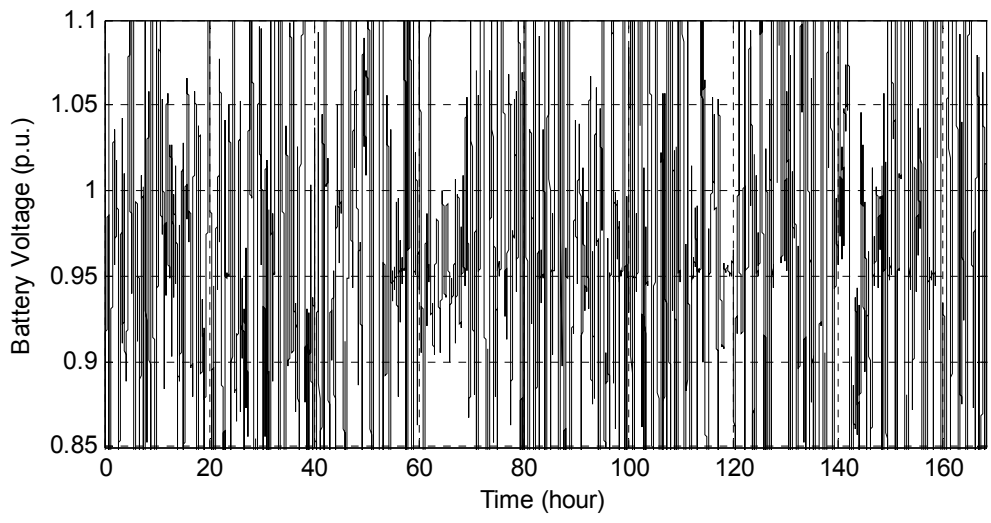
Figure 4-18: 10 MWh BESS performance with 100 sec prediction window. (a) State of charge of one battery. (b) Current profile of one battery (kA). (c) DC link voltage (p.u.). (d) Power injected by the BESS (MW)



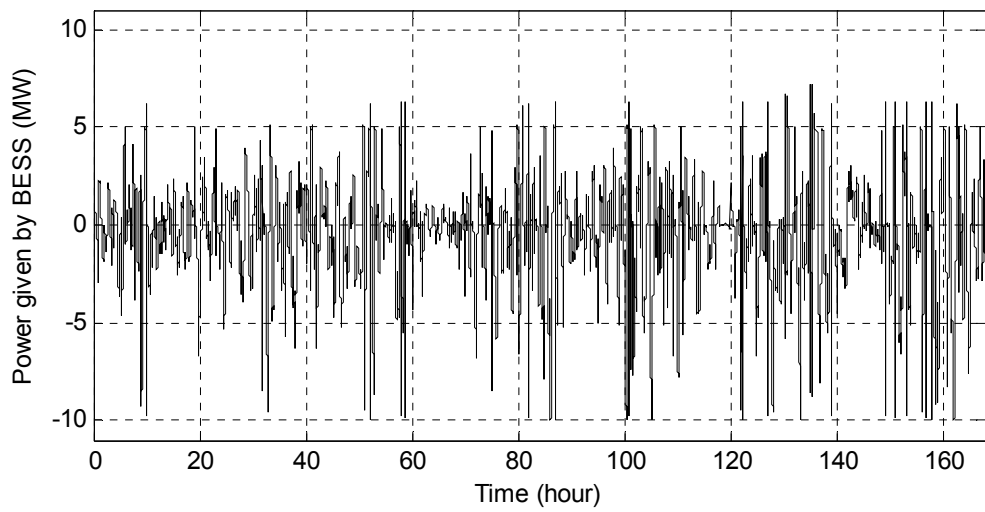
(a)



(b)

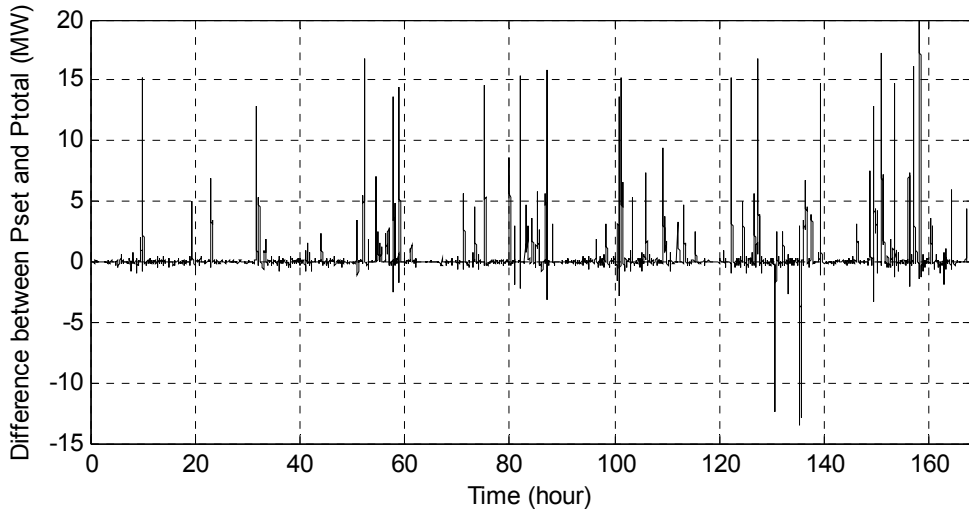


(c)

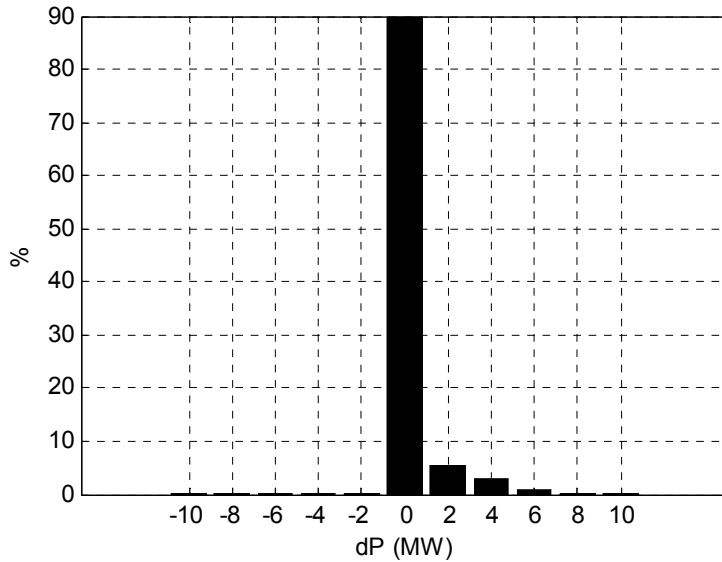


(d)

To assess the effectiveness of dispatchability provided by the BESS and compare it with 30 min prediction window, the difference between the total output and the desired set points is determined. This difference $dP = P_{set} - P_{total}$ is given in Figure 4-19 (a), and Figure 4-19 (b) shows the corresponding histogram. As these figures indicate, most of the time the deviations are within ± 3 MW, and larger deviations occur rarely with 100 sec window, too.



(a)



(b)

Figure 4-19: Power deviations in net power supplied P_{total} around the desired set point P_{set} with 10 MWh BESS. (a) Power deviations $dP = P_{set} - P_{total}$ (in megawatts). (b) Histogram of power deviations (%)

To analyze the effect of different prediction window, the power deviations can be compared with the case without BESS. The result without BESS was shown in Figure 4-6. Assuming that the deviations up to ± 3 MW are acceptable, it is seen that with 10

MWh BESS, we can reduce the undesired deviations from 24% (Figure 4-6 (b)) to 4.6% (Figure 4-19 (b)) with the optimal control method having 100 sec prediction window. From this result, it can be concluded that longer prediction shows better performance (i.e., 3.7% deviation with 30 min prediction window compared to 4.6% deviation with 100 sec window), but the difference in the performance is not that significant. This better performance with longer prediction window is due to minimizing the objective function (i.e. the integral) through a longer time period instead of a shorter one, since using longer prediction window i.e. more data for future will improve the solution by reducing the occurrence of big deviations more compared to shorter prediction window.

The results with 300 kWh BESS connected to a solar PV system of 1.5 MW peak output are presented next. As it was shown that the 30 min prediction window gives better results, a single case with 30 min prediction window is simulated only. Figure 4-20 shows the P_{set} , P_{solar} and the net power injected $P_{total} = P_{solar} + P_{bess}$ for one day zoom-in of the weekly long simulation. It is seen that the total injected power follows the desired set points perfectly most of the time similar to the results obtained with the wind case.

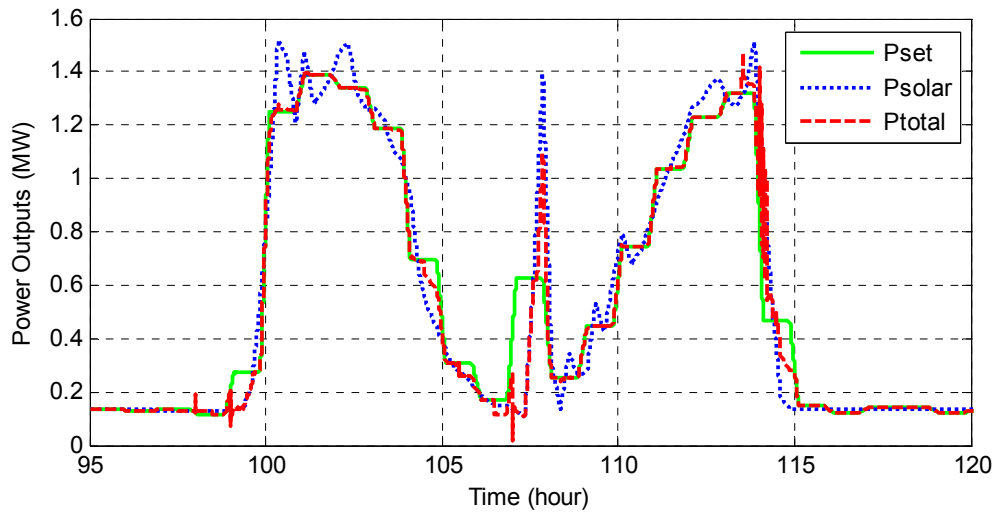
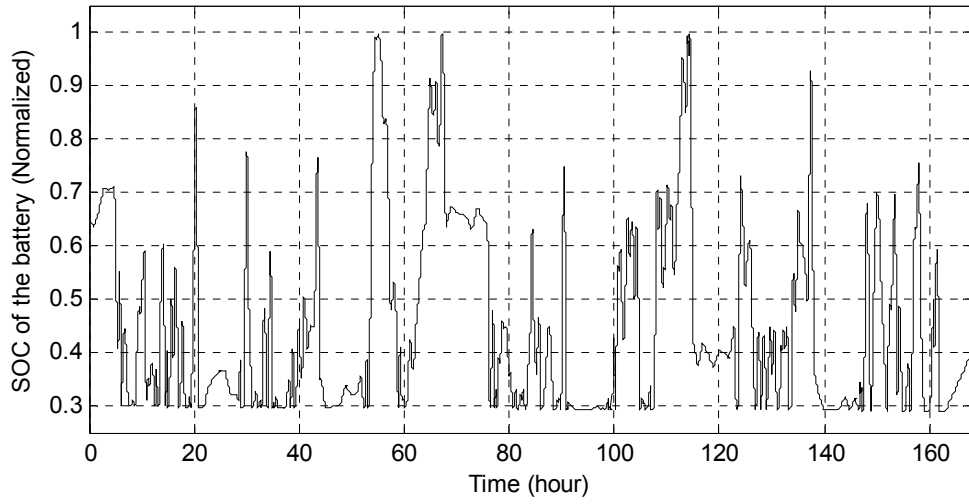


Figure 4-20: Dispatching of solar PV power with BESS; P_{set} : desired set point, P_{solar} : solar power, P_{total} : net injected power (in megawatts) - 30 min prediction window

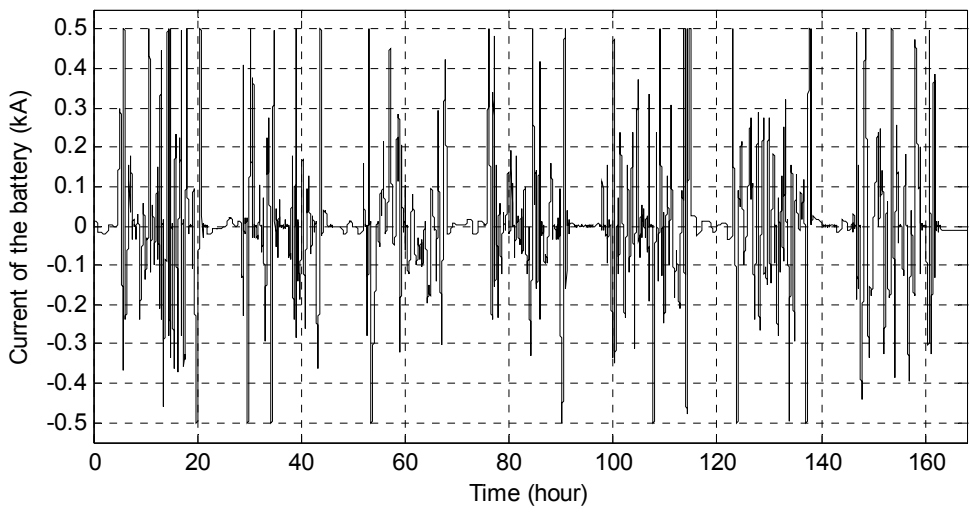
The 300 kWh BESS performance is seen in Figure 4-21. It is seen in Figure 4-21 (a) that the SOC of the battery is kept between 30% - 100%. The current profile of the battery in Figure 4-21 (b) indicates the charge/discharge current levels and cycle frequency. This figure points out that the maximum charge/discharge current is 500 A as defined by the limits and the charge/discharge cycle is approximately every 20 min; but most of the time charging/discharging is partial and occurs during the daytime only. Figure 4-21 (c) shows that the battery voltage stays within acceptable limits (+10/-15 % of rated voltage) during the weekly period. The power output profile of the BESS in Figure 4-21 (d) indicates that the output of the BESS is limited to ± 300 kW as desired.

It should again be noted that by limiting the SOC to be between 30% and 100% similar to the wind case, the deep discharge/charge cycles have been minimized in order to extend the lifetime of the battery.

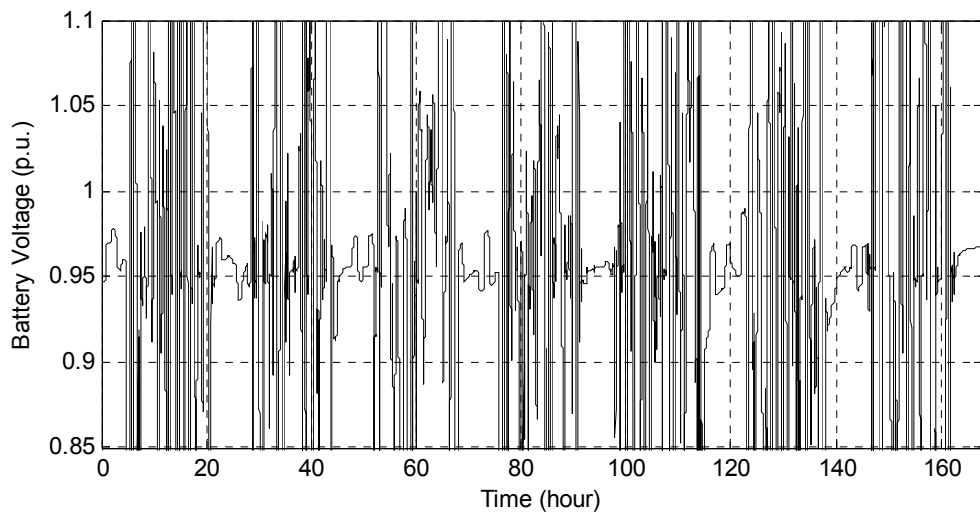
Figure 4-21: 300 kWh BESS performance with 30 min prediction window. (a) State of charge of one battery. (b) Current profile of one battery (kA). (c) DC link voltage (p.u.). (d) Power injected by the BESS (kW)



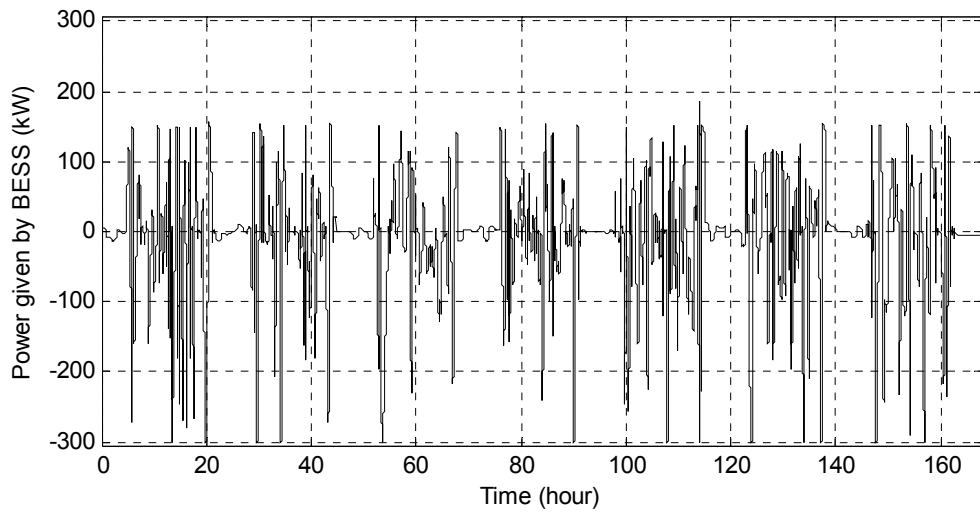
(a)



(b)

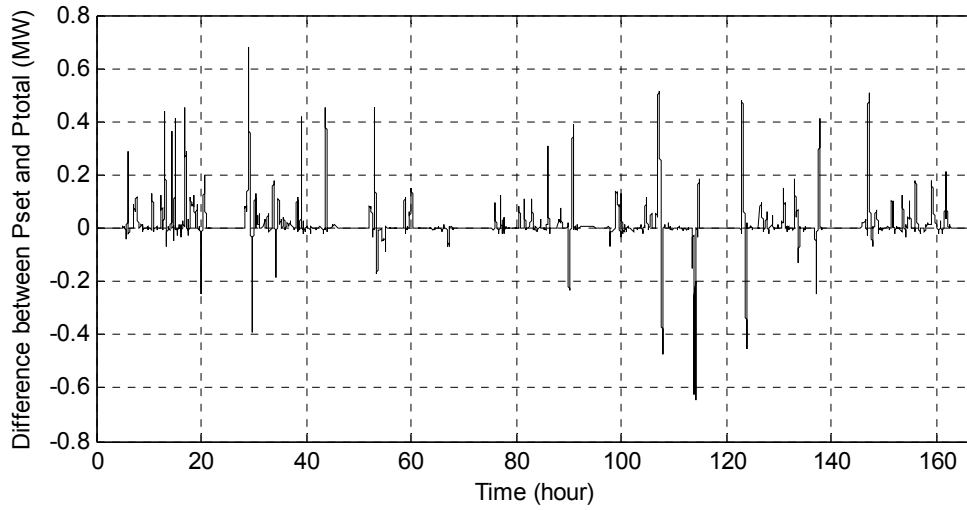


(c)

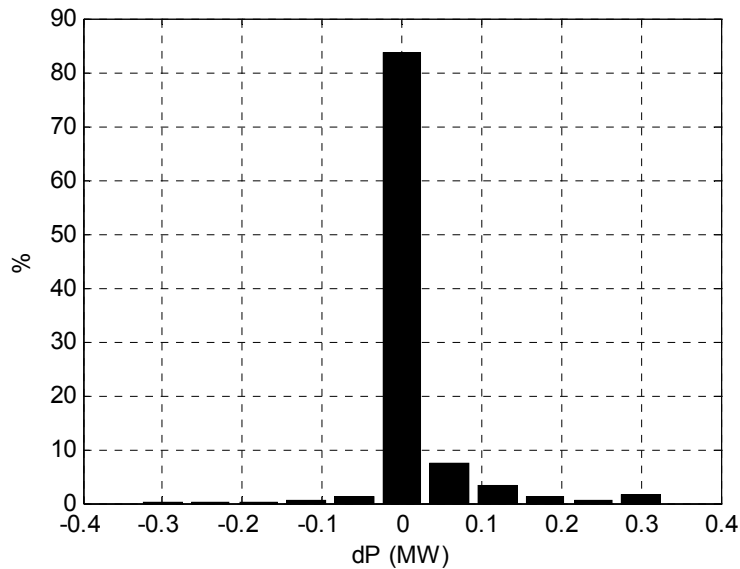


(d)

To assess the effectiveness of dispatchability provided by the BESS, the difference between the total output and the desired set points is determined for solar case, too. This difference $dP = P_{set} - P_{total}$ is given in Figure 4-22 (a), and Figure 4-22 (b) shows the corresponding histogram. As these figures indicate, most of the time the deviations are within ± 0.09 MW, larger deviations occur rarely.



(a)



(b)

Figure 4-22: Power deviations in net power supplied P_{total} around the desired set point P_{set} with 300 kWh BESS. (a) Power deviations $dP = P_{set} - P_{total}$ (in megawatts). (b) Histogram of power deviations (%)

To analyze the improvement obtained with the BESS integration furthermore, the power deviations can be compared with the case without BESS. The result without BESS was already shown in Figure 4-10.

If it is again assumed that the deviations up to ± 0.09 MW are acceptable, it is seen that with 300 kWh BESS, we can reduce the undesired deviations from 27% (Figure 4-10 (b)) to 7.6% (Figure 4-22 (b)).

From the results of the two cases with solar and wind, it is seen that the BESS charge/discharge frequency is relatively high with the optimal control method, too, and as stated before, new type of batteries with high charge/discharge cycling rates would be needed for this application.

The optimal control strategy considered also makes a compromise in that it limits the full utilization of the BESS capacity (i.e. 70% utilization) in order to extend the lifetime of the BESS. However, as the results show, we can decrease the undesired deviations much more with this method compared to SOC feedback control method and hence we need a smaller size BESS compared to the other method – about 15-25% of the wind farm/solar PV capacity – to have an effective and smooth dispatch profile. Even if the optimal control method shows better performance and reduces the undesired deviations from the hourly dispatch set points to a value lower than 10%, it has some drawbacks, too. One of them is the computation time, which is longer with this method since at each control period the optimal control problem needs to be solved. Another disadvantage with this method is that the battery is controlled in open loop scheme for the control window duration which may cause the actual battery states to deviate from the predicted ones. Furthermore, the optimal control method requires a mathematical model for the battery and for some battery types it may be difficult to derive it and the modeling error can worsen the performance of the controller. Because of these disadvantages with optimal control method, a novel third method is developed which will be described next.

4.3 Rule Based Control

Even if optimal dispatching performance is obtained with the optimal control method described, its open loop structure, requirement of a battery model, and long computation time necessitated to develop another novel control method. For this purpose, a rule based control will be developed to determine the current reference for the converter which will charge/discharge the BESS accordingly.

In order to determine our rules, we need to revisit our optimal control problem and define it as an optimal tracking problem for BESS.

As described in section 4.2, our performance index for this problem is:

$$J(u) = \int_0^t (P_{bess,ref}(t) - P_{bess}(t))^2 dt \quad (4-14)$$

which will penalize the deviations from the battery power reference $P_{bess,ref}$ and hence our objective becomes to minimize the deviations between the solar/wind power and hourly dispatch set points using the BESS i.e. optimal tracking for BESS.

Our limitations as discussed before for this problem are:

$$SOC_{LL} \leq SOC(t) \leq SOC_{UL} \quad (4-15)$$

$$i_{max,ch} \leq i_{bess}(t) \leq i_{max,disch} \quad (4-16)$$

where SOC_{LL} and SOC_{UL} represent the minimum and maximum limits of SOC of the BESS, respectively; i_{bess} is the BESS current and it is positive when battery discharges; $i_{max,ch}$ and $i_{max,disch}$ represent the maximum allowable charge and discharge current for the BESS, respectively.

Now, instead of developing a mathematical model for the system in order to complete the problem definition, we will use a single equation to relate the input and output. For this

purpose, it is assumed that the P_{bess} is the output of the system and i_{bess} is the input to the system, and using this, the relation between output and input becomes:

$$P_{bess} = V_{bat} \times i_{bess} \quad (4-17)$$

where the voltage of the BESS, V_{bat} is used to relate the input and output.

This type of optimal tracking problems has attracted considerable attention from control researchers and in order to solve it, the system inversion for exact tracking is developed [60], [61]. In this method, the system's dynamics is inverted in order to get the desired input trajectory (i.e. i_{bess}^*) from the desired output trajectory (i.e. $P_{bess,ref}$). In [60], this method is applied in order to solve the output tracking problem for a general piezo-based positioner and, in [61], it is applied for a nonlinear nonminimum-phase system. For our problem, this method can be applied easily by using the voltage of the battery as the transfer function of our system.

Using the system inversion technique, we can develop our rules for the solution of the optimal tracking problem as follows:

$$\text{For } SOC_{LL} < SOC(t) < SOC_{UL} \quad P_{bess}(t) = P_{bess,ref}(t) \quad (4-18)$$

$$\text{For } SOC_{LL} = SOC(t) \quad \text{if } P_{bess,ref} > 0 \quad P_{bess}(t) = 0 \quad (4-19)$$

$$\text{if } P_{bess,ref} \leq 0 \quad P_{bess}(t) = P_{bess,ref}(t) \quad (4-20)$$

$$\text{For } SOC_{UL} = SOC(t) \quad \text{if } P_{bess,ref} < 0 \quad P_{bess}(t) = 0 \quad (4-21)$$

$$\text{if } P_{bess,ref} \geq 0 \quad P_{bess}(t) = P_{bess,ref}(t) \quad (4-22)$$

where it is assumed that the battery initial SOC is between SOC_{LL} and SOC_{UL} ; and $P_{bess}(t)$ is positive when battery discharges. Having developed the rules that guarantees that SOC is kept within the limits while performing perfect dispatch i.e. exact tracking, now using the $P_{bess}(t)$ obtained above we can define the rules to incorporate the current limit:

$$\text{For } i_{max,ch} < \frac{P_{bess}(t)}{V_{bat}(t)} < i_{max,disch} \quad i_{bess}^*(t) = \frac{P_{bess}(t)}{V_{bat}(t)} \quad (4-23)$$

$$\text{For } i_{\max, ch} \geq \frac{P_{bess}(t)}{V_{bat}(t)} \quad i_{bess}^*(t) = i_{\max, ch} \quad (4-24)$$

$$\text{For } i_{\max, disch} \leq \frac{P_{bess}(t)}{V_{bat}(t)} \quad i_{bess}^*(t) = i_{\max, disch} \quad (4-25)$$

where equation (4-17) is used to relate the input and output as discussed above.

By looking at equations (4-18) to (4-25), we can conclude that our objective, $P_{bess} = P_{bess,ref}$, is satisfied as long as we don't reach any of the limitations, and when we hit these limitations, we limit our reference current according to the corresponding rule. Therefore, the rule based control provides us the optimal solution and since it continuously gets feedback from the BESS (i.e., SOC and V_{bat}) and outputs current reference at each step, it is indeed the closed loop optimal controller for our problem. It should also be emphasized that this method doesn't require the development of a mathematical model for the system and it uses only the battery voltage to relate the input and output. And, hence, it can be applied easily to any other battery type. Moreover, the control scheme can be implemented easily with logic gates which will have less computation time compared to the optimal control method.

Even if the proposed method is given for the BESS constraints, it can also be used for any type of energy storage with different constraints. For example, we can easily add another constraint of DC voltage limitation (i.e. $0.9\text{p.u.} < V_{bat} < 1.1\text{p.u.}$) and create rules similar to above and use that in obtaining $i_{bess}^*(t)$.

4.3.1 Simulation Setup

PSCAD/EMTDC is again used in order to verify the effectiveness of the proposed control method and two different cases, one with PV system and storage; the other with wind farm and storage are simulated. During the simulations in PSCAD, the actual solar and

wind power data is used for P_{solar} and P_{wind} (Figure 1-1 (a) and (b) respectively) and the setup shown in Figure 3-1 is realized similar to the setup used for SOC feedback method.

It is again assumed that the STATCOM can follow the current reference coming from the rule based control perfectly and hence it is represented as a gain block of 0.97 (i.e. 3 % loss).

The same BESS sizes with the SOC feedback method were selected which were 300 kWh (300 kW 1 hour discharge) for the case with solar and 10 MWh (10 MW 1 hour discharge) for the wind case. Moreover, the same realization with SOC feedback method for the BESS is made to get the required battery number.

During the simulations, it is again assumed that each of these batteries contributes the same amount of current and the current limits are selected as $\pm 500\text{A}$ for the batteries and SOC of the batteries are limited to change between 30% and 100%.

The set point P_{set} is again selected as hourly dispatch reference which is obtained by taking the actual next hour average of P_{wind} for wind case and P_{solar} for the solar case and adding 10% noise to it as mentioned before in chapter 3.

Using this setup, one week long simulations were made in PSCAD/EMTDC with a time step of 1 sec.

4.3.2 Simulation Results

The results with 10 MWh BESS connected to 50 MW wind farms are presented first. Figure 4-23 shows the P_{set} , P_{wind} and the net power injected $P_{total} = P_{wind} + P_{bess}$ for one day zoom-in of the weekly long simulation. It is seen that the total injected power follows the desired set points perfectly most of the time and achieves optimal tracking.

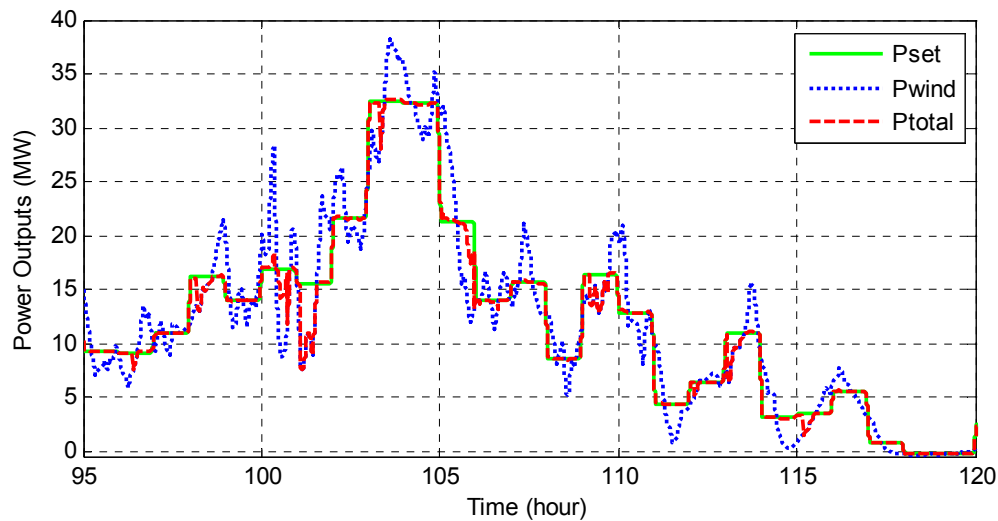
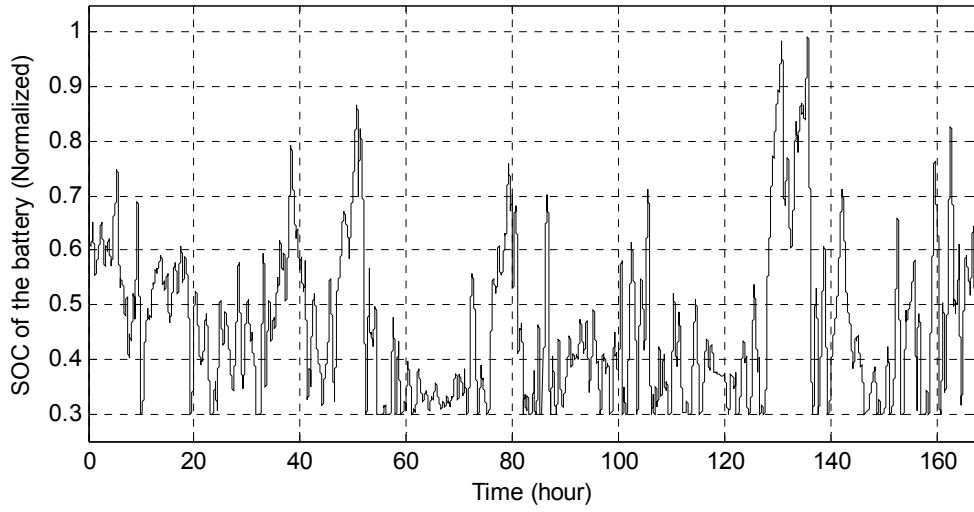


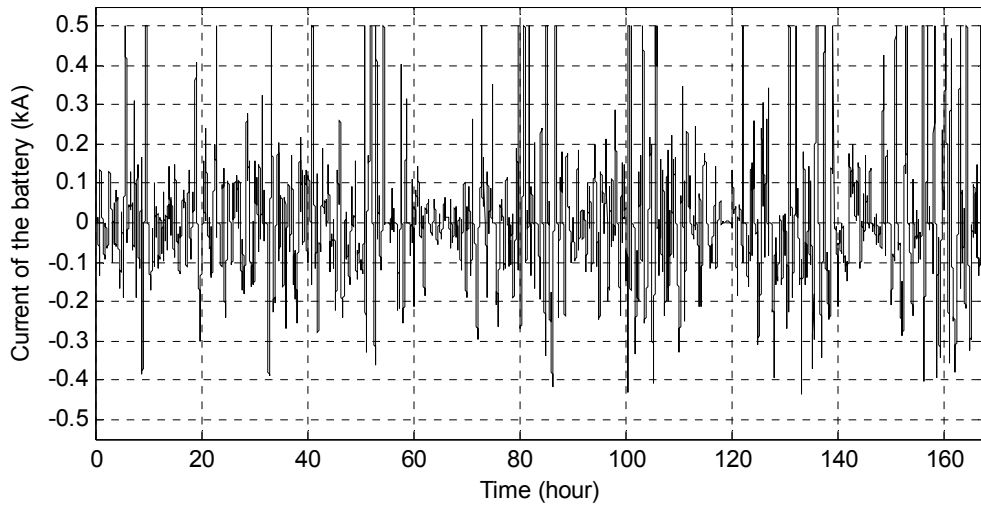
Figure 4-23: Dispatching of wind farm power with BESS; P_{set} : desired set point, P_{wind} : wind power, P_{total} : net injected power (in megawatts)

The 10 MWh BESS performance is seen in Figure 4-24. Figure 4-24 (a) shows that the SOC of the battery is kept between 30% - 100% as limited before. The current profile of the battery in Figure 4-24 (b) indicates the charge/discharge current levels and cycle frequency. This figure points out that the charge/discharge current varies between ± 500 A as set before. The figure also shows that the charge/discharge cycle is approximately every 20 min, but most of the time charging/discharging is partial and shallow. Figure 4-24 (c) shows that limiting the SOC helps to keep the battery voltage within acceptable limits (+10/-15 % of rated voltage) during the weekly period. The power output profile of the BESS in Figure 4-24 (d) indicates that the output of the BESS is limited to change between ± 10 MW.

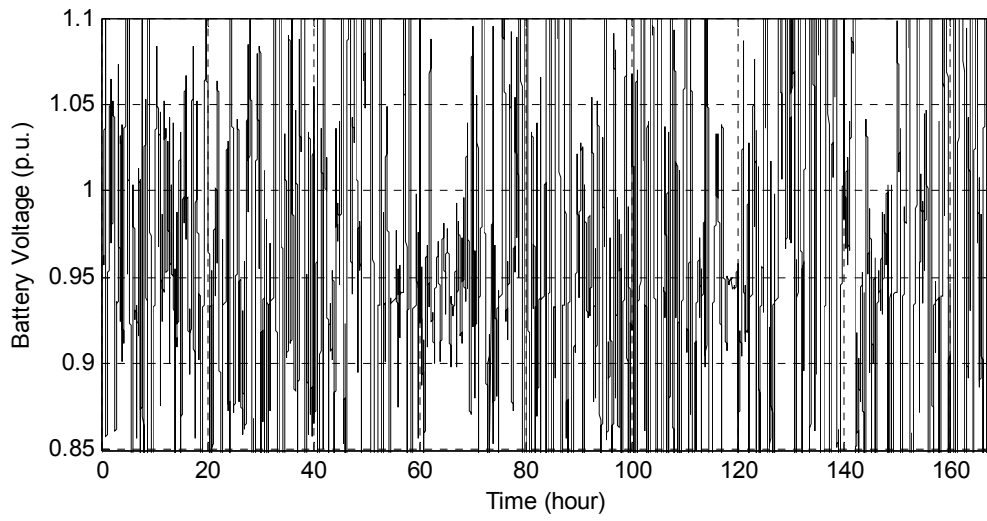
Figure 4-24: 10 MWh BESS performance. (a) State of charge of one battery. (b) Current profile of one battery (kA). (c) DC link voltage (p.u.). (d) Power injected by the BESS (MW)



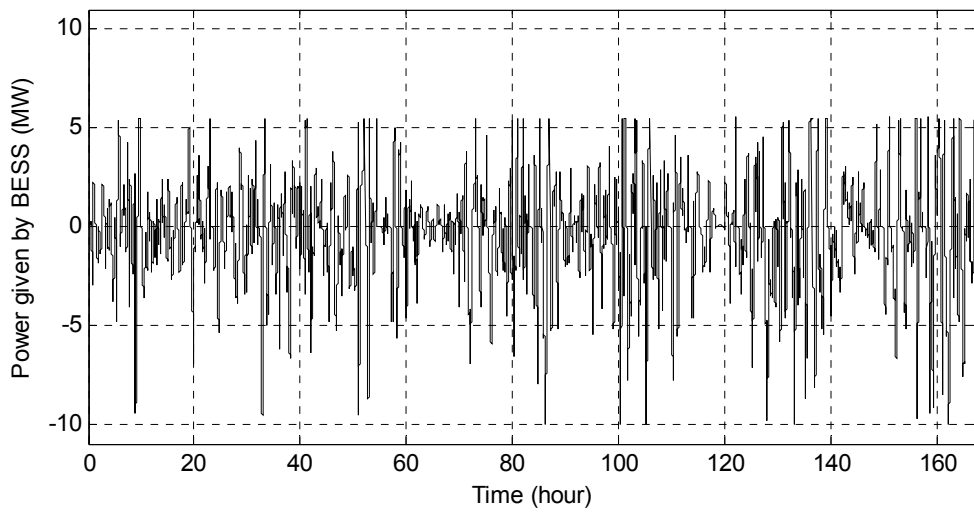
(a)



(b)

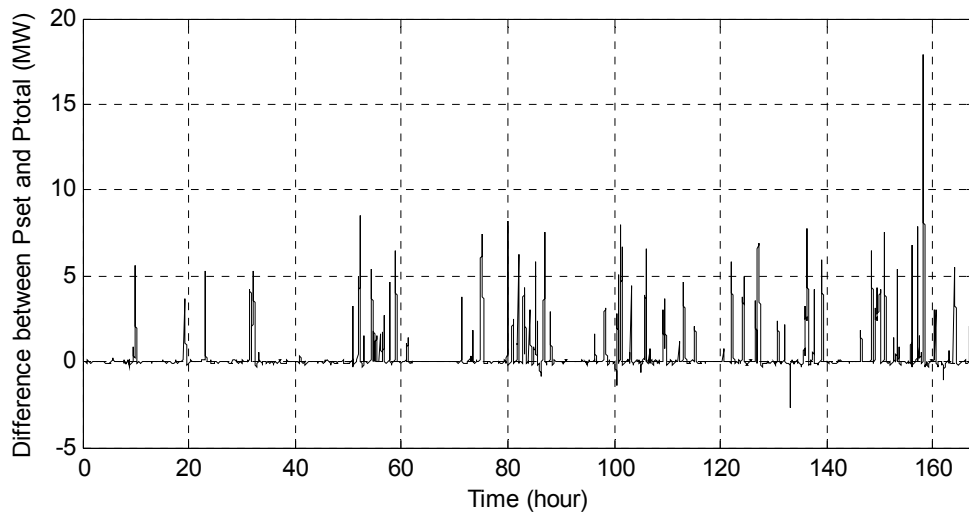


(c)

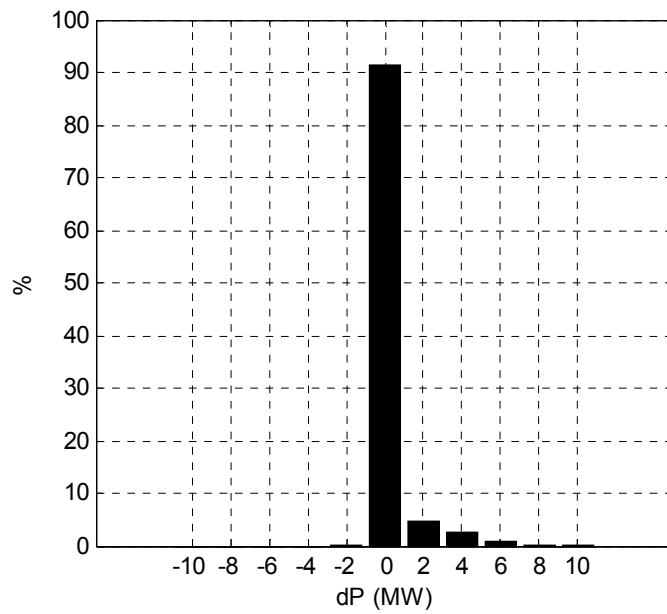


(d)

To assess the effectiveness of dispatchability provided by the BESS, the difference between the total output and the desired set points is once again determined. This difference $dP = P_{set} - P_{total}$ is given in Figure 4-25 (a), and Figure 4-25 (b) shows the corresponding histogram. As these figures indicate, most of the time the deviations are within ± 3 MW, and larger deviations occur rarely with the rule based control method.



(a)



(b)

Figure 4-25: Power deviations in net power supplied P_{total} around the desired set point P_{set} with 10 MWh BESS. (a) Power deviations $dP = P_{set} - P_{total}$ (in megawatts). (b) Histogram of power deviations (%)

To analyze improvement obtained with the BESS integration furthermore, the power deviations can be compared with the case without BESS as done in the SOC feedback

method. The result without BESS was shown in Figure 4-6. If we assume again that the deviations up to ± 3 MW are acceptable, it is seen that with 10 MWh BESS, we can reduce the undesired deviations from 24% (Figure 4-6 (b)) to 4% (Figure 4-25 (b)) with the rule based control.

The results with 300 kWh BESS connected to a solar PV system of 1.5 MW peak output are presented next. Figure 4-26 shows the P_{set} , P_{solar} and the net power injected $P_{total} = P_{solar} + P_{bess}$ for one day zoom-in of the weekly long simulation. It is seen that the total injected power follows the desired set points perfectly most of the time again and achieves optimal tracking similar to the results obtained with wind case.

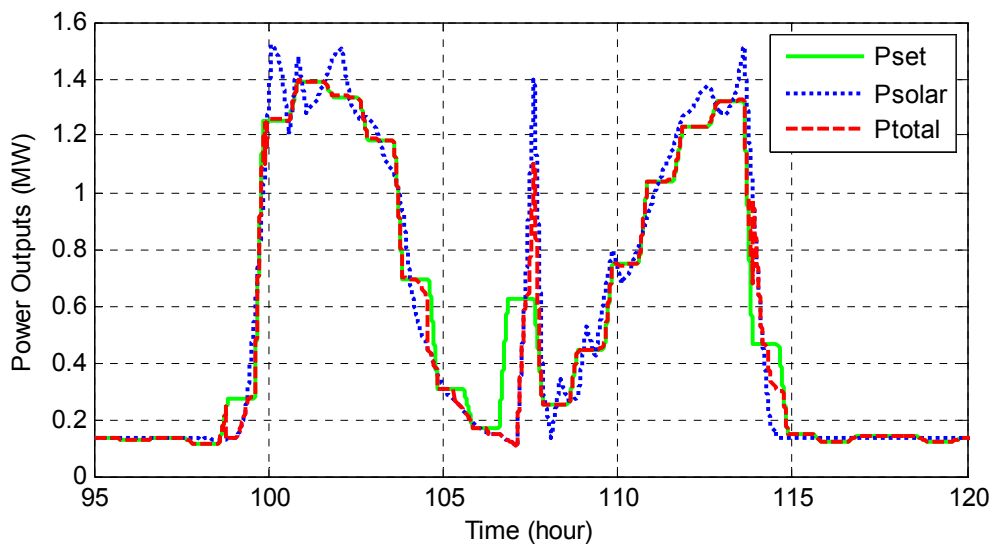
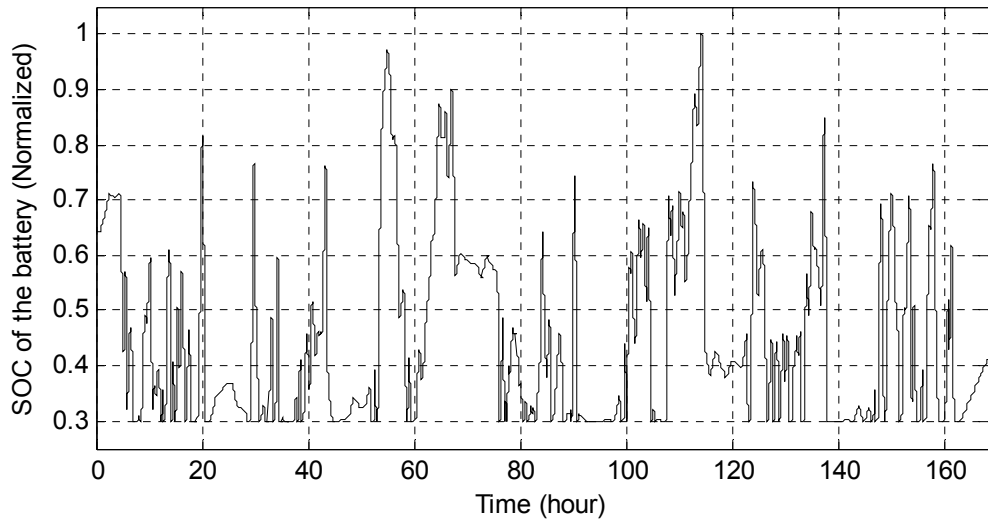


Figure 4-26: Dispatching of solar PV power with BESS; P_{set} : desired set point, P_{solar} : solar power, P_{total} : net injected power (in megawatts)

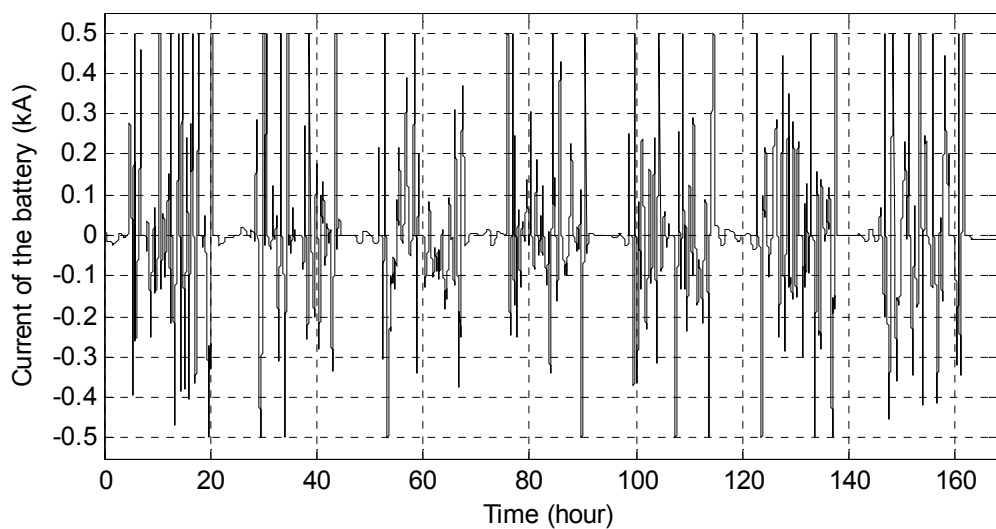
The 300 kWh BESS performance is seen in Figure 4-27. It is seen in Figure 4-27 (a) that the SOC of the battery is only allowed to change between 30% - 100%. By doing this similar to the wind case, the deep discharge/charge cycles have been minimized in order to extend the lifetime of the battery. The current profile of the battery in Figure 4-27 (b) indicates the charge/discharge current levels and cycle frequency. This figure points out

that the maximum charge/discharge current is 500 A as defined by the limits and the charge/discharge cycle is approximately every 20 min; but most of the time charging/discharging is partial and occurs during the daytime only. Figure 4-27 (c) shows that the battery voltage stays within acceptable limits (+10/-15 % of rated voltage) during the weekly period. The power output profile of the BESS in Figure 4-27 (d) indicates that the output of the BESS is limited to ± 300 kW as desired.

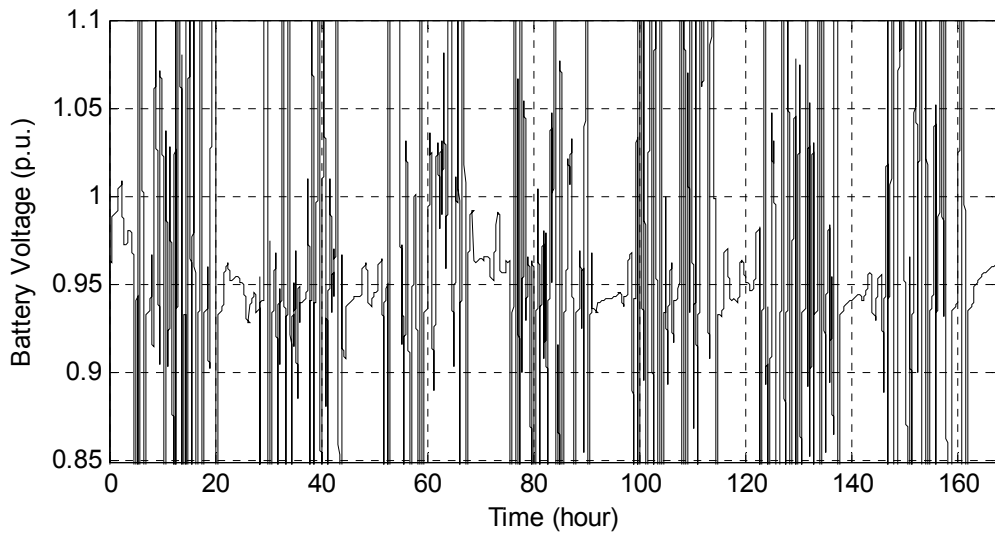
Figure 4-27: 300 kWh BESS performance. (a) State of charge of one battery. (b) Current profile of one battery (kA). (c) DC link voltage (p.u.). (d) Power injected by the BESS (kW)



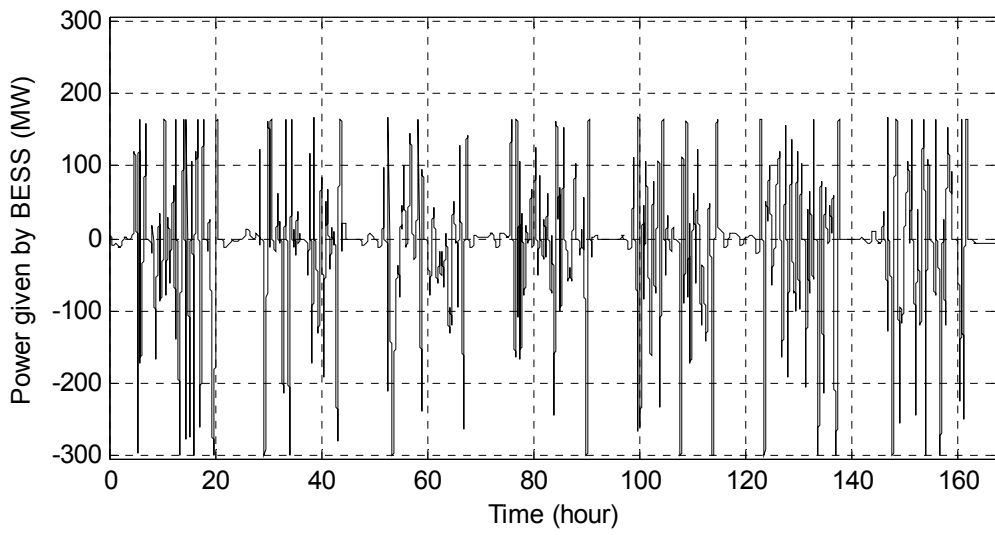
(a)



(b)

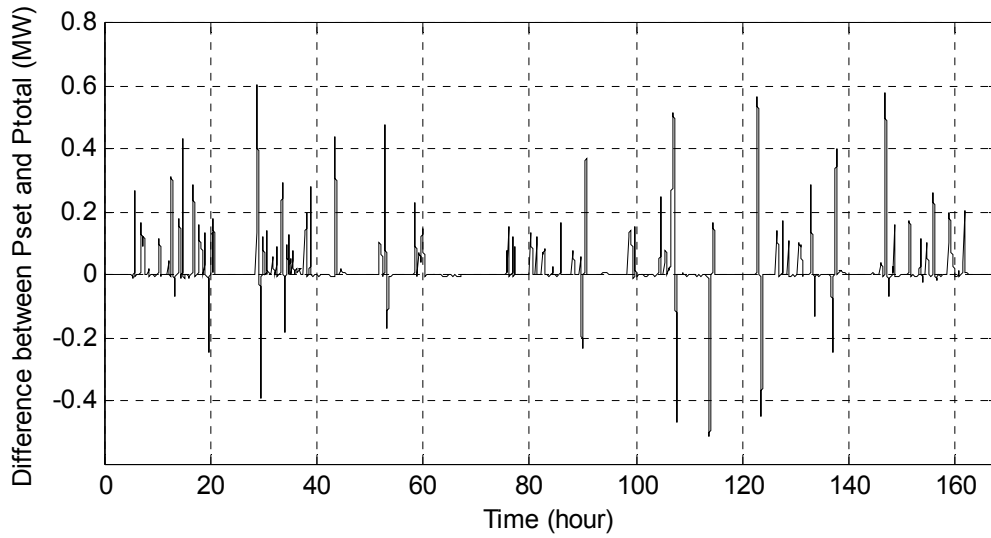


(c)

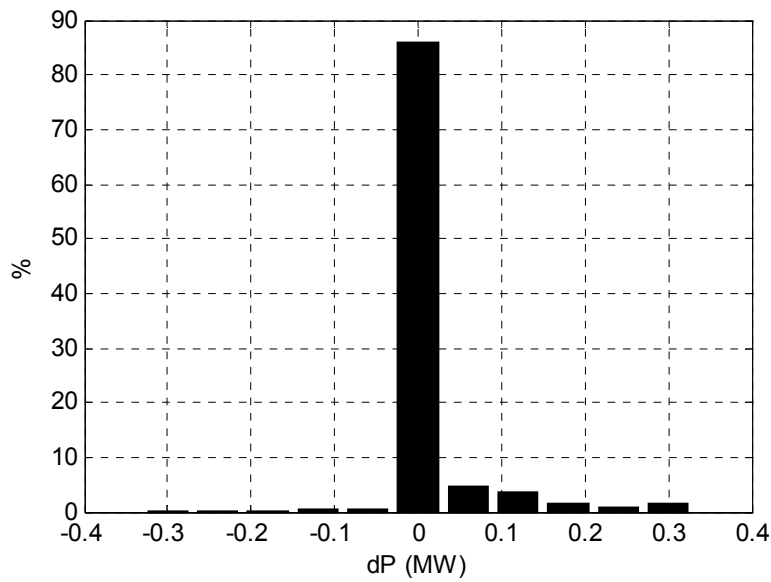


(d)

To assess the effectiveness of dispatchability provided by the BESS, the difference between the total output and the desired set points is determined for solar case too. This difference $dP = P_{set} - P_{total}$ is given in Figure 4-28 (a), and Figure 4-28 (b) shows the corresponding histogram. As these figures indicate, most of the time the deviations are within ± 0.09 MW, larger deviations occur rarely.



(a)



(b)

Figure 4-28: Power deviations in net power supplied P_{total} around the desired set point P_{set} with 300 kWh BESS. (a) Power deviations $dP = P_{set} - P_{total}$ (in megawatts). (b) Histogram of power deviations (%)

To analyze the improvement obtained with the BESS integration furthermore, the power deviations can be compared with the case without BESS. The result without BESS was already shown in Figure 4-10.

If it is again assumed that the deviations up to ± 0.09 MW are acceptable, it is seen that with 300 kWh BESS, we can reduce the undesired deviations from 27% (Figure 4-10 (b)) to 8.7% (Figure 4-28 (b)).

From the results of the two cases with solar and wind, it is seen that the BESS charge/discharge frequency is relatively high with the rule based control method, too, and as stated before, new type of batteries with high charge/discharge cycling rates would be needed for this application.

The rule based control strategy considered also makes a compromise in that it limits the full utilization of the BESS capacity (i.e. 70% utilization) in order to extend the lifetime of the BESS. However, from the results, it is seen that we can decrease the undesired deviations much more with this method compared to SOC feedback control method and hence we need a smaller size BESS compared to the SOC feedback method – about 15-25% of the wind farm/solar PV capacity – to obtain optimal tracking.

It is also seen that rule based control performs very similar to optimal control since it is the closed loop optimal control implementation for the same objective function. Moreover, with the closed loop scheme, we eliminate the disadvantage of leaving the system open loop for the control window duration which was the case with the optimal control. Furthermore, relating the input and output by simply using the battery voltage also eliminated the requirement of mathematical model for the battery which is difficult to obtain usually. Finally, the computation time with this control scheme is lower since there is no need to solve the optimal control problem for each prediction window.

4.4 Control of STATCOM

Having proposed three novel control methods for the outer control shown in Figure 4-1 in order to obtain the current reference, i_{bess}^* , a method for the inner control i.e. for the control of STATCOM is described next.

The control block diagram utilizing the reference signal obtained from the first part of the controller is given in Figure 4-29 [62], [63].

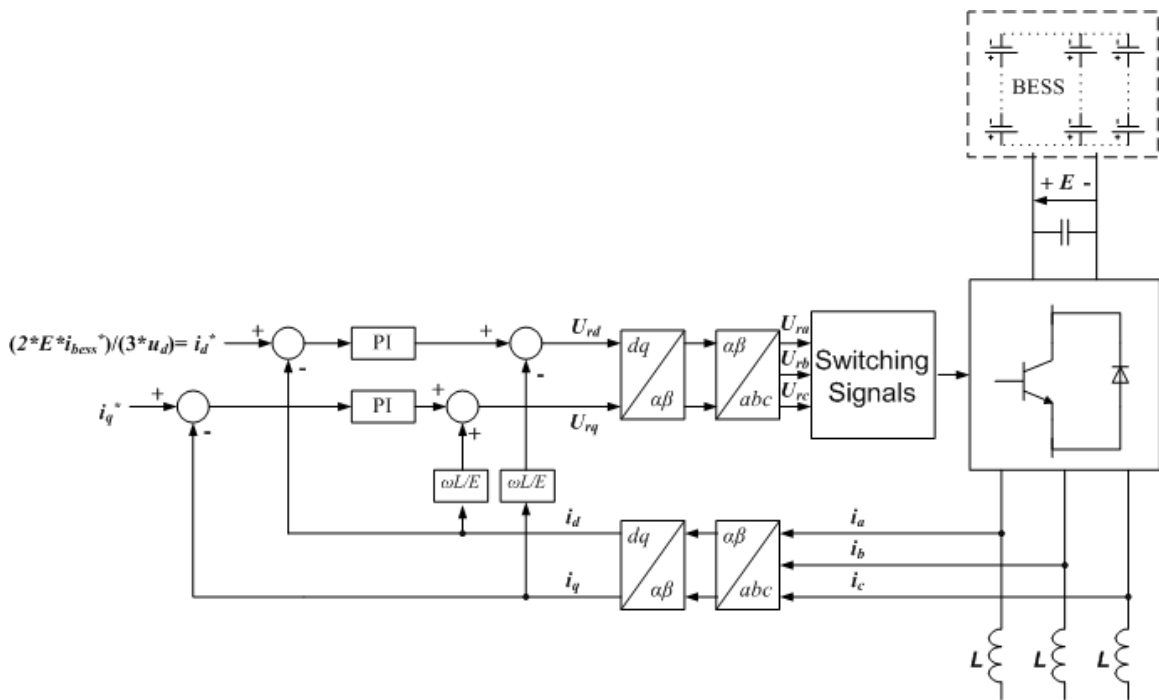


Figure 4-29: Control block diagram of STATCOM

It is seen from Figure 4-29 that vector control technique [64], [65] is used to control STATCOM such that independent control of active and reactive power can be achieved via control of direct and quadrature axis currents namely, i_d and i_q respectively. In order to input our current reference, i_{bess}^* , to this control scheme the following equation which assumes input power to STATCOM is equal to output power of STATCOM is used:

$$P_{in} = E i_{bess}^* = P_o = \frac{3}{2} U_d i_d^* \quad (4-26)$$

Using i_d^* obtained from equation (4-26), the active power flow control can be achieved by charging/discharging BESS dynamically. Furthermore, i_q^* which is the reference current for the quadrature axis can also be used to control the reactive power flow [12].

Having showed the detailed block diagram for dynamic control of STATCOM in Figure 4-29; for long term simulations, it should again be mentioned that, the dynamics of STATCOM can be ignored and represented as a gain block since the STATCOM response time is in the order of ms whereas the charge/discharge time of the battery for this application as shown before is in the order of minutes.

4.5 Comparison of Methods

In order to compare the three proposed methods for the outer control loop, simulations for wind case are repeated with three other BESS sizes; 5 MWh, 15 MWh and 20 MWh. To assess the effectiveness of dispatchability provided by each method, a performance index, namely PI , is defined which adds the undesired deviations i.e. $dP = P_{set} - P_{total}$. To formulate this index, it is again assumed that the deviations up to ± 3 MW are acceptable and hence the equation for PI can be written as:

$$PI = \sum N_x * |dP_x| \quad (4-27)$$

which sums the unacceptable power deviations that are higher than 3 MW. In this equation, N_x represents the number of occurrence of the deviations. According to this index $PI = 0$ means perfect hourly dispatch. For example for the case without energy storage (i.e. Figure 4-6), the PI is 209.89 (worst case, highest PI).

The comparison results obtained with the defined PI is shown in Figure 4-30.

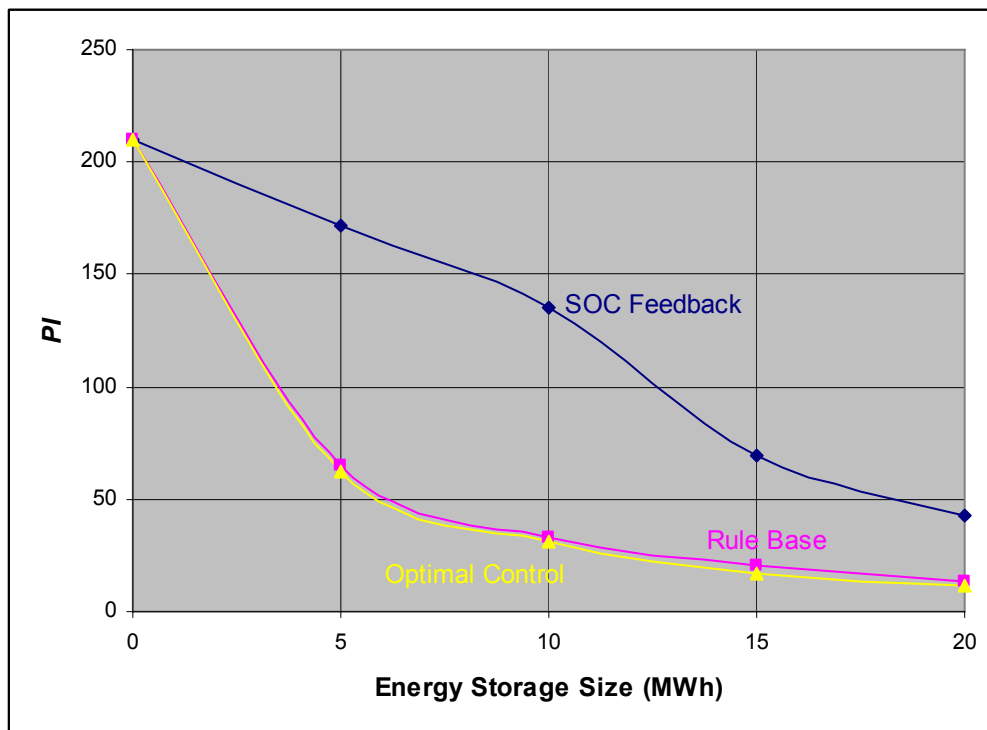


Figure 4-30: Comparison of the three proposed methods

It is seen from Figure 4-30 that the performance obtained with SOC feedback method is quite poor compared to the other two methods proposed. Moreover, it can also be observed that the rule based control and the optimal control performs very similar since rule based control is the closed loop solution of the optimal control problem. There is a slightly better performance with the optimal control scheme due to the 30 min prediction window (the optimal control case simulations are made with 30 min prediction window only).

The comparison results also show that there is a decrease in an order of magnitude in PI when rule based or optimal control scheme is used even with 5 MWh storage. Hence, this shows that quite effective dispatch is obtained with these two methods. Moreover, the PI decrease slows down with increased BESS sizes for the rule based control and the

optimal control cases and hence there is not much difference in the dispatchability obtained between 10 MWh BESS and 20 MWh BESS with these two methods.

4.6 Experimental Validation of the Rule Based Method

In order to verify the simulation results, an experimental setup for the rule based method is developed. For this purpose, the setup shown in Figure 3-1 is simplified such that the BESS is replaced by a single lead-acid battery of 8 Ah, the grid is represented as two lead acid batteries of 8 Ah, and the converter (i.e. STATCOM) is represented by a half bridge circuit. Since P_{wind} and P_{set} are already known, we obtained the battery power reference signal i.e. $P_{bess,ref}$ by taking difference of P_{set} and P_{wind} . As, instead of 10MWh BESS, a single lead acid battery ($8Ah \times 12.5V = 100Wh$) is used, $P_{bess,ref}$ is scaled down by 100k times. The final experimental setup is shown in Figure 4-31.

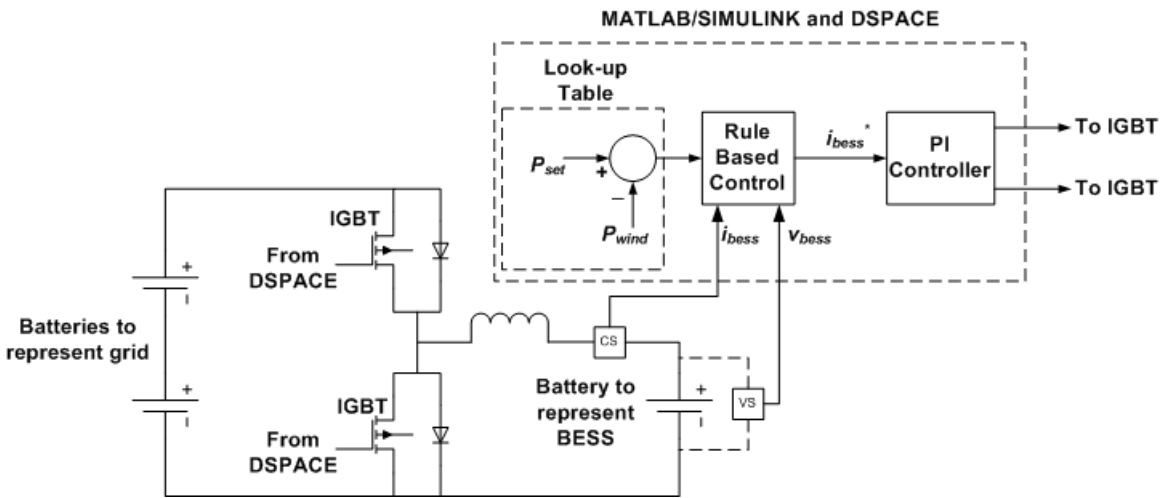


Figure 4-31: Experimental Setup

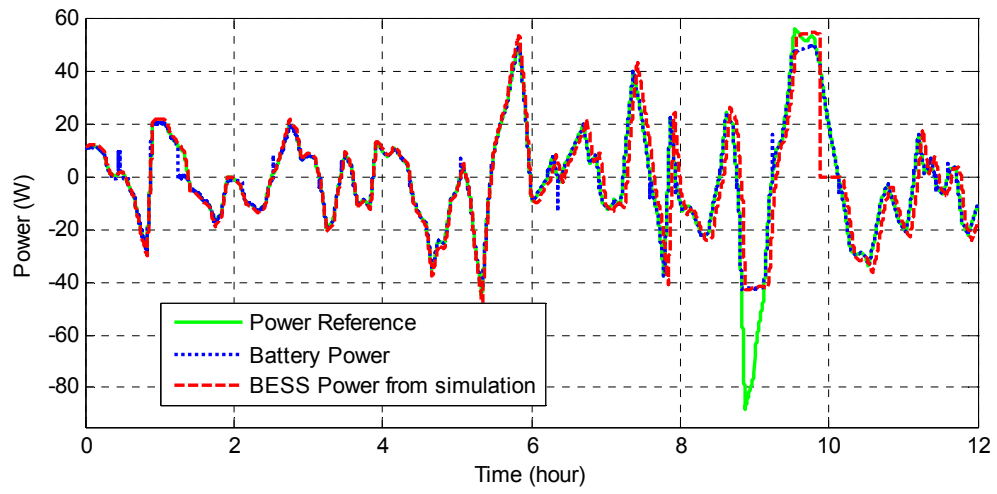
In this setup, IGBTs are used as switches, current sensor is used to measure the battery current and current integration method is used to get the SOC from this measurement. Resistive divider is used to get the battery voltage. A fuse is placed after the inductor for protection, and also a current limit of $\pm 3.6A$ is put for the current reference, i_{bess}^* , which is the output of the rule based control for further protection. Moreover, the rule based

control and control of the half bridge is implemented in Matlab/Simulink and Dspace is used to obtain the PWM signals coming from the control output from Matlab/Simulink. The PWM signals obtained from Dspace are given into the gate driver of the IGBTs. The details of the hardware can be found in Appendix C.

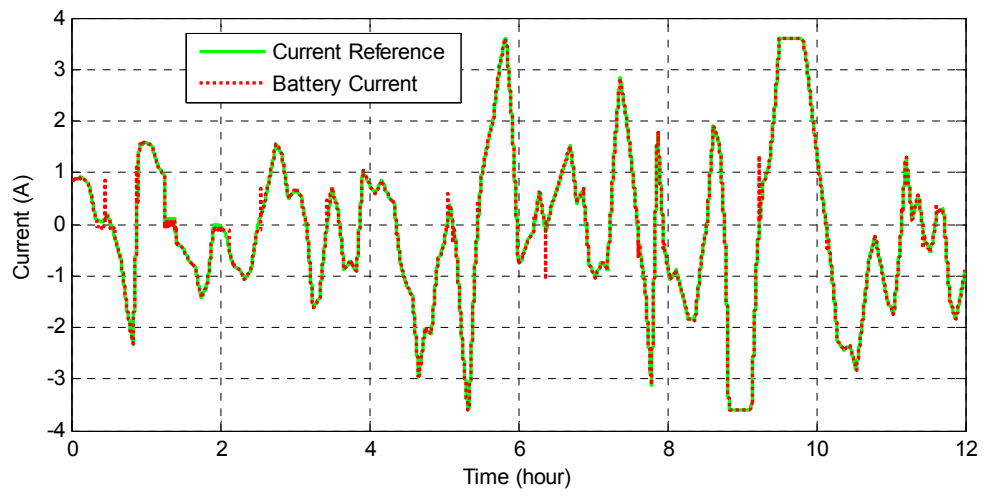
The aim is to show that the lead acid battery can indeed follow the current reference signal coming from the rule based control and charge/discharge the battery accordingly while keeping the battery SOC within 30%-100% and current between 3.6A and -3.6A as limited before.

The experiment results obtained with a sampling time of 0.5 sec are shown in Figure 4-32.

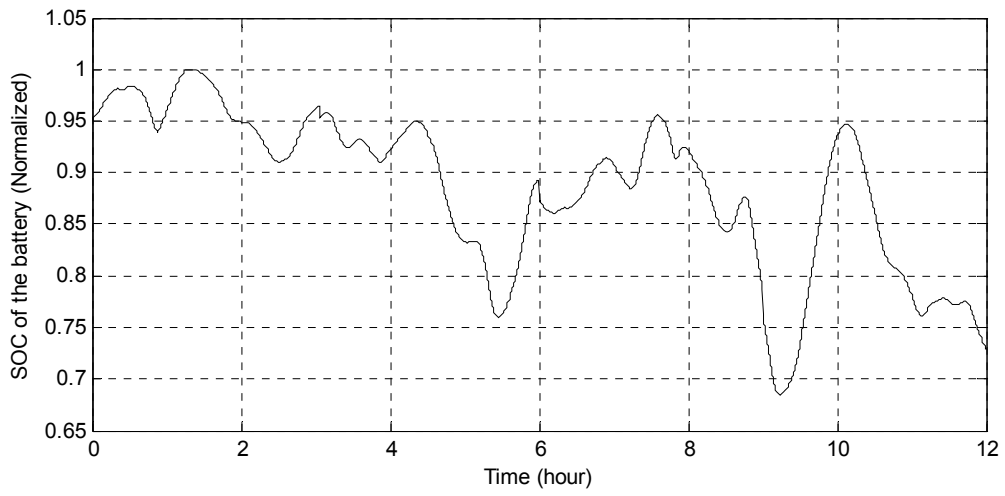
Figure 4-32: Single battery performance with rule based control. (a) Power reference, $P_{bess,ref}$, power injected by the battery, P_{bess} and scaled BESS power from simulation (W). (b) Current reference, i_{bess}^* and current profile of the battery i_{bess} (A). (c) State of charge of the battery. (d) Battery voltage (V)



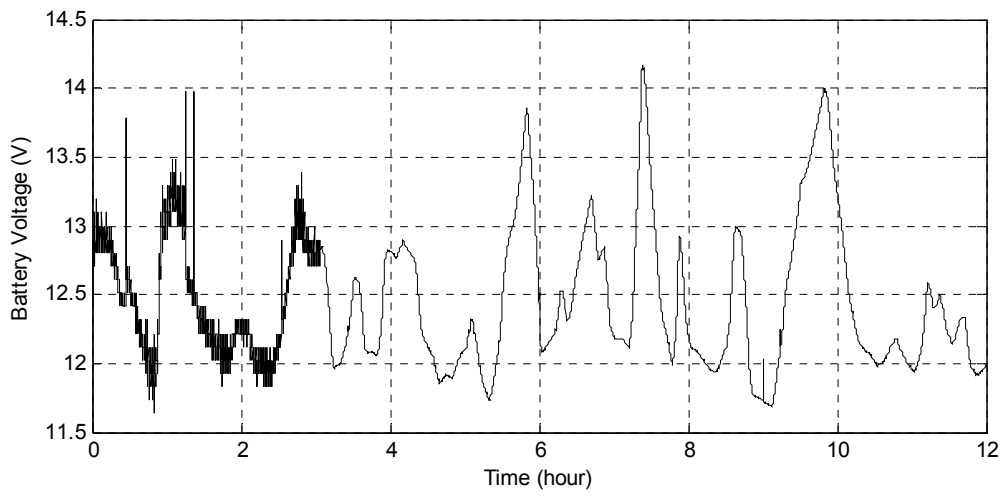
(a)



(b)



(c)



(d)

It is seen in Figure 4-32 (a) that the battery can follow the power reference and charge/discharge accordingly as long as no limit is reached and; moreover, it is seen that the power profile obtained with actual battery is the same as the one obtained from the simulation results with 10 MWh BESS by using the same scale factor. Figure 4-32 (b) shows that the BESS follows the current command perfectly and sets the current to zero when SOC (Figure 4-32 (c)) reaches its limit of 1 p.u. because of the corresponding rule and similarly limits the current to 3.6A according to the current limit. Moreover, it is observed that charge/discharge period is in the order of minutes, and hence, the battery can achieve the ramp up/down required for perfect current following. From these results it can be concluded that the rule based method works perfectly and charges/discharges the battery accordingly while keeping the battery SOC and current within its proper limits. The battery voltage profile seen in Figure 4-32 (d) shows that keeping the SOC within the limits also keeps the battery voltage within safe levels. Moreover, it should be noted that a filter in Matlab/Simulink is placed in order to read the voltage values clearly coming from the resistive voltage divider after the 3rd hour.

5. BESS for Contingency Support

Having showed that the rule based control provides the optimal solution and validated it with an experiment; another case study is made to show that BESS can also be used to absorb the wind generation during a contingency and hence wind curtailment could be avoided. For this purpose, the actual wind data shown in Figure 5-1 is used.

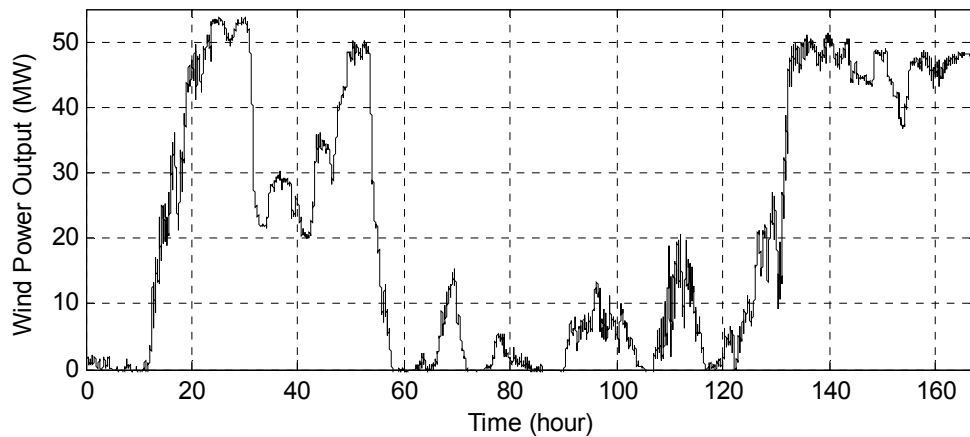


Figure 5-1: Wind farm power output (MW)

Currently, the transmission lines that carry the power output of the wind farm get overloaded under contingency occurring in this wind generation area and in order to prevent the voltage collapse, wind farm curtailments take place. In order to prevent this curtailment, BESS can be used to store the excess wind generation during the contingency.

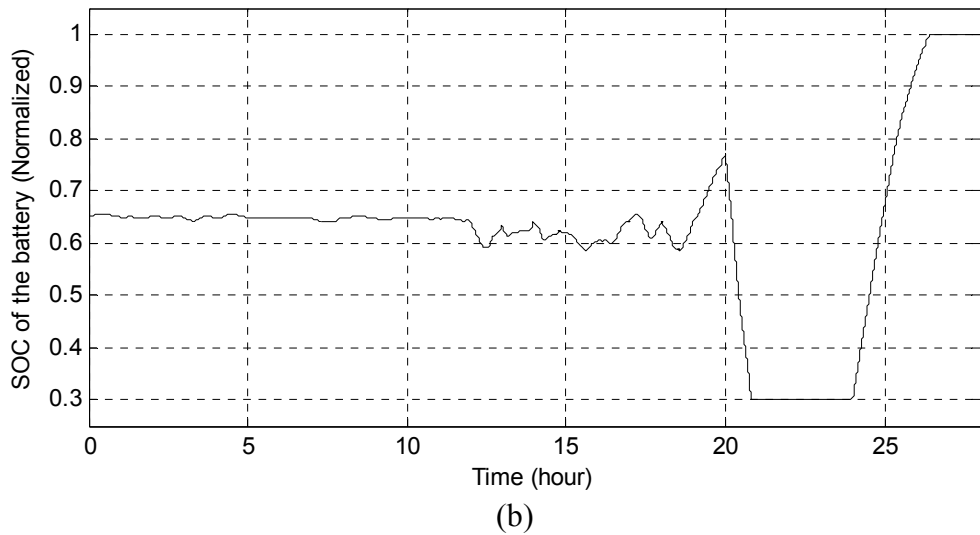
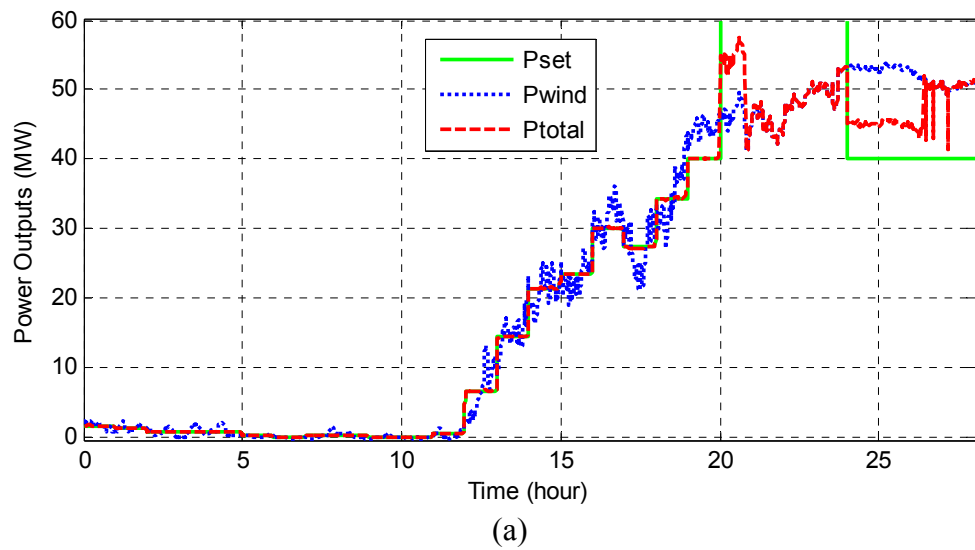
To demonstrate the application of BESS for this problem, the rule based control will again be used with some modifications as described below:

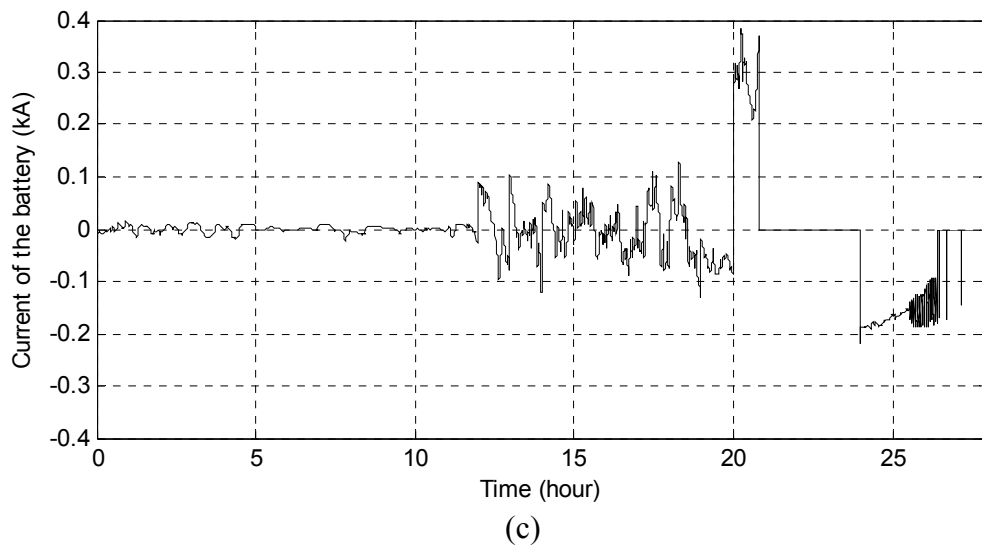
- Batteries charge/discharge according to the rule based control based on hourly dispatch profile, when the wind farm power output is less than 80% of its rated power (i.e. 55 MW).

- When the wind power output is more than 80% of its rated, the battery discharges to reach 30% SOC in preparation for a potential contingency. No hourly dispatch is done during the time when power output is at 80% or more of its rated value.
- If a contingency happens, the battery absorbs energy to minimize wind farm curtailments and avoid transient instability during the time following the contingency on the system.
- If the contingency is fixed before the battery SOC is at 100% and power output is less than 80% of the rated, battery goes back to hourly dispatch.
- If the contingency is not fixed and the battery reaches 100% SOC, wind curtailments take place.

To show the effectiveness of the BESS for this application, 32 MWh (8 MW 4 hour discharge) BESS size is selected. The same simulation setup with the rule base control is used for the simulations with the changes in the control as mentioned above. The simulation results obtained with 32 MWh BESS is shown in Figure 5-2.

Figure 5-2: BESS application for contingency support. (a) P_{set} : desired set point, P_{wind} : wind power, P_{total} : net injected power (in megawatts). (b) State of charge of one battery.
(c) Current profile of one battery (kA)





It is seen from Figure 5-2 (a) that optimal hourly dispatch is obtained as long as the wind farm power output doesn't reach its 80% of rated power. When it reaches 80% of its rated power (around 20th hour), it immediately begins discharging which can be seen by observing the decrease in the SOC of the battery in Figure 5-2 (b). When the contingency occurs at the 24th hour, the BESS instantaneously begins to absorb the excess power until it reaches 100% SOC. The current is kept within the limits during this operation which is seen in Figure 5-2 (c). By absorbing the excess power with BESS, it is seen that the total injected power to the grid can be reduced from 53 MW (before the contingency) to 45 MW for two and half hours, i.e., until the BESS is fully charged.

From this case study, it can be concluded that besides optimal hourly dispatch for wind power, prevention of wind farm curtailment can be achieved with the help of BESS.

6. Conclusions and Future Work

In this thesis, three different control methods for BESS, which is to be integrated with renewable energy sources are proposed so that the intermittent renewable resource can be dispatched on an hourly basis like any other conventional generator.

In order to develop the controllers, the reference power profile selection is made for the intermittent renewable energy source of interest and the required minimum BESS power and energy ratings are obtained. Furthermore, the challenges with BESS are determined for this application and the battery operation is characterized in terms of charge/discharge duration and lifetime.

Having determined the reference power profile and characterized the battery operation, the three methods are explained and simulated. From the results of the simulations and analysis of the methods, it is observed that:

- The dispatch performance obtained with SOC feedback method is quite poor compared to the other two methods namely optimal control and rule based control
- The rule based control and the optimal control performs very similar since rule based control is the closed loop solution of the optimal control problem
- There is a slightly better dispatch performance with the optimal control scheme due to the 30 min prediction window
- The rule based method has several advantages over the optimal control such as less computation time, closed loop implementation, no need for mathematical model of the BESS
- The BESS charge/discharge frequency is relatively high in this application; and hence, new type of batteries with high charge/discharge cycling rates are needed
- The control methods considered make a compromise in that they didn't utilize the BESS capacity fully in order to extend the lifetime of the BESS

- A large size BESS – about 15%-25% of the solar PV/wind farm capacity – is needed to have an effective hourly dispatch

After the analysis of the simulation results, the validation of the best novel method proposed, i.e. the rule based control, is made by a simple experimental setup and moreover another case study with this method for contingency support is presented.

For future study, other storage types suitable for this type of application, such as flywheels or different battery types can be analyzed, simulated and tested. Moreover, an improvement for testing of the rule based control can be made by letting the SOC of the battery to reach its lower limit and observe if the battery can give the desired power during low SOC levels (around 30%).

Another important recommendation for future work will be to modify the rule based control so that when the battery is close to its lower (i.e. 30%) or upper SOC (i.e. 100%) limits, the rule based control should limit the power demand from the BESS due to the fact that the battery may not absorb all the desired power when it is close to its full capacity (around 95% SOC); and similarly, it can not provide the desired power when it is at a low SOC level (around 35% SOC). This characteristic of the battery can also be incorporated in the battery model in order to represent a more realistic battery.

Finally, the solar data used in this study was obtained from a small scale PV system and scaled in order to represent utility scale PV system; however, for a better representation of utility scale PV system, actual power data from a PV system of 1 MW or bigger size can be used.

References

- [1] Renewable Energy Policy Network for the 21st Century (REN21), “Renewables Global Status Report 2009 Update,” 2009 [Online]. Available: http://www.ren21.net/pdf/RE_GSR_2009_Update.pdf
- [2] J. Bebic, R. Walling, K. O'Brien, B. Kroposki, “The sun also rises,” *IEEE Power and Energy Mag.*, vol. 7, no. 3, pp. 45 - 54, May-June 2009.
- [3] X. Y. Wang, D. Mahinda Vilathgamuwa, S. S. Choi, “Determination of Battery Storage Capacity in Energy Buffer for Wind Farm,” *IEEE Trans. Energy Conv.*, vol. 23, no. 3, pp. 868 - 878, Sept. 2008.
- [4] S. Teleke, M. E. Baran, A. Huang, S. Bhattacharya, L. Anderson, “Control Strategies for Battery Energy Storage for Wind Farm Dispatching,” *IEEE Trans. Energy Conv.*, vol. 24, no. 3, pp. 725 - 732, Sept. 2009.
- [5] C. Abbey, G. Joos, “Supercapacitor Energy Storage for Wind Energy Applications,” *IEEE Trans. Ind. Appl.*, vol. 43, no. 3, pp. 769 - 776, May-June 2007.
- [6] A.E. Curtright, J. Apt, “The Character of Power Output from Utility-Scale Photovoltaic Systems,” Carnegie Mellon Electricity Industry Center, Working Paper CEIC-07-05, 2007. [Online]. Available: <http://wpweb2.tepper.cmu.edu/ceic/papers/ceic-07-05.asp>
- [7] C. Han, A.Q. Huang, M.E. Baran, S. Bhattacharya, W. Litzemberger, L. Anderson, A.L. Johnson, A.-A. Edris, “STATCOM Impact Study on the Integration of a Large Wind Farm into a Weak Loop Power System,” *IEEE Trans. Energy Conversion*, vol. 23, no. 1, pp. 226 – 233, March 2008.
- [8] R. Hara, H. Kita, T. Tanabe, H. Sugihara, A. Kuwayama, S. Miwa, “Testing the technologies,” *IEEE Power and Energy Mag.*, vol. 7, no. 3, pp. 77 - 85, May-June 2009.
- [9] D.M. Logan, J.S. Baylor, D. Cotcher, D. Krauss, “Communicating the Value of Dispatchability for Non-Utility Generation Projects,” *IEEE Trans. Power Sys.*, vol. 10, no. 3, pp. 1408 – 1413, Aug. 1995.

- [10] D. Hawkins, M. Rothleder, "Evolving Role of Wind Forecasting in Market Operation at the CAISO," IEEE Power Systems Conference and Exposition, pp. 234 – 238, Oct. 29-Nov. 1 2006.
- [11] Bonneville Power Administration, "Renewable Energy Technology Roadmap," Technology Innovation Office, September 2006. [Online]. Available: http://www.bpa.gov/corporate/business/innovation/docs/2006/RM-06_Renewables-Final.pdf.
- [12] C. Han, A.Q. Huang, W. Litzemberger, L. Anderson, A.-A. Edris, M. Baran, S. Bhattacharya, A. Johnson, "STATCOM Impact Study on the Integration of a Large Wind Farm into a Weak Loop Power System," IEEE PSCE, pp. 1266 – 1272, Oct. 29-Nov. 1 2006.
- [13] E. Muljadi, C.P. Butterfield, R. Yinger, H. Romanowitz, "Energy Storage and Reactive Power Compensator in a Large Wind Farm," 42nd AIAA Aerospace Sciences Meeting and Exhibit, 5 - 8 January 2004.
- [14] P. F. Ribeiro, B. K. Johnson, M. L. Crow, A. Arsoy, and Y. L. Liu, "Energy storage systems for advanced power application," in Proc. IEEE, vol. 89, no. 12, pp. 1744–1756, Dec. 2001.
- [15] J. McDowall, "Conventional battery technologies—Present and future," in Proc. IEEE Power Engineering Society Summer Meeting, vol. 3, July 2000, pp. 1538–1540.
- [16] M. A. Casacca, M. R. Capobianco, and Z. M. Salameh, "Lead-acid battery storage configurations for improved available capacity," IEEE Trans. Energy Conversion, vol. 11, pp. 139–145, Mar. 1996.
- [17] N.W. Miller, R. S. Zrebiec, R.W. Delmerico, and G. Hunt, "Design and commissioning of a 5 MVA, 2.5 MWh battery energy storage," in Proc. IEEE Power Engineering Society Transmission and Distribution Conf., 1996, pp. 339–345.
- [18] B. Roberts, "Capturing grid power," IEEE Power and Energy Mag., vol. 7, no. 4, pp. 32 - 41, July-Aug. 2009.
- [19] The Electropaedia, "Lead Acid Batteries," Battery and Energy Technologies, 2005 [Online]. Available: <http://www.mpoweruk.com/leadacid.htm>

- [20] I. Buchmann, "The Lithium Ion Battery," Batteries in a Portable World, 2001 [Online]. Available: <http://www.buchmann.ca/chap2-page6.asp>
- [21] Electricity Storage Association, "Technologies," 2009 [Online]. Available: <http://www.electricitystorage.org/site/technologies/>
- [22] I. Buchmann, "The nickel-based battery, its dominance and the future," Battery University, 2003 [Online]. Available: <http://www.batteryuniversity.com/partone-4.htm>
- [23] L. Chung, M.F.M. Siam, A.B. Ismail, Z.F. Hussien, "Modeling and simulation of sodium sulfur battery for battery-energy storage system and custom power devices," National Power and Energy Conference Proceedings, pp. 205-210, 29-30 Nov. 2004.
- [24] The Electropaedia, "Flow Batteries," Battery and Energy Technologies, 2005. [Online]. Available: <http://www.mpoweruk.com/flow.htm>
- [25] I. Buchmann, "What's the role of the Supercapacitor?," Battery University, 2003 [Online]. Available: <http://www.batteryuniversity.com/partone-8.htm>
- [26] P. Taylor, L. Johnson, K. Reichart, P. DiPietro, J. Philip, and P. Butler, "A summary of the state of the art of superconducting magnetic energy storage systems, flywheel energy storage systems, and compressed air energy storage systems," Sandia National Labs, SAND99-1854, 1999.
- [27] R. B. Boom and H. A. Peterson, "Superconductive energy storage for power systems," IEEE Trans. Magn., vol. MAG-8, pp. 701–704, Sept. 1972.
- [28] California Energy Commission, "DER Equipment- Energy Storage/UPS Systems," Distributed Energy Resource Guide, 2002 [Online]. Available: http://www.energy.ca.gov/distgen/equipment/energy_storage/energy_storage.html
- [29] A. Arulampalam, M. Barnes, N. Jenkins, J.B. Ekanayake, "Power quality and stability improvement of a wind farm using STATCOM supported with hybrid battery energy storage," IEE Proc. Generation, Transmission and Distribution, vol. 153, no. 6, pp. 701 – 710, November 2006.
- [30] J. Zeng, B. Zhang, C. Mao, Y. Wang, "Use of Battery Energy Storage System to Improve the Power Quality and Stability of Wind Farms," International Conference on Power System Technology, pp. 1 – 6, 2006.

- [31] K.Yoshimoto, T.Nanahara, G.Koshimizu, “New Control Method for Regulating State-of- Charge of a Battery in Hybrid Wind Power/Battery Energy Storage System,” IEEE PES, pp. 1244 – 1251, Oct. 29-Nov. 1 2006.
- [32] C. Banos, M. Aten, P. Cartwright, T.C. Green, “Benefits and control of STATCOM with energy storage in wind power generation,” IEE International Conference on AC and DC Power Transmission, pp. 230 – 235, 28-31 March 2006.
- [33] P. A. Coppin, “Using Intelligent Storage to Smooth Wind Energy Generation,” Electrical Energy Storage Applications and Technologies, September 2007.
- [34] H. T. Le, S. Santoso, W. M. Grady, “Development and analysis of an ESS-based application for regulating wind farm power output variation,” in Proc. IEEE Power and Energy Soc. Gen. Meeting, July, 26–30, 2009.
- [35] M. Mehos, D. Kabel, P. Smithers, “Planting the seed,” IEEE Power and Energy Mag., vol. 7, no. 3, pp. 55 - 62, May-June 2009.
- [36] J. P. Barton and D. G. Infield, “Energy storage and its use with intermittent renewable energy,” IEEE Trans. Energy Convers., vol. 19, no. 2, pp. 441–448, Jun. 2004.
- [37] The Electropaedia, “State of Charge (SOC) Determination,” Battery and Energy Technologies, 2005. [Online]. Available: <http://www.mpoweruk.com/soc.htm>
- [38] S. Pang, J. Farrell, J. Du, M. Barth, “Battery State-of-Charge Estimation,” American Control Conference, vol. 2, pp. 1644 – 1649 25-27 June 2001.
- [39] J. Chiasson, B. Vairamohan, “Estimating the state of charge of a battery,” IEEE Trans. Control Systems Tech., vol. 13, no. 3, pp. 465 – 470 May 2005.
- [40] Il-Song Kim, “Nonlinear State of Charge Estimator for Hybrid Electric Vehicle Battery,” IEEE Trans. Power Elec., vol. 23, no. 4, pp. 2027 – 2034 July 2008.
- [41] O. Caumont, P. Le Moigne, C. Rombaut, X. Muneret, and P. Lenain, “Energy Gauge for Lead-Acid Batteries in Electric Vehicles,” IEEE Trans. Energy Convers., vol. 15, no. 3, pp. 354 – 360 Sept. 2000.
- [42] A. J. Salkind, C. Fennie, P. Singh, T. Atwater, D. E. Reisner, “Determination of state-of-charge and state-of-health of batteries by fuzzy logic methodology,” Journal of Power Sources, vol. 80, pp. 293 – 300, 1999.

- [43] C.C. Chan, E.W.C. Lo, S. Weixiang, "The available capacity computation model based on artificial neural network for lead-acid batteries in electric vehicles," *Journal of Power Sources*, vol. 87, pp. 201 – 204, 2000.
- [44] S. Piller, M. Perrin, A. Jossen, "Methods for state-of-charge determination and their applications," *Journal of Power Sources*, vol. 96, pp. 113 – 120, 2001.
- [45] M. Dürr, A. Cruden, S. Gair, J.R. McDonald, "Dynamic model of a lead acid battery for use in a domestic fuel cell system," *Journal of Power Sources*, vol. 161, no. 2, pp. 1400-1411, 27 October 2006.
- [46] H.L. Chan, "A new battery model for use with battery energy storage systems and electric vehicles power systems," *IEEE PES Winter Meeting*, vol. 1, pp. 470 – 475, 23-27 Jan. 2000.
- [47] Z.M. Salameh, M.A. Casacca, W.A. Lynch, "A mathematical model for lead-acid batteries," *IEEE Trans. Energy Convers.*, vol. 7, no. 1, pp. 93 – 98, March 1992.
- [48] *Battery Application Manual*, Gates Energy Products, Inc., Gainesville, FL, 1989.
- [49] M. Ceraolo, "New Dynamical Models of Lead-Acid Batteries," *IEEE Trans. Power Syst.*, vol. 15, no. 4, pp.1184-1190, November 2000.
- [50] S. Barsali, M. Ceraolo, "Dynamical Models of Lead-Acid Batteries: Implementation Issues," *IEEE Trans. Energy Convers.*, vol. 17, no. 1, pp.16-23, March 2002.
- [51] R. A. Jackey, "A Simple, Effective Lead-Acid Battery Modeling Process for Electrical System Component Selection," *SAE Paper 2007-01-0778*, SAE International, Warrendale, PA, 2007.
- [52] The Electropaedia, "Battery Life (and Death)," *Battery and Energy Technologies*, 2005. [Online]. Available: <http://www.mpoweruk.com/life.htm>
- [53] M. Ahlstrom, L. Jones, R. Zavadil, W.S Grant, "The future of wind forecasting and utility operations," *IEEE Power and Energy Magazine*, pp. 57-64, no.6, Nov.-Dec. 2005.
- [54] B. Ernst, "Wind Power Forecast for the German and Danish Networks," *Wind Power in Power Systems*, T. Ackermann, Ed. John Wiley & Sons, 2005, pp. 365-381.

- [55] J. Cao, X. Lin, “Study of hourly and daily solar irradiation forecast using diagonal recurrent wavelet neural networks,” *Energy Conversion and Management*, vol. 49, no. 6, pp. 1396 – 1406, February 2008.
- [56] V.M. Becerra, “Development and Applications of Novel Optimal Control Algorithms”. PhD Thesis, City University, London, UK, 1994 [Online]. Available: http://www.personal.rdg.ac.uk/~shs99vmb/files/PhD_thesis_vmb.pdf
- [57] B. Chachuat, *Nonlinear and Dynamic Optimization: From Theory to Practice*, Automatic Control Laboratory, EPFL, Switzerland, 2007.
- [58] J. Akesson, *MPCtools 1.0 — Reference Manual*, Department of Automatic Control, Lund Institute of Technology, January 2006
- [59] DIDO, a MATLAB Application Package for Solving Optimal Control Problems developed by I. M. Ross, 2007. [Online]. Available: <http://www.elissar.biz/Elissar.html>
- [60] D. Croft, S. Stilson, S. Devasia, “Optimal tracking of Piezo-based Nanopositioners” *The Sixth Foresight Conference on Molecular Nanotechnology*, 1998. [Online]. Available: <http://www.foresight.org/conferences/MNT6/Papers/Devasia/index.html>
- [61] S. Devasia, D. Chen, B. Paden, “Nonlinear inversion-based output tracking,” *IEEE Trans. Automatic Control*, vol. 41, no. 7, pp.930-942, July 1996.
- [62] M.E. Baran, S. Teleke, A. Huang, S. Bhattacharya, L. Anderson, S. Atcitty, “STATCOM with Energy Storage for Smoothing Intermittent Wind Farm Power,” *IEEE PES GM*, pp. 1 – 6, 20-24 July 2008.
- [63] M.E. Baran, S. Teleke, A. Huang, S. Bhattacharya, L. Anderson, S. Atcitty, “Dispatching of wind farms using battery energy storage,” *Int. J. of Power Electronics*, Vol. 1, No.2 pp. 164 – 175, 2008.
- [64] S. Sirisukprasert, A. Q. Huang, J. S. Lai “Modeling, analysis and control of cascaded-multilevel converter-based STATCOM,” *IEEE PES general meeting*, vol. 4, pp. 2561 - 2568, July 2003.
- [65] C. Schauder, H. Mehta, “Vector analysis and control of advanced static VAR compensators,” *IEE Proceedings of Generation, Transmission and Distribution*, Volume 140, Issue 4, pp. 299 – 306, July 1993.

Appendices

Appendix A: Battery Model

The equations for the circuit components shown in Figure 3-3 can be written as follows [49]:

$$Em = Emo - K_E (273 + \theta)(1 - SOC) \quad (A-1)$$

$$C1 = \frac{\tau_1}{R1} \quad (A-2)$$

$$R1 = -R_{10} \ln(DOD) \quad (A-3)$$

$$R2 = R_{20} \frac{e^{A_{21}(1-SOC)}}{1 + e^{(A_{22} \ln/I^*)}} \quad (A-4)$$

$$Ip = V_{pn} G_{po} e^{\left(\frac{V_{pn}}{V_{po}} + A_p \left(1 - \frac{\theta}{\theta_f}\right)\right)} \quad (A-5)$$

$$Rp = \frac{V_{pn} - Ep}{Ip} \quad (A-6)$$

$$R0 = R_{00} [1 + A_0 (1 - SOC)] \quad (A-7)$$

$$Ep = \text{constant} \quad (A-8)$$

where Em was the open-circuit voltage (EMF) in volts, Emo was the open-circuit voltage at full charge in volts, K_E was a constant in volts/°C, $C1$ was a main branch capacitance in farads, τ_1 was a main branch time constant in seconds, $R1$ was a main branch resistance in ohms, R_{10} was a constant in ohms, $R2$ was a main branch resistance in ohms, R_{20} was a constant in ohms, A_{21} was a constant, A_{22} was a constant, Im was the main branch current in amps, Ip was the current loss in the parasitic branch, V_{pn} was the voltage at the parasitic branch, G_{po} was a constant in seconds, V_{po} was a constant in volts, A_p was a constant, Rp was a parasitic resistance in ohms, $R0$ was a resistance in ohms, R_{00} was the value of $R0$ at $SOC=1$ in ohms, A_0 was a constant. Typical values of these constants can be found in [49]. Moreover, the definition for SOC is already provided in equation (3-1) and the DOD can be defined as:

$$DOD = 1 - \frac{Q_e}{C(I_{avg}, \theta)} \quad (A-9)$$

$$I_{avg} = \frac{Im}{\tau_1 s + 1} \quad (A-10)$$

where I_{avg} was the mean discharge current in amps and the definition for Q_e and C were given in equation (3-2) and equation (3-3) respectively.

Appendix B: Derivation of the mathematical model

By looking at Figure 4-11 we can derive the equations as follows:

$$I_{cap} = C1 \frac{dV_{C1}}{dt} = C1 \frac{d[R1(I_{bat} - I_{cap})]}{dt} \quad (\text{B-1})$$

$$V_{bat} = Em - I_{bat}(R0 + R2) - R1(I_{bat} - I_{cap}) \quad (\text{B-2})$$

$$P_{bess} = V_{bat} \times I_{bat} \quad (\text{B-3})$$

After simplification we get:

$$\frac{dI_{cap}}{dt} = -\frac{1}{R1 \times C1} I_{cap} + \frac{dI_{bat}}{dt} = -\frac{1}{\tau_1} I_{cap} + \frac{dI_{bat}}{dt} \quad (\text{B-4})$$

$$V_{bat} = Em - I_{bat}(R0 + R1 + R2) + R1 \times I_{cap} \quad (\text{B-5})$$

$$P_{bess} = R1 \times I_{bat} \times I_{cap} + Em \times I_{bat} - (R0 + R1 + R2) I_{bat}^2 \quad (\text{B-6})$$

Appendix C: Experimental Setup details

The following components are used in the experiment:

Table A.1: Used Parts

Component Name	Detail
IGBT Module	Powerex CM300DY-12E
Gate Driver	Powerex BG2B
Batteries	Lawn and Garden
Current Sensor	Tamura L18P015D15
Inductor	440 μ H
Resistive Divider	2x 510 k Ω
Dspace	DS1104
Matlab	7.1.0
Fuse	4 A